Spring 5-15-2022

Control of Intestinal Turnover and Cell Death through Canonical Autophagy Pathways within Mouse and Human Epithelia

John Steven Ekman
Washington University in St. Louis

WASHINGTON UNIVERSITY IN ST. LOUIS

Division of Biology and Biomedical Sciences
Immunology

Dissertation Examination Committee:
Mentor: Thaddeus S. Stappenbeck
Clay Semenkovich, Chair
Megan Baldridge
Stuart Kornfeld
Nima Mosammaparast
Gwendalyn Randolph
Robert Schreiber

Control of Intestinal Turnover and Cell Death through Canonical Autophagy Pathways within Mouse and Human Epithelia

by
John Steven Leal Ekman

A dissertation presented to
The Graduate School
of Washington University in
partial fulfillment of the
requirements for the degree
of Doctor of Philosophy

May 2022
St. Louis, Missouri

Table of Contents

Contents

List of Figures

List of Abbreviations

ANOVA: analysis of variance; *Atg14*: autophagy related 14; *Atg16l1*: autophagy related 16-like 1 (S. cerevisiae); *Atg5*: autophagy related 5; cCASP3: cleaved CASP3/caspase-3; cCASP8: cleaved CASP8/caspase-8; CHX: cycloheximide; Cflar/Cflip: CASP8 and FADD-like apoptosis regulator; EdU: 5-ethynyl-2´-deoxyuridine thymidine; f/f: flox/flox; Fadd: Fas (TNFRSF6)-associated via death domain; H&E: hematoxylin and eosin; MTT: 3-(4,5-dimethylthiazol-2-yl)-2,5-diphenyltetrazolium bromide; Nec-1: necrostatin-1; *Rb1cc1/Fip200*: RB1-inducible coiled-coil 1; *Ripk1*: receptor (TNFRSF)-interacting serine-threonine kinase 1; *Ripk3*: receptor (TNFRSF)-interacting serine-threonine kinase 3; Sqstm1/p62: Sequestosome 1 *Tnfrsf1a/Tnfr1*: tumor necrosis factor receptor superfamily, member 1a; *Tnf/ Tnfsf1a*: tumor necrosis factor; VC: *Vil1/villin 1*-Cre.

Acknowledgments

I want to foremost thank my mentor, Thad Stappenbeck for my development as a future physician scientist. You have generously supported me in lab and outside of lab, and I am truly grateful. You have provided innumerable resources towards my project and helped me become a better scientist. I'm looking forward to working together as I take the next steps through residency, fellowship, and starting my own lab.

I want to thank my entire lab for so much support, advice, and great times. To my co-authors and friends, thank you. I want to thank Qiuhe for being an amazing mentor and friend, generating tools that were essential for moving my project forward, and for your critical insight and scientific feedback. Umang you have been an outstanding colleague and friend, offering me advice and the opportunity to contribute to your work; may we collaborate on scientific projects in the years ahead! To Nikki, we have spent many years literally back-to-back in NTA 1020, I was the recipient of so much your generous help, guidance, and support. To Feidi for many hours of histology prep, and research; wishing you continued success in residency. To Haerin for the many hours working side-by-side as we deciphered the *Atg14* phenotype. Ta, you have emphasized to me the art and skill of being a rigorous, and thoughtful scientist. To my fellow grad students: RC, Taka, Derek, Clara and those before including Khushbu, Lulu and others, I appreciate your support and continuing our dear friendship, as we keep moving forward to residency, fellowship, research and beyond.

To the current lab: Satoru, Ted, Shanshan, and Kevin. I'm so happy that you will all keep the lab legacy and work going strong. Pat, I am so grateful that we have you to navigate our way through CCF. Thank you very much for dedicating your time to us and getting our lab off the ground during the start of a pandemic! To all those who mentored me including, but not limited to Hiroyuki, Kelli, Gerard I will always be grateful of the expertise you have shared with me,

and I hope to continue to cross paths as colleagues!

Thank you to Dr. Skip Virgin for serving as the initial chair on my committee and for your great advice, support and generously sharing the p62 mouse with me. Thank you, Dr. Clay Semenkovich, for being a scientific and career mentor, and an amazing thesis chair. Thank you Darren, for your countless hours generating my mouse models that have formed the foundation for my project. Thank you Wandy for your microscopy expertise and generation of the TEM data. Thank you all the technicians in the Histo Core for countless hours of slide prep.

To all the administrative assistants that have supported me and make scheduling a breeze.

To my committee members, thank you for all of your thoughtful scientific and career advice. Presenting to you has been an honor. I have learned so much from you, and you challenge me to become the best scientist I can. I look forward to staying in touch as research colleagues.

To the MSTP office and committee who accepted me into this fantastic program and supported me along the way. Thank you! To my MSTP classmates: Thank you for so much support and great times. Looking forward to following your successes through residency and beyond!

Last, but certainty not least, I would like to thank my family for the love and support throughout my entire life. You have believed in me and made me who I am. I would like to thank God for keeping me strong in my faith and for guiding me through challenging times. I will keep moving forward knowing that I carry the DNA and heritage of Leal, Villa, Gutierrez, and Alvarado with me at all times. I will run my race.

Funding for this work was provided in part by the MSTP training grant T32GM007200-39, the Pulmonary Training grant T32HL007317-41 and Crohn's & Colitis Foundation; Kenneth Rainin Foundation; National Heart, Lung, and Blood Institute [T32 HL007317]; National Institutes of Health [P30DK052574]

J. Steven Leal-Ekman

Washington University in St. Louis
May 2022

Dedicated to my Grandfather Tony Leal
and Grandmother Yolanda Villa Leal

ABSTRACT OF THE DISSERTATION

Control of Intestinal Turnover and Cell Death through Canonical Autophagy Pathways within Mouse and Human Epithelia

by J. Steven Leal Ekman

Doctor of Philosophy in Biology and Biomedical Sciences

Immunology

Washington University in St. Louis, 2022

Professor Clay Semenkovich, Chair

Professor Thaddeus Stappenbeck, Co-Chair, Mentor

Regulation of epithelial turnover is essential for the maintenance of the structure and function of the intestine. The balance of intestinal epithelial turnover is known to be modulated by cell-extrinsic cytokines such as Tumor Necrosis Factor (TNF). Likewise, cell-intrinsic modulation of survival and death is afforded by a highly-conserved, multi-step pathway termed autophagy. In this body of work, I have characterized a specific and potent role for autophagy in protecting mouse intestinal epithelial cells (enterocytes) from TNF-triggered cell death. Specifically, I have found that the autophagy initiation factor Atg14 is central to mediating this protective role. Utilizing conditional loss of function mouse models of *Atg14* and its upstream regulator *Rb1cc1/Fip200*, I have demonstrated that canonical autophagy factors are required for maintenance of the intestinal architecture and the viability of enterocytes. I furthermore demonstrate through genetic and pharmacologic approaches that TNF signaling through its cognate receptor Tnfr1 is required for the induction of apoptotic death of autophagy-deficient enterocytes. Through a candidate approach to profile the TNF signaling and autophagic pathways in the Atg14 deficient mouse cell, I have identified both an autophagy associated factor (Sqstm1/p62) and a TNF induced cell death factor (Cflar/Cflip) isoform that

accumulate within the autophagy deficient mouse cell. Genetic ablation of *Sqstm1/p62* rescues mouse intestinal architecture and epithelial cell death within the *Atg14* deficient mouse model. These findings define the critical molecular pathways that mediate sensitivity to apoptosis in the *Atg14* deficient mouse enterocyte. Lastly, my research has identified that human *ATG14* KO cells (HeLa) share a defect in SQSTM1/p62, but are not sensitive to enhanced TNF-triggered death, and do not express the pathogenic isoform of the cell death regulator CFLAR/CFLIP. This finding lays the foundation for further basic science research to understand the divergence between human and mouse with respect to cell death pathways. This work provides insight into the limited success, thus far, of autophagy-oriented therapeutics in the context of human disease, while promoting novel approaches for such therapies.

Chapter 1:

Introduction

Autophagy is a fundamental, highly conserved cellular process that functions to degrade protein aggregates and maintain homeostasis [2]. This process is important in the intestine as genetic mutations in autophagy genes are associated with Crohn's disease (CD) [3]. The overarching aim of this dissertation project in the Stappenbeck lab is to define the role of canonical autophagy in the context of cellular turnover and intestinal epithelial tissue renewal. The small intestinal epithelium provides an appropriate model system for this work because in a single histological section, one can visualize proliferating stem cells, professional absorptive enterocytes, and senescent enterocytes in preparation for apoptotic cell death [4]. Furthermore, our knowledge of factors that regulate turnover is incomplete: only a handful of factors that control cell maturation, division, and death are characterized and these pathways only explain a small proportion of intestinal biology [5] [6]. The cells of the intestinal epithelium are highly responsive to cytokines such as TNFα [7]. How cellular housekeeping pathways crosstalk with cytokine signaling has yet to be fully characterized.

In the Stappenbeck lab, I am interested in elucidating the function of autophagy in the intestinal epithelium using mouse and *in-vitro* spheroid models, the latter of which have been pioneered by our group [8]. My work builds upon previous publications from our group demonstrating that mice conditionally deficient for proteins of the autophagy cascade (i.e. Atg16l1), in the intestinal epithelium are viable, but carry morphological and functional defects in secretory epithelial cells, and are sensitive to pathogen-triggered inflammation [9]. These factors model relevant aspects of the epithelial defects found in patients with Inflammatory Bowel Disease (IBD) [10]. The intestinal roles of other autophagy factors such as Atg14, Beclin-1, and Rb1cc1/Fip200 have not yet been characterized.

I generated mice (*Atg14* $^{f/f}$; *VC*$^{+}$) with an intestinal epithelial specific deletion of *Atg14*. *Atg14*

$^{f/f}$; VC^{+} mice were distinct from similar deletions of *Atg5* and *Atg16L1* as these animals failed to thrive after weaning, leading to spontaneous lethality beginning at week six. Histologically there was severe villus atrophy in the small intestine. I also detected increased apoptotic bodies in the epithelium, an indicator of increased cell death. **This work presents the first comprehensive analysis of the autophagy initiator *Atg14* in the intestinal epithelium**. [11].

Chapter 1 reviews the relevant literature regarding the three distinct, yet interconnected pathways addressed within this dissertation: TNFα (Tumor Necrosis Factor alpha), autophagy, and cell death. It also provides pertinent background detailing the biology of the intestine and the known factors that control its homeostasis.

Chapter 2 presents the published findings to characterize the role of Atg14 and another autophagy initiation factor (Rb1cc1/Fip200) within the intestinal epithelium. It also presents the finding that these animals are profoundly sensitive to intestinal cell death by endogenous TNF.

Chapter 3 defines a molecular scaffold (Sqstm1/p62) that potentiates TNF-triggered cell death. It highlights a molecular link downstream of TNF connecting the autophagic and caspase-8 pathways.

Chapter 4 determines the role of ATG14 in human cells. This ongoing work seeks to answer the question: “To what degree is the association between autophagy and cell death conserved between mice and humans?” The answer to this question has major implications for targeting the autophagy and cell death pathways therapeutically during disease.

1.1 The Intestine

Structure of the intestinal epithelium

The small intestinal epithelium is a monolayer of highly specialized cells that line the surface of the gastrointestinal tract. The epithelium covers the surface of two distinct domains: the crypts that invaginate away from the lumen, lined by the intestinal stem and progenitor cells, and the villi which

protrude toward the lumen with a large surface area lined by absorptive enterocytes and secretory cells. [12] **(Figure 1**). The small intestinal epithelium undergoes the fastest rate of basal division in the body, turning over every 2-3 days [13]. New cells are generated within the crypts and mature as they approach the villus. As cells reach the villus tip, they are specified to die and extrude out of the monolayer, making room on the villus for new cells [14]. In order to achieve this, they undergo a process of programmed cell death called apoptosis [15].

Apoptosis is visually characterized by cell shrinkage, chromatin condensation, nuclear compartmentalization and fragmentation [16]. Apoptosis is mediated through the action of Caspase-3, a serine-threonine protease that, when activated (cleaved Casp-3) cleaves numerous protein substrates throughout the cell for degradation. There are two primary apoptotic cascades that can be initiated: intrinsic and extrinsic. The intrinsic cascade is initiated by cellular insults as DNA or mitochondrial damage. This form of damage releases the mitochondrial protein Cytochrome C into the cytoplasm, where it binds with the protein Apaf-1 to activate Caspase-9. Caspase-9 in turn initiates the activation of the effector caspases Casp-3 and Casp-7 through proteolytic cleavage [17]. In contrast, the extrinsic pathway is initiated through the ligation of a death receptor with its cognate cytokine death ligand. Some of the most common death ligands include TRAIL, FAS, and Tumor Necrosis Factor (TNF) [18]. TNF stimulates the formation of a Death Inducing Signaling Complex (DISC), consisting of the initiator caspase, Caspase-8 and several regulatory subunits [19]. When the DISC is activated, Caspase-8 is cleaved, in turn proteolytically activating Casp-3 and Casp-7 to commit the cell to death [20].

Figure 1 Schematic of intestinal architecture:

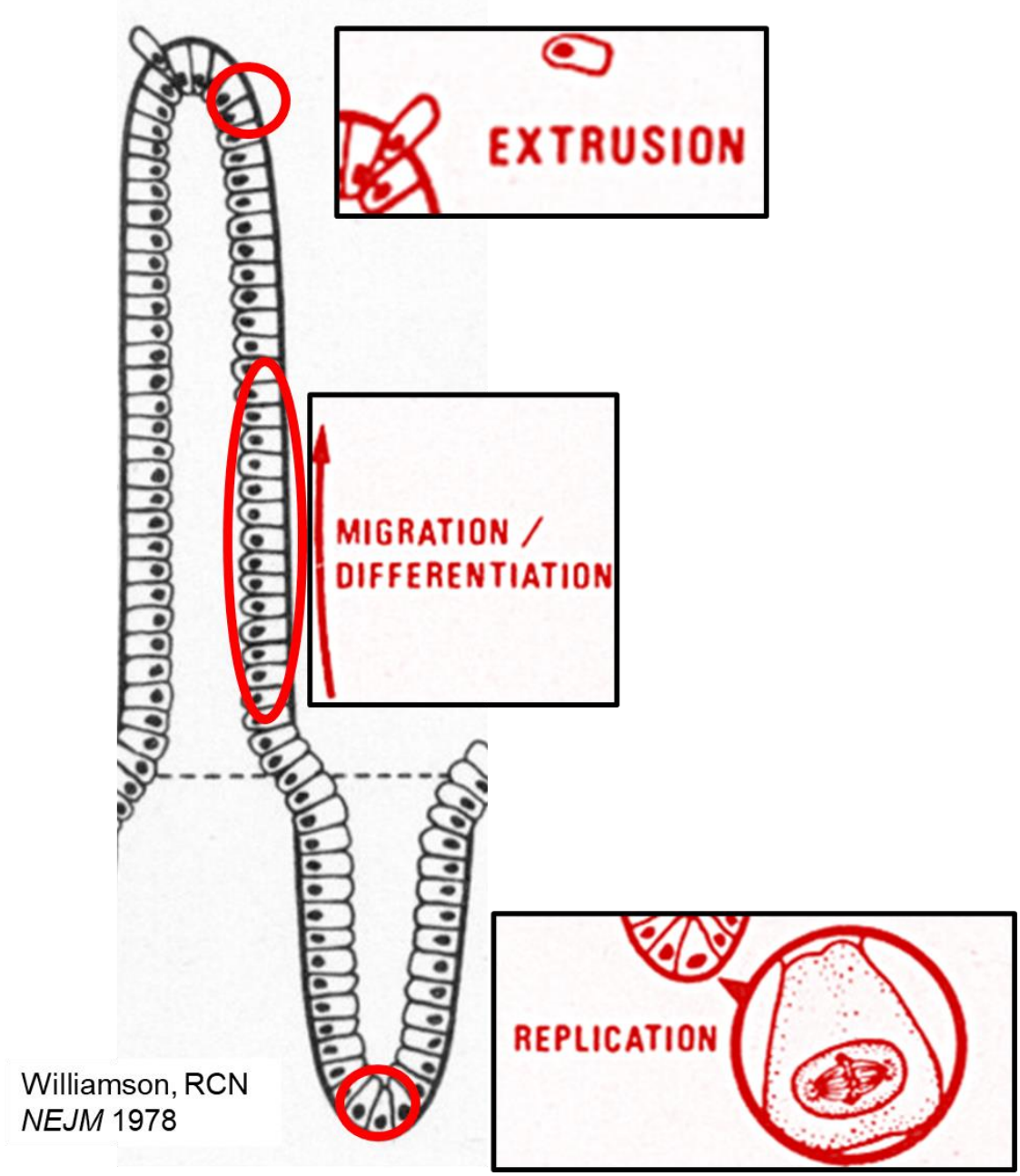

The intestinal epithelium maintains domains of proliferation, multi-lineage differentiation and maturation, and cell death; domains of interest are circled in red. Adapted from Williamson, NEJM. 298(25) 1393-1402 [12].

1.2 Autophagy

In the most general sense, autophagy is a catabolic process through which cytoplasmic cargo (protein, organelles, etc…) are sequestered within double-membraned vesicles called autophagosomes

and degraded by the lysosome. This pathway functions in virtually every eukaryotic cell to mediate a catabolic response to starvation but also functions to mediate protein degradation, trafficking, and secretion [21]. The focus of this dissertation will be on the core catabolic protein factors that carry out this pathway: The Serine Kinase complex (Rb1cc1/Fip200), the Lipid Kinase complex (Atg14, Beclin-1), the Lipid Ligase complex (Atg5, Atg16l1), the Vesicle Fusion complex (Atg14, Stx17) and the autophagy cargo receptors (Sqstm1/p62) [22]. The proximal factors that sense nutrients and energy such as the AMPK or mTOR pathways, will not be discussed here [23].

Atg14 is a component of the lipid kinase nucleation (initiation) complex [24]. This complex, comprised of Atg14, Beclin-1, Vps15, and Vps34, functions to nucleate the assembly of a double-membraned vesicular structure that will expand to become an autophagosome. Current models propose that Atg14 functions to localize the lipid kinase complex to the ER membrane, where autophagosome biogenesis commences [11]. From there, the effector lipid kinase subunit, Vps34, phosphorylates the membrane lipid Phosphatidylinositol (PI), generating the phospholipid PI3P. Deposition of PI3P on membranes recruits subsequent effectors that are required for autophagosome maturation as well as endosome maturation [25] [26].

The primary methodological approach to study the autophagy pathway has been through genetic loss of function studies. Recent studies support the hypothesis that not all autophagy gene knockouts lead to the same phenotype [27]. Rb1cc1/Fip200 functions as part of a complex that phosphorylates and activates the Atg14 lipid kinase complex. Lipid kinase function requires antecedent activity of the serine kinase complex [28]. The lipid ligase complex including Atg16L1 and Atg5, play a direct role in maturing and expanding the PI3P containing autophagosome through the action of conjugating a protein binding moiety called LC3 to the autophagosome membrane [29]. In the absence of lipid ligase function, autophagosomes are still produced, but they are not matured nor

degraded effectively. In contrast, the loss of *Atg14* results in the absence of bona fide autophagosomes, but does not appreciably change the conjugation or protein binding of LC3 on endosomal membranes [30].

Figure 2 Schematic of the core autophagy pathway: Highlighting the four discrete, sequential complexes of the core degradation machinery and the autophagy cargo receptor

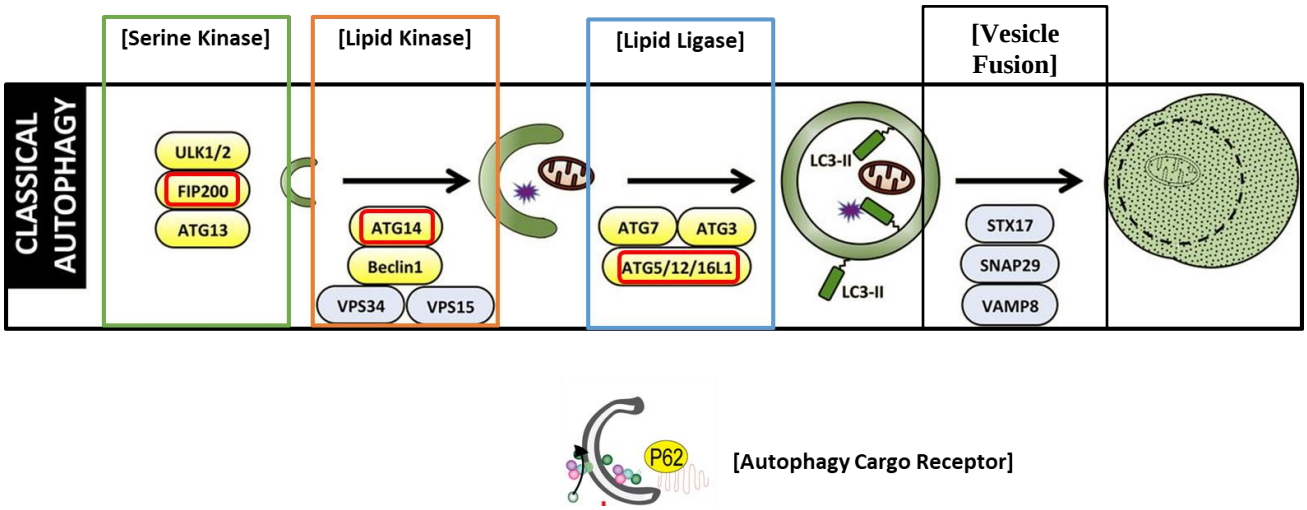

The canonical autophagy pathway consists of 4 major independent, yet stepwise processes: initiation, nucleation, elongation, and vesicle fusion. Each of these processes is carried out by a unique protein complex: The Fip200-Ulk1 serine kinase complex, the Atg14-Beclin1-Vps34 lipid kinase complex, the Atg5-Atg12-Atg16L1 lipid ligase complex, and the SNAP-SNARE proteins that mediate vesicular fusion. These 4 complexes are indicated above in green, orange, blue, and black, respectively. The autophagy cargo receptor is not a part of the core catabolic machinery, but plays a critical role in bringing cargo to the autophagosome to be degraded. Adapted from Cadwell, K, Debnath, J. et. al. JCB 2018;217(3):813-822 and Patel, K. and Stappenbeck, TS, Annu Rev Physiol 2013;75:241-62 [22].

The Sequestosome1/ p62 Autophagy Cargo Receptor

Sequestosome1/p62 is the dominant and prototypical member of the family of autophagy cargo receptors, proteins which deliver cargo (proteins and organelles) to the autophagosome for

degradation [31]. They function in concert with the members of the core catabolic machinery to mediate canonical degradative autophagy, but are functionally independent; they have no role in generating the autophagosomal vesicle. Furthermore, these proteins are substrates for autophagy [32]. If autophagy is induced, these proteins will be degraded along with the proteinaceous cargo they bind. Therefore, it is important to note that autophagy-deficient cells will have increased levels of p62 [33] [34].

Sqstm1/p62 functions as a platform for cellular signaling pathways; p62 was initially discovered as an interacting factor of RIPK1 to facilitate TNF-triggered NF-κB stimulation [35]. Specifically of interest to this work are the reports of SQSTM/p62 mediating TNF triggered cell death signaling through its interaction with both RIPK1 (which is now recognized as a master regulator of cell fate) [36] and with Caspase-8 (CASP8) [37]. In each of these reports, the respective authors found that within the context of TRAIL-stimulated cancer cells, SQSTM/p62 can form a scaffold to activate cell death pathways. The results presented in chapter 3 will expand upon the known role of p62 in the context of intestinal cell death.

In the context of disease, mutations and polymorphisms in the autophagy pathway directly increase the cellular abundance of SQSTM/p62 [34] and also that of ubiquitinated protein inclusions [38]. Specifically patients with tauopathies demonstrate p62 aggregates (otherwise referred to as p62 bodies, or p62 puncta) in the brain, in association with ubiquitinated protein complexes [39]. The formation of these large ubiquitinated proteinaceous bodies is incompletely understood, but histologically similar structures are readily observed under experimental conditions of cell culture when components of the *initiation* steps of autophagy are deleted [40] [41] [42]. Subsequent studies have ascribed a function to these aggregates, proposing that p62 functions as a scaffold to mediate signaling of growth and proliferative signaling pathways [43]

and the aberrant activation of such signaling pathways leads to disease states such as cancer and metabolic disease [44] [45].

1.3 TNF

Intestinal TNF signaling

Tumor necrosis factor-alpha (TNF-α, subsequently referred to as TNF) is a pleiotropic cytokine that is present at basal levels systemically. In healthy individuals, it plays a largely benign, pro-inflammatory and proliferative role as part of the innate immune response. TNF is produced primarily in activated macrophages [46], including the Kupffer cells of the liver (and released in bile) [47] [48], as well as in mast cells [49], and intestinal epithelial cells [50]. Owing to the many proximal sources of this molecule, the intestinal epithelium is regularly exposed to TNF. TNF is clinically relevant in Inflammatory Bowel Disease (IBD): affected patients have elevated serum levels of the molecule and TNF levels are directly correlated with severity of disease [51]. TNF neutralization is an extremely effective therapy for many patients with IBD [52]. In this chapter, I hypothesize that *Atg14* loss sensitizes the cell to TNF-mediated apoptosis. Linking autophagy, a genetic pathway associated with IBD, with TNF, a soluble factor implicated in IBD, would significantly advance the understanding of this disease.

TNF signaling yields two disparate outcomes downstream of TNF Receptor Signaling: A) Pro-survival, pro-inflammatory transcription or B) apoptotic cell death. The former is the default outcome in most cells and is mediated by the rapid activation of the NF-κB signaling cascade. There are two TNF receptors: TNF receptor 1 (Tnfr1) or TNF receptor 2 (Tnfr2) [53]. While both receptors can mediate signaling, only the former can trigger cell death [54]. Tnfr2 has a limited repertoire, it is expressed primarily in immune cells. TNF binding to either Tnfr1 or Tnfr2 leads to the recruitment of a number of intracellular adapter proteins, such as Tradd, Ripk1, Traf2, and cIap1/2 [55]. A polyubiquitination cascade is rapidly triggered within 5-10 minutes to form a scaffold that facilitates

the recruitment and activation of the I-KappaB alpha-Kinase (IKK) complex that cleaves IκB to liberate the canonical NF-κB subunit RelA/p65 [56]. p65 transits to the nucleus to induce the rapid transcription of a panel of inflammatory response genes [57].

An alternate outcome is mediated solely by Tnfr1: apoptosis. As of today, the triggers that induce this alternate outcome are incompletely understood, but there are three known prerequisites for apoptotic activation. These steps include A) the loss of the of the NF-κB polyubiquitin scaffold, B) the endocytic internalization of the TNF receptor, and C) the recruitment of initiator caspases to the DISC. [58]

Clathrin-mediated endocytosis is rapidly induced after ligand binding as a means to negatively downregulate TNF stimulation. The initial induction of NF-κB occurs at the plasma membrane and biochemical studies have demonstrated that the NF-κB signaling cascade is still functional in the early endosome [59]. However, experimental blockade of TNFR1 internalization though genetic deletion of the internalization domain or though pharmacological means, impairs induction of apoptosis [59].

The final prerequisite for the apoptotic cascade is the formation of the Death Inducing Signaling Complex (DISC). The DISC is a secondary signaling complex comprised of several proteins that, when activated, can induce apoptosis [60, 61]. The primary effector of this complex is Caspase-8. This work hypothesizes that autophagy is a pathway to sequester and clear the DISC; blocking autophagy is sufficient to allow pathogenic DISC complexes to activate and trigger cell death.

The cell can generate multiple classes of Death Induced Signaling Complexes, each with a different complement and stoichiometry of proteins such as Ripk1, Fadd, Casp8, and Cflar [62]. Reports cite that these complexes can measure greater than 2 mDa [63]. The subcellular localization of such large complexes is controversial; publications characterize that this complex is

subcellularly localized to the cytoplasm, often forming insoluble aggregates or in association with cellular membranes [64]. Owing to the size of the complex, and its membrane localization, the lysosome is well suited to the degradation and inactivation of such large protein signaling complexes[65]. Correspondingly, the lysosome, not the proteasome, is experimentally recognized as the endpoint of the TNF receptor signaling complex [66].

Figure 3 Schematic of the TNF-triggered apoptotic pathway

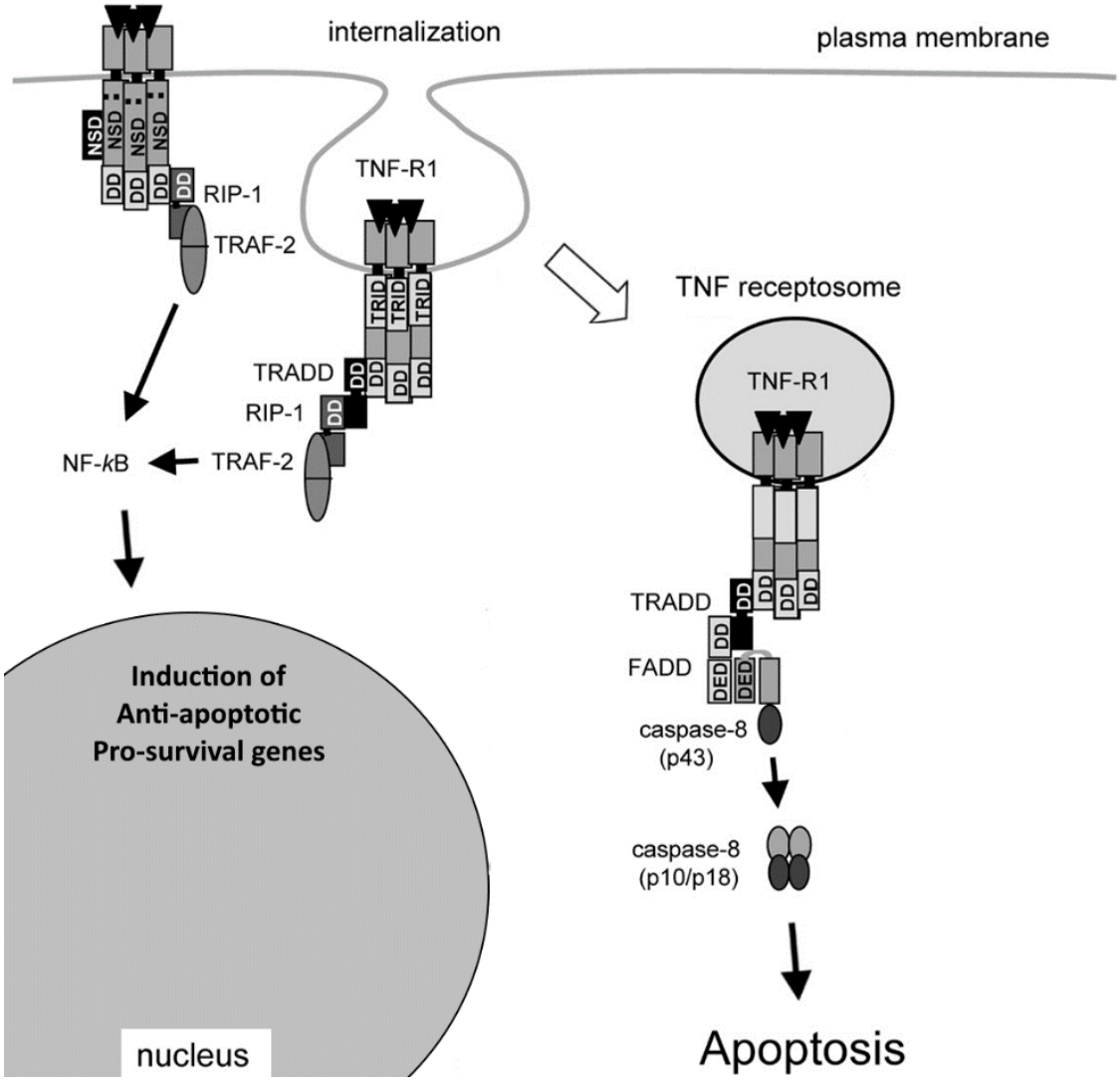

This figure illustrates the opposing outcomes mediated by TNF. In most cells and in wild-type intestinal epithelial cells, the default outcome upon TNF ligation is transcription of NF-kB induced genes. Under selected circumstances and in *Atg14* $^{f/f}$*; VC*$^{+}$ cells, apoptosis is favored. Internalization is a prerequisite for the activation of apoptotic cascade[59]. Figure adapted from Schneider-Brachert et. al. *Immunity*.

1.3 Cell Death

Autophagy and Cell death

Multiple studies have demonstrated that loss of canonical degradative autophagy within the mouse intestinal epithelium sensitizes enterocytes to death. This prevailing model is grounded through the observations from at least four independent publications where mice with a floxed allele of an autophagy-related gene are crossed to a Cre driver under control of the *Villin* promoter, a promoter expressed in nearly all intestinal epithelial lineages. Three of these studies generated conditional knockout mice targeting autophagy lipid ligases, Atg5 and Atg16l1, within the intestinal epithelium and in the context of intestinal infection and damage models.

The Cadwell group challenged the *Atg16L1* $^{F/F}$ *VC+* mouse model to either an intestinal damage model (DSS colitis) coupled with a viral infection model (oral Murine Norovirus [MNV]), or alternately a model of graft versus host disease (T-cell transfer colitis model). In both challenge conditions, these mice had an increased incidence of epithelial death shown to be driven by increased levels of TNF [67]. Additionally, the mode of cell death seen in these studies was necroptosis, an inflammatory, caspase-independent form of death. The Yarovinsky group challenged the *Atg5* $^{F/F}$ *VC+* mouse model as well as the *Atg5* $^{F/F}$ *Defa5+* mouse model (to delete *Atg5* from crypt-based Paneth cells) to an infection model with Toxoplasma Gondii [68]. In both genetic models, there was villus atrophy and inflammatory cell death driven by increased circulating levels of TNF and interferon gamma. The Maloy group challenged the *Atg16L1* $^{F/F}$ *VC+* mouse model to an infectious and inflammatory cocktail which combined intraperitoneal injection of Anti-IL10 with oral gavage of *Helicobacter hepaticus* [69]. Animals did not have an increased inflammatory response (as was cited by the previous two papers), but there was an increase in epithelial cell death, as measured by generation of cleaved caspase-8 and increased TUNEL+ enterocytes. Consistent with the other reports, the phenotype was driven by increases in circulating TNF.

The publications from these groups studied loss of function of intestinal epithelial autophagy complexes in conjunction with distinct damage models, but shared a conclusion that defects in autophagy, leads to an enhancement in intestinal epithelial cell death. All three groups implicated the clinically relevant cytokine TNFα as a trigger for cell death. The study presented in Chapter 2, published contemporaneously with the aforementioned studies investigates the role of two genes that serve in the more proximal steps of the autophagy pathway, *Fip200* and *Atg14* [70]. In brief, mice conditionally deficient in the intestinal epithelium for either of these genes develop robust, spontaneous cell death in the absence of an injury or infection model. The cell death is TNF-mediated, but is non-inflammatory and results in apoptotic, not necroptotic death. Taken together, current data supports the model that canonical degradative autophagy, plays a critical role in modulating the cytotoxic effects of TNF within the intestinal epithelium.

Receptor Interacting Kinase 1 (Ripk1)

Research beginning in the mid to late 1990's, characterized RIPK1/RIP as a novel kinase that interacts with multiple death receptors of the TNF family, namely FAS and TNFR1 [71]. Initial reports cited that it facilitated apoptotic signaling [72] [73] while subsequent reports cited that it was required for NF-kB signaling [74] [73]. The development of the first *Ripk1* knockout mouse by Phil Leder's group, reveals an intriguing phenotype in that mice "fail to thrive" shortly after birth, and that this phenotype is mediated by an enhanced sensitivity to TNFα-triggered cell death [75]. An open question for the field was the contribution of RIPK1 in tissues like the intestinal epithelium, where TNF regulation has been shown to have significant disease associated relevance [51].

This question was addressed within a pair of landmark *Nature* articles that demonstrate that intestinal epithelial specific deletion of *Ripk1* was sufficient to cause spontaneous intestinal damage, loss of crypt-villus architecture, and enhanced death both in-vivo and during in-vitro organoid culture

[76] [77]. Furthermore there have been recent reports of human *RIPK1* loss of function mutations that yield a similar pattern of multi organ immunodeficiency and intestinal damage, though the phenotype is blunted compared to that of the mouse models [78] [79].

Current research paints a much more complex picture of this regulatory factor. It can mediate both survival signaling and death signaling in a kinase-dependent and through a kinase-independent (scaffolding dependent) manner [80] [81] [82] [83]. Per the former mechanism, RIPK1 activates a related family member, RIPK3, to mediate necroptosis, a, inflammatory, immunogenic form of cell death [84]. Per the latter kinase-independent mechanism, RIPK1 promotes the association of Caspase-8 complexes. Both Rip kinases have been shown to co-localize with SQSTM/p62, through the significant of such an association is unclear [85].

What is becoming clearer is the paradigm that post-transcriptional modifications (via phosphorylation and ubiquitination) are critical for defining the interacting partners and activation state of the RIPK proteins [81]. These modifications as well as the abundance and activation states of the modifiers themselves (including TAK1, LUBAC, PELI1, and CHIP/STUB1) define the extent to which RIPK1 and RIPK3 undergo pro-survival or pro-apoptotic modifications [86] [87]. They can also define the timing and extent of protein turnover by the proteasome and/or the lysosome to alter the balance between survival and apoptosis [88] [89] [86] [90] [91]. Furthermore both RIPK1 and RIPK3 can serve as a substrate for caspase-8 cleavage to reinforce apoptosis [92] [93]. In Chapter 2 (**Figure 11**) and in Chapter 4 (**Figure 44**) data are presented regarding the expression of Ripk1 in mouse and human cells within the context of the *Atg14* knockout.

CASP8 and FADD-like apoptosis regulator/ Cellular FLICE-inhibitory protein (Cflar/Cflip)

Two TNF-induced factors of note are Sqstm1/p62 and Cflar/Cflip (cFLIP). cFLIP is a master regulator of caspase activity. It directly binds to Caspase-8, forming a heterodimer though its Death

Effector Domain (DED) to modulate caspase activity (**Figure 4**) [94]. CASP8 activity can be enhanced or suppressed depending upon the splice isoform that is expressed in the cell. The functions of the different splice isoforms are not completely understood, and further detail will be discussed in Chapter 4.2. In brief, it is important to note that splice isoforms vary by species, by cell type, and additionally by the genetic background of the mouse[1, 95]. Human cells predominantly express a form of CFLAR/CFLIP that blocks caspase activation (cFLIP-S), while B6 background mice favor an isoform of Cflar/Cflip that promotes caspase activation (cFLIP-L).

Expression of CFLIP is inducible in both human and mouse: this gene is a classical TNF-induced gene through the transcriptional transactivation of NF-kB inducible elements. Blockade of CFLIP through tool compounds such as the translation inhibitor Cycloheximide (CHX) results in induction of cell death in part because Casp8 is unopposed and self-activates [96].

Figure 4 Schematic of cFLIP control of Caspase-8 activation

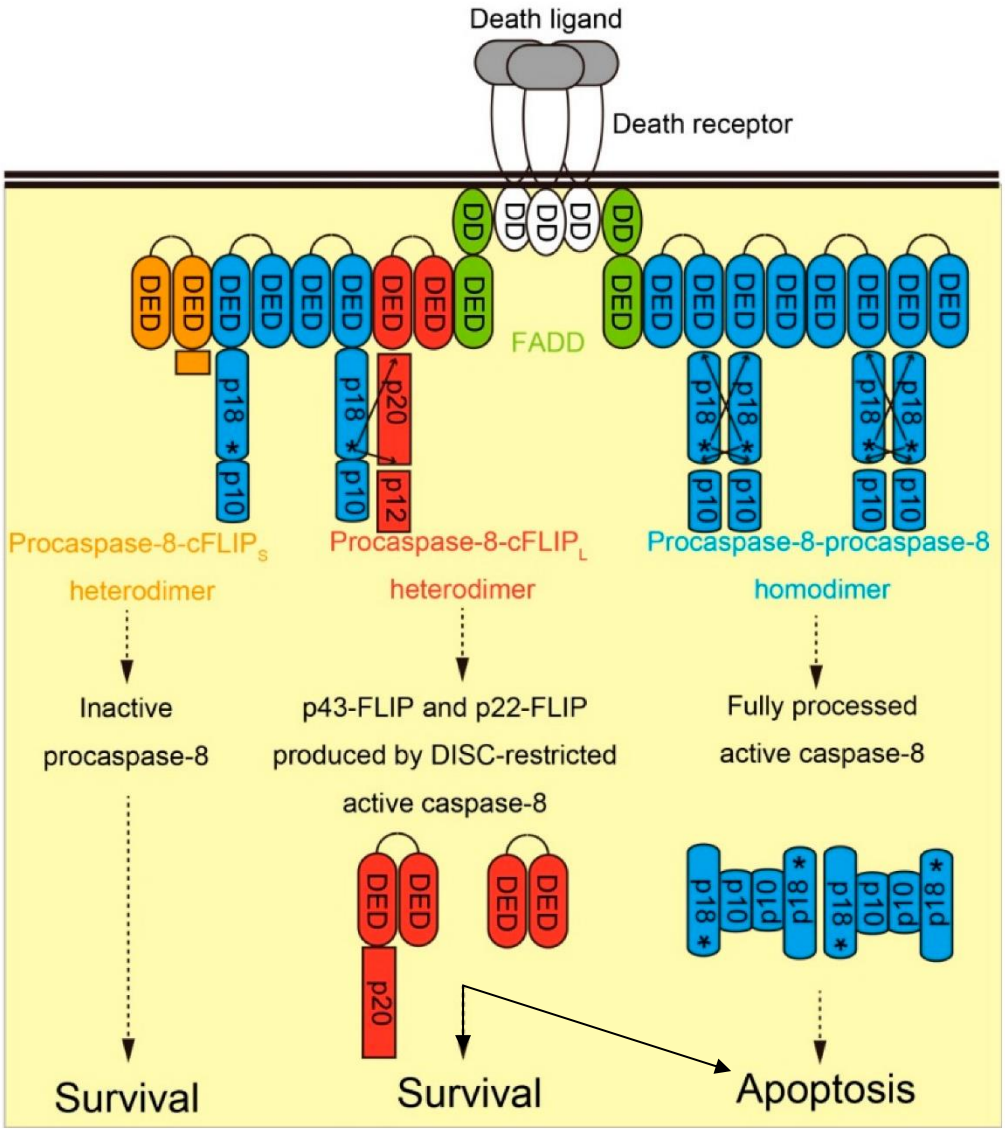

Published model of cFLIP interaction with Casp8. The model demonstrates that cFLIP-s is the only isoform to conclusively block Casp8 self-processing and activation. cFLIP-p43 leads to active caspase-8 that is spatially restrained to the cellular complex called the DISC. Restrained Casp8 can lead to survival or cell death . Adapted from Tsuchiya, Y et. al. *Int. J. Mol. Sci.* **2015**, *16*(12), 30321-30341 [1]

Chapter 2:

Atg14 protects the intestinal epithelium from TNF-triggered villus atrophy

In this chapter, I present my published findings that an intestinal epithelial specific deletion of *Atg14*, an autophagy initiation factor, results in spontaneous villous atrophy after weaning. Villous atrophy is a result of enterocyte apoptosis triggered by endogenous expression of the cytokine TNFα. Lastly, I present data suggesting robust, spontaneous villous atrophy and apoptosis is shared by other mouse loss of function autophagy models (*Rb1cc1/Fip200*) but that later steps of the autophagy pathway have a much more attenuated phenotype.

2.1 Abstract

Regulation of intestinal epithelial turnover is a key component of villus maintenance in the intestine. The balance of cell turnover can be perturbed by various extrinsic factors including the cytokine TNF, a cell signaling protein that mediates both proliferative and cytotoxic outcomes. Under conditions of infection and damage, defects in autophagy are associated with TNF-mediated cell death and tissue damage in the intestinal epithelium. However, a direct role of autophagy within the context of enterocyte cell death during homeostasis is lacking. Here, we generated mice lacking *Atg14* (autophagy related 14) within the intestinal epithelium [Atg14 $^{f/f}$ *Vil1*-Cre (*VC*)+]. These mice developed spontaneous villus loss and intestinal epithelial cell death within the small intestine. Based on marker studies, the increased cell death in these mice was due to apoptosis. *Atg14* $^{f/f}$ *VC+* intestinal epithelial cells demonstrated sensitivity to TNF-triggered apoptosis. Correspondingly, both TNF blocking antibody and genetic deletion of *Tnfrsf1a/Tnfr1* rescued villus loss and cell death phenotype in *Atg14* $^{f/f}$ *VC+* mice. Lastly, we identified a similar pattern of spontaneous villus atrophy and cell death when Rb1cc1/Fip200 was conditionally deleted from the intestinal epithelium (*Rb1cc1* $^{f/f}$ *VC+*). Overall, these findings are consistent with the hypothesis that factors that control entry into the autophagy pathway are also required during homeostasis to prevent TNF triggered death in the intestine.

2.2 Introduction

Regulation of epithelial turnover is a key mechanism underlying the protection afforded by mucosal barriers [97]. This is particularly true for the mouse small intestinal epithelium; it is a rapid turnover system based on a single, continuous layer of epithelial cells organized into repeating units of Crypts of Lieberkühn and villi. The crypts contain intestinal epithelial stem and progenitor cells that perpetually and continuously produce multiple differentiated lineages.

Most epithelial lineages (other than Paneth cells located at the crypt base) migrate out of crypts onto adjacent villi where upward migration is organized in coherent columns [4]. Epithelial turnover is completed through a process of regulated cell death (apoptosis) that is concentrated at villus tips, where apoptotic cells are extruded into the lumen [98]. However, cell death and extrusion can also occur along the length of the villi as well as in crypts [99]. In order to maintain crypt-villus architecture, the rate of apoptotic cell death that occurs along the crypt-villus axis must balance the rate of proliferation in crypts [100]. Various perturbations to this system such as infection and inflammation can increase the rate of epithelial turnover [101] and in some cases skew towards an increase in epithelial stem and progenitor cells in the crypt [102].

Intestinal epithelial cell death can be modulated by several pathways including pyroptosis [103], genotoxic and endoplasmic reticulum stress [6, 104], loss of contact with the basement membrane that induces anoikis [105] and activation of death receptors through high levels of stimulation by TNF (tumor necrosis factor) family cytokines [7]. Loss of function studies of negative regulators of TNF-induced cell death (such as *Tnfaip3*/*A20*, *Tnip1*/*Abin-1*, and *Ripk1*) show increased apoptosis and necroptosis in the intestinal epithelium [76, 77, 106]. One conclusion from these studies is that host genetic factors can regulate the intrinsic sensitivity of the intestinal epithelium to TNF-mediated death signaling.

The process of autophagy is a candidate pathway to regulate cell death in the intestinal epithelium. Conditional loss of function studies of various autophagy enzymes [notably the conjugation system enzymes ATG5 (autophagy related 5) and ATG16L1(autophagy related 16-like 1 [S. cerevisiae])] show an important role for autophagy within the intestine [107]. None of these models display a substantial alteration in epithelial cell death during homeostasis. However, a number of recent studies demonstrate that autophagy allows protection against TNF-

mediated epithelial cell death in the presence of pertinent environmental exposures: smoking, colonic damage (dextran sulfate sodium, DSS), infection (*Helicobacter* or *Toxoplasma*), or combination of infection and DSS [67-69, 108].

Despite these studies, open questions remain. First and foremost, is the process of autophagy required to protect the intestinal epithelium against cell death during homeostasis? Thus far only superimposition of infection/damage on mice with autophagy defects (namely ATG5 or ATG16L1) can increase epithelial cell death. Secondly, recent work suggests that residual autophagy can occur even in the complete absence of ATG5 or ATG16L1. In contrast, factors such as ATG14 (autophagy related 14) demonstrate a complete block in autophagic flux [27]. ATG14 and RB1CC1/FIP200 are well-characterized factors that mediate autophagy initiation through the class III phosphatidylinositol 3-kinase complex I (PIK3C3/VPS34-BECN1-PIK3R4/VPS15-ATG14) or ULK1 complex (ULK1-RB1CC1/FIP200-ATG13-ATG101), respectively [24, 109, 110] Thus, it is critical to test the role of intestinal epithelial death and turnover in the context of loss-of function of proteins critical for autophagy initiation.

To test the role of ATG14 in epithelial turnover, we generated a mouse strain with a conditional deletion of *Atg14* within the intestinal epithelium. Five-week-old mice spontaneously developed widespread small intestinal villus atrophy. CASP3/caspase-3 mediated apoptosis was the major driver of villus atrophy in these mice. *Atg14*-deficient intestinal epithelial cell lines were highly sensitive to TNF-induced apoptosis. Correspondingly, neutralization of TNF ligand and deletion of *Tnfrsf1a/Tnfr1* (TNF Receptor 1) rescued spontaneous villus atrophy in these mice. Taken together, our results suggest that ATG14 protects intestinal epithelial cells from TNF-mediated programmed cell death.

2.3 Materials and Methods

Mice.

Atg14$^{flox/flox}$ (*Atg14*^{tm1Aki}), *Rb1cc1*$^{flox/flox}$ (*Rb1cc1*$^{tm1.1Guan}$), *Atg5*$^{flox/flox}$ (*Atg5*^{tm1Myok}) mouse strains [111] were bred to *Vil1*-Cre mice [112](Jackson labs) to conditionally delete *Atg14, Fip200* and *Atg5*, respectively, from the intestinal epithelium. *tnfrsf1a*$^{-/-}$ (*Tnfrsf1a*^{tm1Imx}) mice [113] were obtained from Jackson Laboratories and crossed to *Atg14*$^{flox/flox}$ *VC*$^{+}$ to generate *Atg14*$^{flox/flox}$*tnfrsf1a*$^{-/-}$ *VC*$^{+}$ mice. All mice were maintained at the SPF animal facilities of Washington University in St. Louis and kept in enhanced autoclaved cages with autoclaved regular chow diet and water. All lines were maintained on a C57BL/6 genetic background. All experimental animals were handled according to the institutional and national American animal regulations. Animal protocols were approved by the ethics committee of Washington University.

Serum Cytokine Analysis.

Mouse blood was collected through terminal cardiac puncture in accordance with all animal protocols and regulations. Serum was isolated by centrifugation of blood at 18,000 x g and collecting the supernatant. Serum was stored at -80˚C before analysis. Serum TNF concentrations were measured using a sandwich ELISA utilizing mouse TNF-α ELISA MAX Standard kit (Biolegend, 430902).

Primary intestinal epithelial cell culture.

Small intestinal jejunal crypts were isolated and cultured from mice as previously described [114]. Briefly, stem cell media containing 50% L-WRN (WNT3A, RSPO3 and NOG) conditioned medium: was used to culture epithelial spheroids enriched for stem cells [8]. To differentiate spheroids into enterocytes, spheroids were incubated in Advanced DMEM/F-12 (Invitrogen, 12634028), with 2 mM L-glutamine, 100 units/ml penicillin, and 0.1 mg/ml streptomycin, freshly supplemented with 50 ng/ml EGF (Peprotech, 315-09), 10 µM ROCK1/ROCK2 inhibitor Y-27632 (R&D Systems, 1254) and 10 µM PTGER4 inhibitor L-

161,982 (R&D Systems, 2514).

All enterocyte differentiated spheroids were cultured in differentiation media for 24 h followed by differentiation media ± (1-100 ng/ml) of recombinant mouse TNF (Biolegend, 575206) for another 12 h for optimal cell death assay (unless indicated otherwise). Cycloheximide (50 μg/ml; Enzo, ALX-380-269-G001) along with 100 ng/ml of TNF (Biolegend, 575206) were used as positive control for cell viability assays. Additionally, 20 μg/ml Z-VAD-FMK (APExBIO, A1902), 10 μM necrostatin-1 (MedChemExpress, HY-15760), 1 μM Staurosporine (MedChemExpress, HY-15141), and 20 μM GDC-0152 (APExBIO, A4224) were used as indicated to rescue or induce cell death, respectively.

Intestinal spheroid viability assays.

Small intestinal spheroids were collected in cell recovery solution (Corning, 354253), fixed in 4% paraformaldehyde in PBS for 16 h at 4˚C, immersed in 20% sucrose solution for 16 h at 4˚C and then processed in O.C.T. compound (Fisher, 23-730-571). 5 μm sections were additionally fixed with 4% PFA prior to immunohistochemical staining. Spheroid imaging was performed using published methods [115]

Small intestinal epithelial stem cells were cultured as previously described and plated in a 96 well plate for 3 days for MTT (3-[4,5-dimethylthiazol-2-yl]-2,5-diphenyltetrazolium bromide) cell proliferation assay (American Type Culture Collection, 30-1010K). MTT reagent was added to each well in 1:10 dilution and the cells were incubated at 37˚ degree for 2 h. Next, 100 μL of MTT detergent reagent was added to each well and incubated in the dark at room temperature for 2 h. Absorbance reads were measured at 570 nm using Cytation 5. Cell proliferation was measured as fold change with values at day 3 of culture normalized to day one.

For EdU proliferation assays, small intestinal epithelial cells were cultured for 24 h then

stained for EdU for 2 h. Next, the cells were trypsinized into single cells, washed and collected for fixation and EdU labeling. The cells were fixed in 10% formalin for fifteen minutes, washed and stained with 488-Azide Fluorophore for thirty minutes in the dark. The cells were then washed and sorted through Fluorescence activated cell sorting (FACS) and analyzed for % live EdU positive cells. EdU assay was performed using Click-iT EdU Alexa Fluor 488 Imaging Kit (Invitrogen, C10639).

Small intestinal spheroids were expanded as previously described and plated in a 96 well clear bottom white-walled plate (Corning, 3610). Spheroids were differentiated to enterocytes in the presence of PTGER4 inhibitor [116] and treated for 12 h with recombinant mouse TNF or other listed compounds. Dose-dependent viability was measured in jejunal enterocyte differentiated spheroids using Cell Titer Glo 3D ATP viability reagent (Promega Life Sciences, G9682), and luminescence was detected using a Cytation 5 multi-mode plate reader (Biotek). Luminescence values were averaged by treatment group and normalized to the vehicle control group per genotype.

Immunoblot analysis.

Protein lysates were prepared from differentiated enterocytes cultured from small intestinal crypts as previously described [114]. Differentiated enterocytes were collected in cell recovery solution (Corning, 354253), centrifuged at 4˚C at 200 x g for 10 min, lysed using 200 µl of RIPA buffer (Sigma, R0278) containing protease and phosphatase inhibitor (Cell Signaling Technologies, 5872) and sonicated (QSonica). Proteins were separated by SDS-PAGE (Bio-Rad), transferred to nitrocellulose, and analyzed by immunoblotting. Microsoft Office was used to convert scanned immunoblot images to grayscale and to crop images.

Histology.

Freshly isolated small intestine and colon tissue were pinned and fixed in 10% neutral buffered

formalin (Sigma, HT501128). Tissues were then processed for paraffin embedding and hematoxylin and eosin staining using published protocols [117].

For immunohistochemistry, paraffin embedded sections were deparaffinized by incubating the sections in xylene and isopropanol for 3 washes (5 min each). The sections were then incubated in 10% hydrogen peroxide in methanol, rinsed in PBS, and boiled in Trilogy solution (Cell Marque, 920P-09) for 20 min. The sections were incubated in blocking buffer, (10 mg/ml bovine serum albumin/0.1% Triton-X 100) for 30 min and incubated with primary antibody overnight at 4˚C. After overnight primary antibody incubation, sections were rinsed in PBS, incubated with species specific biotinylated secondary antibodies (Invitrogen, 31820) and Vectastain ELITE ABC kit was used to label streptavidin-HRP (Vector Laboratories, PK-6100). Staining were then visualized by DAB (2, 2'-diaminobenzidine) peroxidase substrate (Vector laboratories, SK-4100). Olympus BX51 microscope and DP Controller software were used to obtain bright-field images.

Antibodies and reagents.

Immunohistochemistry was performed using rabbit monoclonal anti-cleaved CASP3 Asp175 (Cell Signaling Technologies, 9664), rabbit monoclonal anti-cleaved CASP8 Asp387 (Cell Signaling Technologies, 8592), mouse polyclonal anti-ACTB (Abcam, ab6276), rat monoclonal LY6G (BioLegend, 127602), and corresponding species-specific secondary antibodies.

Immunoblotting was performed using rabbit monoclonal anti-cleaved CASP3 (Cell Signaling Technology, 9664), mouse polyclonal anti-ACTB (Abcam, ab6276), rabbit monoclonal anti-cleaved CASP8 (Asp387) (D5B2) (Cell Signaling Technology, 8592). All antibodies were diluted 1:1000 in Blocking One solution (Nacalai, 03953-95) and incubated 16 h at 4˚C. Species appropriate HRP-conjugated secondary antibodies (ThermoFisher, 32260; Abcam,

ab102448) were diluted 1:15,000 in Blocking One solution (Nacalai, 03953-95) and incubated one hour at 24˚C. Clarity ECL (Bio-Rad, 1705060) and Prosignal Dura ECL (Prometheus, 20-301) was used for detection with autoradiography film.

Mouse TNF neutralization Studies.

For TNF neutralization in mice, low endotoxin rat anti mouse TNF (clone MP6-XT22) 1.0 mg/ml; (Biolegend, 506332) or rat IgG1 Isotype, κ control (Biolegend, 400432) was administered by 500 µl intraperitoneal injections twice per week during the entire experimental period. Littermates were used as controls in all experiments. Groups of mice for the experiment include male and female animals.

PCR genotyping and qPCR.

The *Atg14*$^{f/f}$ strain was genotyped by PCR of tail DNA using a forward primer, 5'-CCC ATC TCC ATT CCT GGA TTA CTG GAC-3', a reverse primer #1, 5'-ACA AGA TGC AGA ACT GAT GGC AGG-3', and a reverse primer #2, 5'-ACA GAG TTA GTT CCA GGA CAG CCA GG-3' to generate a 430 base pair PCR fragment for the wild-type allele and a 530 base pair PCR fragment for the *Atg14* floxed allele. The genotyping PCR protocol for *Atg14*$^{f/f}$ mice is as follows: 1 min at 94˚C, 30 cycles of annealing of 1 min at 94˚C, 1 min at 65˚C and 2 min at 72˚C, elongation period of 10 min at 72˚C, and final 4˚C incubation. *Vil1*-Cre mice were genotyped using a forward primer 5'- GTG TGG GAC AGA GAA CAA ACC -3' and a reverse primer 5'- ACA TCT TCA GGT TCT GCG GG -3'. *Tnfrsf1a* was genotyped by PCR using a forward primer 5'- GCT ACT TCC ATT TGT CAC GTC C -3', a reverse primer #1, 5'-ATG GGG ATA CAT CCA TCA GG -3', and a reverse primer #2, 5' GGG GAA CAT CAG AAA CAA GC -3' to generate a 362 base pair PCR fragment for the wild-type allele and a 270 base pair PCR fragment for the TNF receptor 1 allele. Vendor PCR protocol for TNF receptor was used to genotype TNF receptor 1 allele. *Tnfrsf1a* mRNA was measured through qPCR

using forward primer, 5'- GCT CTG CTG ATG GGG ATA CAT C-3', and a reverse primer, 5'-ACC TGG GAC ATT TCT TTC CGA C-3'.

Statistical analysis.

All statistical analysis were performed using GraphPad Prism software (version 7.01) by either unpaired Student's t test or 2-way ANOVA Sidak's multiple T-test or Tukey's T-test, as indicated.

2.4 Results

2.4.1 Deleting *Atg14* in mouse intestinal epithelial cells elicits spontaneous villus atrophy and failure to thrive

The major unexpected phenotype of mice with deletion of *Atg14* in the intestinal epithelium [$Atg14^{f/f}$ *Vil1*-Cre $(VC)^{+}$] [112] as compared to littermate controls (includes $Atg14^{f/f}$ VC^{-} and $Atg14^{f/+}$ VC^{+}) was divergent body weights during post-weaning development. This phenotype was not anticipated as similar conditional deletions of autophagy pathway genes in the intestinal epithelium such as *Atg5*, *Atg7* and *Atg16l1*, do not show this spontaneous phenotype [9, 118, 119]. Tracking of body weights over time showed that $Atg14^{f/f}$ VC^{+} mice displayed a failure to thrive during a period that spanned maturation to early adulthood (3-6 weeks of age) (**Figure 5 A-B**). During this period of time, $Atg14^{f/f}$ VC^{+} mice did not show increased mortality as compared to controls, enabling further studies to understand the underlying mechanism of this phenotype.

Failure of weight gain in $Atg14^{f/f}$ VC^{+} mice correlated with villus loss. Whole mount analysis of the intestinal mucosal surface of 5-week-old $Atg14^{f/f}$ VC^{+} mice showed a discrete area in the mid-jejunum that did not contain villi in each mouse (**3.6.1Figure 6 A**). Histological analysis confirmed that only rudimentary villi were present in this sharply demarcated area of the small intestine (**Figure 5 C-E**; **3.6.1Figure 6 B-D**). The underlying crypts in areas of villus loss showed expansion and

epithelial hyperproliferation as determined by quantification of M-phase bodies per crypt (**Figure 5 F-G**). The finding that crypt proliferation was maintained or even expanded in *Atg14$^{f/f}$ VC^{+}* mice suggests that villus loss was not secondary to loss of the regenerative potential of the intestinal crypts as previously described in mouse models with targeted deletion of cell cycle genes [120].

The jejunal villus phenotype tracked with the divergence of weight loss of *Atg14$^{f/f}$ VC^{+}* mice and controls that occurred as the mice aged. Three-week-old *Atg14$^{f/f}$ VC^{+}* mice did not show any obvious villus or crypt defects by whole mount or histological analysis and overall weights were comparable with controls at this time (**Figure 5 C-E**). Conversely, at 6 weeks of age, the affected area of villus loss in *Atg14$^{f/f}$ VC^{+}* mice showed extensive expansion both proximally and distally beyond the area of the mid-jejunum (**Figure 5 E, 3.6.1Figure 6 B-D**). Histological analysis of intestinal sections from *Atg14$^{f/f}$ VC^{+}* mice at 6 weeks of age showed a mix of hyperproliferative and hypoproliferative cystic crypts that were associated with areas of villus loss (**Figure 5 G, 3.6.1Figure 6 E**). Despite the loss of villi, we observed no significant differences in the serum levels of glucose, cholesterol and triglyceride as compared to controls (**Figure 7 A-C).** This finding may explain the survival of the *Atg14$^{f/f}$ VC^{+}* mice during this period, suggesting that the remaining villi in the proximal and distal small intestine were sufficient for adequate nutrient absorption.

Focal villus blunting was the major alteration in the intestine of *Atg14$^{f/f}$ VC^{+}* mice. This phenotype was not associated with complete breakdown of the epithelial barrier, as we detected no ulcerations in the intestinal mucosa. In addition, despite the loss of villi in *Atg14$^{f/f}$VC^{+}* mice, we found only a small increase in lamina propria neutrophils in areas of villus loss; the highest value in any sample was one neutrophil per 100 crypts. As a reference, values >10 neutrophils/crypt can be detected in models with severe acute inflammation [121]. In addition, the number of neutrophils in the epithelial compartment of *Atg14$^{f/f}$ VC^{+}* mice were comparable to littermate controls (**Figure 5 H**).

These data suggest that acute inflammation was not a primary driver of villus loss.

2.4.2 Atg14$^{f/f}$ VC^{+} *mouse small intestinal epithelial cells exhibit spontaneous apoptosis*

Intestinal epithelial deletion of *Atg14* resulted in spontaneous and progressive small intestinal villus atrophy that was most prominent in the mid-jejunums of 5-week-old mice. Comparable models of villus atrophy within the small intestine include mice with an intestinal epithelial deletion of RIPK1 (*Ripk1$^{f/f}$ VC^{+}*) [76, 77]. Interestingly, villus atrophy within the *Ripk1$^{f/f}$ VC^{+}* model is accompanied by increased epithelial cell death in the intestinal epithelium [76, 77]. Thus, we next determined if villus loss in *Atg14$^{f/f}$ VC^{+}* mice correlated with epithelial cell death.

Analysis of the crypt epithelial cells from hematoxylin and eosin (H&E) stained intestinal sections of *Atg14$^{f/f}$ VC^{+}* mice and controls showed elevated numbers of apoptotic bodies (as defined by nuclei undergoing karyorrhexis) in *Atg14$^{f/f}$ VC^{+}* mice that were 5 and 6 weeks of age (**3.6.1Figure 8 A**). These findings represent a substantial amount of spontaneous cell death within the intestinal epithelium of *Atg14$^{f/f}$ VC^{+}* mice. Immunohistochemical analysis of a marker of active apoptosis, cleaved CASP3/caspase-3 (cCASP3), suggested an increase in apoptotic cell death within *Atg14$^{f/f}$ VC^{+}* epithelial cells at weeks 5 and 6 (**3.6.1Figure 8 B-D**). Increased abundance of cCASP3 was found in both crypts and villi. At week 3, prior to the development of villus or weight loss, there was a significant increase in the number of cCASP3 positive cells in crypts and a trend towards an increase in cCASP3 positive cells in villi of *Atg14$^{f/f}$ VC^{+}* mice (**3.6.1Figure 8 B-D**). This increase in apoptotic cell death correlates with the villus loss and body weight defects seen within this model.

2.4.3 TNF triggers caspase-mediated apoptosis within *Atg14$^{f/f}$ VC^{+}* intestinal epithelial cells

With the finding that *Atg14$^{f/f}$ VC^{+}* mice undergo robust and spontaneous cell death in the

intestinal epithelium, we next sought to assess the proliferation and survival of primary intestinal epithelial cells in vitro. To test this hypothesis, we isolated and cultured small intestinal stem cells from *Atg14*$^{f/f}$ *VC*$^{+}$ and control mice [8]. We first compared intestinal epithelial cell growth and survival in culture over time using MTT and EdU assays (see methods) and found no intrinsic differences in these parameters (**3.6.1Figure 9 A-B**).

Based on these results, we hypothesized that an extrinsic factor triggers cell death in *Atg14*$^{f/f}$ *VC*$^{+}$ epithelial cells in vivo. We performed a screen on *Atg14*$^{f/f}$ *VC*$^{+}$ and control epithelial cells using sub-lethal doses of various cytokines and chemicals that are expressed in the intestine (**Figure 10**). We cultured these epithelial cells under conditions that enriched for enterocytes [116] as these cells are the predominant cell type on villi which are lost in this model. We found that recombinant mouse TNF was the most potent inducer of cell death; this cytokine reduced cell viability in a dose-dependent manner in *Atg14*$^{f/f}$ *VC*$^{+}$ enterocytes relative to littermate derived controls (**3.6.1Figure 9 C**). These data suggest that TNF triggers apoptotic cell death within *Atg14*-deficient epithelial cells.

We next evaluated the effects of TNF on cleaved CASP3 (cCASP3) and cleaved CASP8/caspase-8 (cCASP8), markers of apoptosis. We found that the relative abundance of cCASP3 was increased in cryo-sections of TNF-treated *Atg14*$^{f/f}$ *VC*$^{+}$ enterocytes as compared to control enterocytes (**3.6.1Figure 9 D-E**). By immunoblot analysis, cCASP3 and cCASP8 were first detected after 4 h of TNF-treatment of *Atg14*$^{f/f}$ *VC*$^{+}$ enterocytes but not similarly treated controls (**3.6.1Figure 9 F**). We next tested the effects of a pan-caspase inhibitor Z-VAD-FMK in this system. After 12 h of TNF stimulation, cCASP3 and cCASP8 remained elevated within *Atg14*$^{f/f}$ *VC*$^{+}$ enterocytes as compared to controls. The addition of Z-VAD-FMK reduced the abundance of the active form of cCASP3 as well as the p18 active form of cCASP8 **(3.6.1Figure 9 G**). Under both these conditions, we neither detected phosphorylation of RIPK1 on S166, nor of

RIPK3 on T231/S232, markers that correlate with necroptosis, a caspase-independent form of cell death. As a positive control for this assay, these markers were detected when jejunal enterocytes were challenged with a combination of TNF, the cell death inducer GDC-0152, and the pan-caspase inhibitor Z-VAD-FMK **(Figure 11 A-B)**. Additionally, we measured the viability of *Atg14*-deficient spheroids through the Cell Titer Glo ATP assay when exposed to TNF in conjunction with Z-VAD-FMK (Z-VAD), a pan-caspase inhibitor and/or necrostatin-1 (Nec-1), a chemical inhibitor of RIP Kinase 1-mediated forms of cell death. Treatment with Z-VAD, but not Nec-1, rescued TNF-triggered death within $Atg14^{f/f}\,VC^{+}$ cells (**3.6.1Figure 9 H**). Together, these data suggest that $Atg14^{f/f}\,VC^{+}$-deficient cells are specifically and potently sensitive to a caspase-dependent form of cell death triggered by the cytokine TNF.

2.4.4 *TNF blockade prevents intestinal pathology in* $\mathbf{Atg14^{f/f}\,VC^{+}}$ *mice*

The differential response to TNF treatment of *Atg14*-deficient enterocytes versus controls supports the hypothesis that ATG14 inhibits sensitivity to TNF mediated cell death. To connect these in vitro findings to the in vivo mouse model, we measured serum TNF levels in $Atg14^{f/f}\,VC^{+}$ mice and controls. At 3 weeks of age, a time point that precedes villus loss but still showed evidence of increased apoptosis, TNF serum levels were at or below levels of detection on both groups of mice; by 5 and 6 weeks of age, $Atg14^{f/f}\,VC^{+}$ mice showed only a modest increase in TNF levels that ranged from 3-10 pg/ml (**0A**). Interestingly, TNF levels did not show a further increase at week 6 (as compared to week 5 values), a time when the area of villus loss was substantially increased. For comparison, mouse models with severe spontaneous intestinal inflammation (e.g. mice with deletion of *Il10rb/Il10r2* (interleukin 10 receptor, beta) and T cell specific mutation of *Tgfbr2* (transforming growth factor, beta receptor II), have serum levels of TNF that reach 400 pg/ml [121]. Thus, we propose that the primary effect of ATG14 loss of function in intestinal epithelium is increased

sensitivity to TNF mediated cell death.

To functionally test the role of TNF in vivo, we administered TNF blocking and isotype control antibodies [122] to groups of mice twice a week from 3 to 5 weeks of age (**Figure 13 A)**. *Atg14$^{f/f}$ VC^{+}* mice injected with TNF blocking antibodies exhibited similar weight gain as their littermate controls, while *Atg14$^{f/f}$ VC^{+}* mice treated with isotype control showed failure to thrive (**3.6.1Figure 12 B**). In addition, histological sections of small intestines of *Atg14$^{f/f}$ VC^{+}* mice treated with anti-TNF showed complete rescue of intestinal pathology as these intestines were devoid of villus loss and crypt atrophy as well as disruption of intestinal architecture (0**C**). Furthermore, *Atg14$^{f/f}$ VC^{+}* mice treated with anti-TNF had similar numbers of apoptotic bodies and cCASP3 positive cells as their littermate controls (**3.6.1Figure 12 D-E; Figure 13 B**). Conversely, *Atg14$^{f/f}$ VC^{+}* mice injected with isotype control showed severe intestinal pathology and increased cCASP3 staining (**3.6.1Figure 12 D-E; Figure 13 B**). Accordingly, *Atg14$^{f/f}$ VC^{+}* mice treated with anti-TNF showed significant restoration in crypt and villus height as well as M-phase cells, to that of controls; *Atg14$^{f/f}$ VC^{+}* animals treated with isotype control demonstrated crypt hyperplasia, villus loss, and elevated numbers of M-phase bodies (**Figure 13 C-E**). Taken together, systemic TNF neutralization shows that this cytokine is necessary to alter the pathology of *Atg14$^{f/f}$ VC^{+}* mice.

2.4.5 Atg14$^{f/f}$ VC^{+} tnfrsf1a$^{-/-}$ *mice do not show villus loss and epithelial apoptosis*

We next used a genetic model to test the role of the TNF receptor in driving the pathology of *Atg14$^{f/f}$ VC^{+}* mice. Under basal conditions, TNF signals through two distinct receptor signaling complexes, TNFRSF1A/TNFR1 and TNFRSF1B/TNFR2, to activate NF-κB -mediated transcription and promote proliferation and inflammation [123]. However, functional [124] and molecular [125] studies have solely implicated TNFRSF1A for apoptosis. Therefore, we generated *Atg14$^{f/f}$ VC^{+} tnfrsf1a$^{-/-}$* double knockout mice to confirm the requirement of TNF signaling through TNFRSF1A

for the development of the *Atg14$^{f/f}$ VC^{+}* phenotype.

We found that *Atg14$^{f/f}$ VC^{+} tnfrsf1a$^{-/-}$* showed divergent weight gain as compared to *Atg14$^{f/f}$ VC^{+} Tnfrsf1a$^{+/-}$* littermates **(Figure 14 A)**. Furthermore, when analyzing the histology sections of 5-week-old *Atg14$^{f/f}$ VC^{+} tnfrsf1a$^{-/-}$* small intestines, villus and crypt height was unremarkable (**Figure 14 B, Figure 15 A-B**). While *Atg14$^{f/f}$ VC^{+} Tnfrsf1a$^{+/-}$* mice showed loss of villi, *Atg14$^{f/f}$ VC^{+} tnfrsf1a$^{-/-}$* showed complete protection from villus loss and crypt hyperplasia (**Figure 14 B**). Furthermore, quantitative analysis of histology, proliferation and cell death showed that *Atg14$^{f/f}$ VC^{+} tnfrsf1a$^{-/-}$* were comparable to *Atg14* sufficient controls while *Atg14$^{f/f}$ VC^{+} Tnfrsf1a$^{+/-}$* showed increased cell death in crypts and increased epithelial proliferation (**Figure 14 C-E, Figure 15 C**). Levels of TNF in the serum were also reduced in all *Atg14$^{f/f}$ VC^{+} tnfrsf1a$^{-/-}$* mice below 5 pg/ml (**Figure 14 F**). Furthermore, *Atg14$^{f/f}$ VC^{+} tnfrsf1a$^{-/-}$* enterocytes treated with TNF showed no alterations in survival consistent with an epithelial cell specific role for TNFRSF1A (**Figure 15 D**). As a control, we confirmed that the transcript abundance of *Tnfrsf1a* was similar in *Atg14$^{f/f}$ VC^{+}* and *Atg14$^{f/f}$ VC^{-}* intestinal epithelial cells (**Figure 16**). Collectively, these results indicate *Atg14$^{f/f}$ VC^{+}* intestinal pathology is dependent on TNFRSF1A signaling and reveal a novel role of *Atg14* in protection of TNF-induced apoptosis.

2.4.6 Rb1cc1$^{f/f}$ VC^{+} *mice show spontaneous villus atrophy and epithelial apoptosis similar to* Atg14$^{f/f}$ VC^{+} *mice*

Our hypothesis is that ATG14 prevents intestinal epithelial apoptosis due to its role in autophagy initiation. To test this hypothesis, we evaluated the effects of loss of function for RB1CC1 in the intestinal epithelium; RB1CC1 functions in a separate, more proximal step of autophagy initiation as part of the ULK1 complex [110]. The small intestines of mice with an intestinal epithelial specific deletion of *Rb1cc1*/*Fip200* (*Rb1cc1$^{f/f}$ VC^{+}*) demonstrated a pattern of villus loss in

the mid-jejunum beginning at 5 weeks of age similar to the phenotype of *Atg14*$^{f/f}$ *VC*$^{+}$ mice (**3.6.1Figure 17 A-C**). The villus loss and crypt hypertrophy was accompanied by increased apoptosis and crypt cell proliferation (**3.6.1Figure 17 D-G**). Primary small intestinal spheroids isolated from *Rb1cc1*$^{f/f}$ *VC*$^{+}$ mice and differentiated to the enterocyte lineage demonstrated a dose-dependent decrease in viability when challenged by recombinant mouse TNF for 12 hours (**3.6.1Figure 17 H**). Taken together, loss of function of RB1CC1 in the intestinal epithelium led to similar effects as loss of function of ATG14, both in vivo and in isolated intestinal epithelial cells.

In contrast, small intestinal sections from *Atg5*$^{f/f}$ *VC*$^{+}$ mice demonstrated no significant alternations in either villus or crypt height relative to littermate control animals (**Figure 18 A-B).** ATG5 functions at a distinct step of the autophagy pathway. It is not involved in the entry steps of the pathway and there are no spontaneous defects in villus homeostasis, nor cell death [126]. Meanwhile ATG14 and RB1CC1 share a common function as part of two distinct complexes to regulate entry into the autophagy pathway [127]. These data suggest that *Atg14* and *Rb1cc1* loss of function models share a common defect that sensitize the small intestinal cell to TNF-triggered apoptosis.

2.5 Discussion

This work establishes an essential role for *Atg14* within the intestinal epithelium as its conditional loss of function in these cells leads to spontaneous and rapidly progressive villus atrophy. Furthermore, we found that the villus atrophy is a consequence of increased intestinal epithelial cell death that is mediated by TNF–triggered apoptosis. As the loss of function of *Rb1cc1* in the intestinal epithelium also results in a similar phenotype, we propose that initiation of autophagy is required to regulate intestinal epithelial cell turnover and homeostasis.

Our findings expand upon the known roles of autophagy within the intestinal epithelium. Polymorphisms in *Atg16l1* are associated with Crohn disease and result in defective morphology of secretory cells in the intestinal epithelium [9]. Mouse loss of function studies of *Atg5*, *Atg7* and *Atg16l1* in the intestinal epithelium identify that the autophagy pathway is required for the secretory function of Paneth and goblet cells [111, 118]. Increased cell death of the absorptive enterocyte lineage is not noted in these experiments; however increased cell death in Paneth cells occurs when *Atg16l1* hypomorphic mice are crossed to *Xbp1* (x-box binding protein 1) knockout mice due to an enhanced unfolded protein response [104, 128].

Mice that are deficient or mutant for autophagy proteins at ATG5 and ATG16L1 in the intestinal epithelium show enhanced intestinal epithelial cell death when challenged by intestinal infection (*Toxoplasma Gondii*, *Helicobacter hepaticus*, mouse Norovirus) or cell damage (DSS, GVHD, smoking) [67, 68, 129]. This is in contrast to the effects of loss of function of the autophagy initiation factors RB1CC1 and ATG14 that we have demonstrated to have spontaneous, more severe intestinal pathology. It is interesting that for all of these models, the cytokine TNF was central to the development of pathology.

TNF signaling is well known to mediate two specific outcomes: survival through the stimulation of NF-κB stimulated genes and death through CASP3 and CASP8 mediated apoptosis or alternative forms of programmed cell death [125, 130, 131]. Matsuzawa-Ishimoto, et al show that $Atg16l1^{f/f}$ VC^{+} organoids demonstrate programmed cell death upon long-term TNF treatment, modeling the susceptibility of $Atg16l1^{f/f}$ VC^{+} to TNF-triggered intestinal epithelial death secondary to a combination of intestinal viral infection and damage (i.e. murine norovirus and DSS). Within the context of our model of *Atg14* intestinal deficiency, we demonstrated an increase in CASP3 mediated apoptosis. Furthermore, we demonstrated that within 8 hours, there is a potent activation of

the CASP8, CASP3 axis that is not observed in littermate control cells. Cell death is rescued though the addition of the caspase-inhibitor Z-VAD in vitro, validating the role of caspases in mediating loss of cell viability. This work provides a robust spontaneous model to study the interaction between the intestinal autophagy pathway and the TNF-triggered apoptotic pathways that govern cellular turnover.

In other cell lineages, defects in factors that mediate the initial steps of the autophagy pathway have been linked to the TNF triggered apoptotic cascade. *Atg13*-deficient mice undergo spontaneous apoptotic cell death within the heart and the liver [40]. Mouse embryonic fibroblasts (MEFs) derived from *Atg13*$^{-/-}$ and *Rb1cc1*$^{-/-}$ animals are sensitive to apoptotic cell death when challenged with TNF [129]. Furthermore, *Becn1* deletion within a subset of neurons results in defective autophagy and increased apoptosis [132]. These reports all highlight phenotypes where defects in the initiation steps of the autophagy pathway, not terminal steps of conjugation or egress, lead to cellular lethality.

Numerous reports highlight a functional distinction among factors that regulate initiation into the autophagy pathway as compared to termination factors regulating LC3 conjugation (ATG5, ATG16L1, and ATG7) or lysosomal fusion [27, 133-135]. In particular, the LC3 conjugation complex, ATG5, ATG16L1, and ATG7, is required to suppress pathogenicity of the parasite Toxoplasma gondii, while ATG14 and other components of the initiation and fusion steps of autophagy are not required for this function [133, 135]. Furthermore, recent reports demonstrate that cells deficient in components of the autophagy conjugation complex, such as ATG5, remain able to undergo a basal level of autophagic flux, while loss of ATG14 completely blocks autophagic fusion with lysosomes to degrade cargo [27]. Therefore, we propose a model in the intestinal epithelium in which initiation factors such as ATG14 and RB1CC1 have unique and critical roles to protect against

TNF-induced apoptosis. However, the molecular mechanism that distinguishes the function of initiation and conjugation/termination complexes still needs to be resolved.

This work lays a foundation for future studies of the interaction between autophagy and TNF signaling in the intestinal epithelium. We propose that the intestine is an amenable system to study this question. There are predictable spatial and temporal effects in the small intestine for loss of autophagy (i.e. phenotype begins in the mid small intestine and spread proximally and distally). The relative sensitivity of intestinal epithelial cells in different regions of the intestine suggests that there may be additional as of yet unknown factors involved in the spatial control of sensitivity to TNF mediated cell death. Future work is also needed to assess in human the extent to which polymorphisms in autophagy mediators also sensitize the intestine and other organs to TNF mediated cell death.

2.6 Figures

Figure 5 Deletion of *Atg14* in the mouse intestinal epithelium leads to spontaneous villus loss

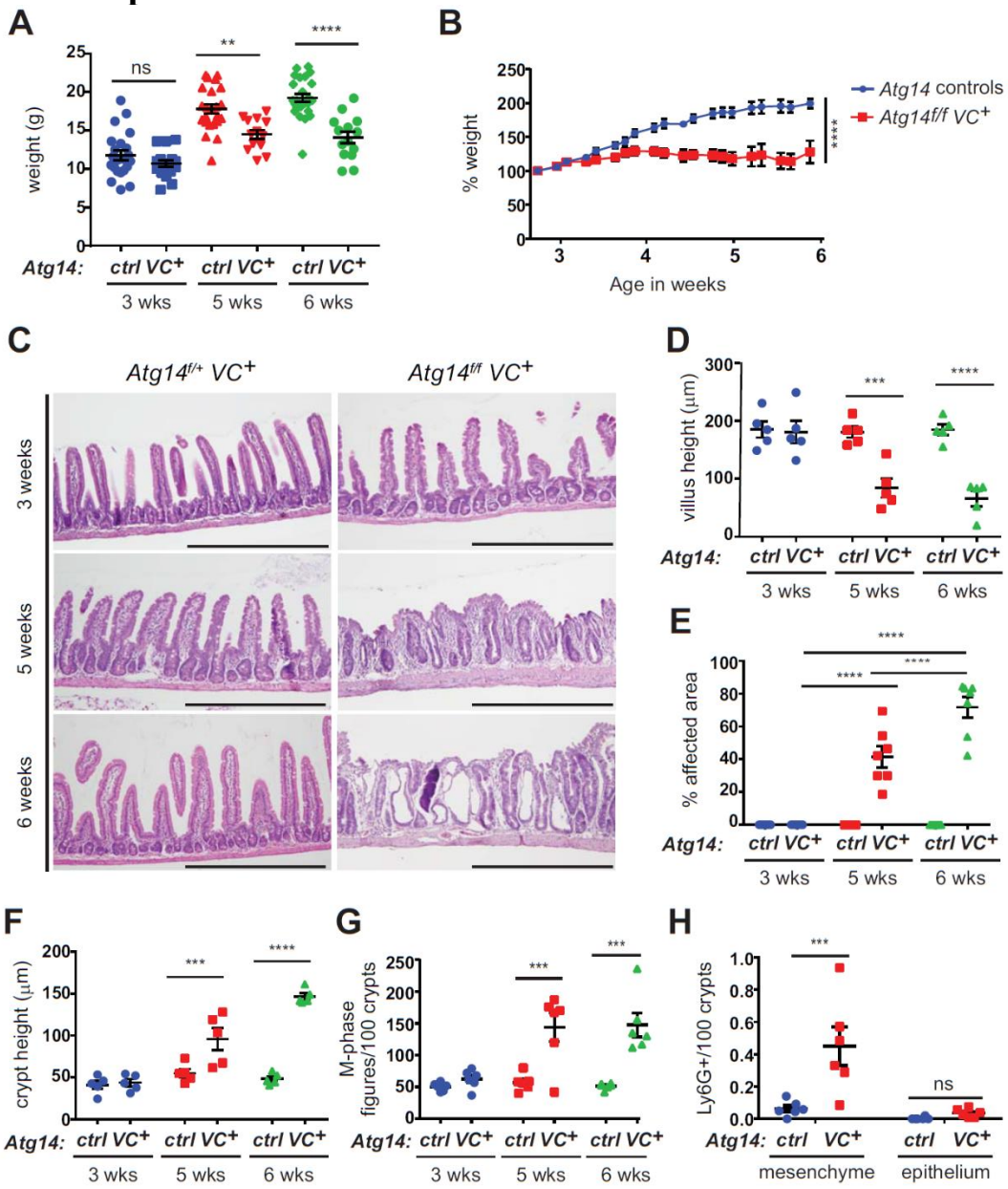

(A) Measured weights of *Atg14*$^{f/f}$ *Vil1*-Cre (*VC*)$^{+}$ and littermate control mice (*Atg14*$^{f/f}$ *VC*$^{-}$ and *Atg14*$^{f/+}$ *VC*$^{+}$) grouped by indicated age at time of sacrifice; n=13-24 mice/group, >4 litters/group, two-way ANOVA with Sidak's multiple comparisons test. (B) Percent weight gain ± SEM of *Atg14*$^{f/f}$ *VC*$^{+}$ and littermate control mice; repeated measures two-way ANOVA. (C-H) Histological analysis of H&E and immuno-stained small intestine sections of *Atg14*$^{f/f}$ *VC*$^{+}$ and littermate controls from 3, 5, and 6-week-old mice; n=5-7 mice/group, ≥

100 crypt-villus units quantified/mouse; two-way ANOVA with Sidak's multiple comparisons test. (C) Representative H&E staining of jejunal sections demonstrating villus loss starting at 5 weeks of age and cystic crypts at 6 weeks of age within *Atg14*$^{f/f}$ *VC*$^{+}$ mice; bars: 500 μm. (D) Mean villus height ± SEM. (E) Percent intestinal length affected ± SEM. (F) Mean crypt height ± SEM. (G) Mean M-phase figures per 100 crypts ± SEM. (H) Mean lamina propria neutrophils ± SEM identified by LY6G immunohistochemical staining from 5- and 6-week-old mice; n=6 mice/group from n=2 independent experiments. **P<0.01, ***P<0.001, ****P<0.0001, ns: not significant.

Figure 6 Spontaneous epithelial cell death with loss of crypt and villi in *Atg14* deficient mice

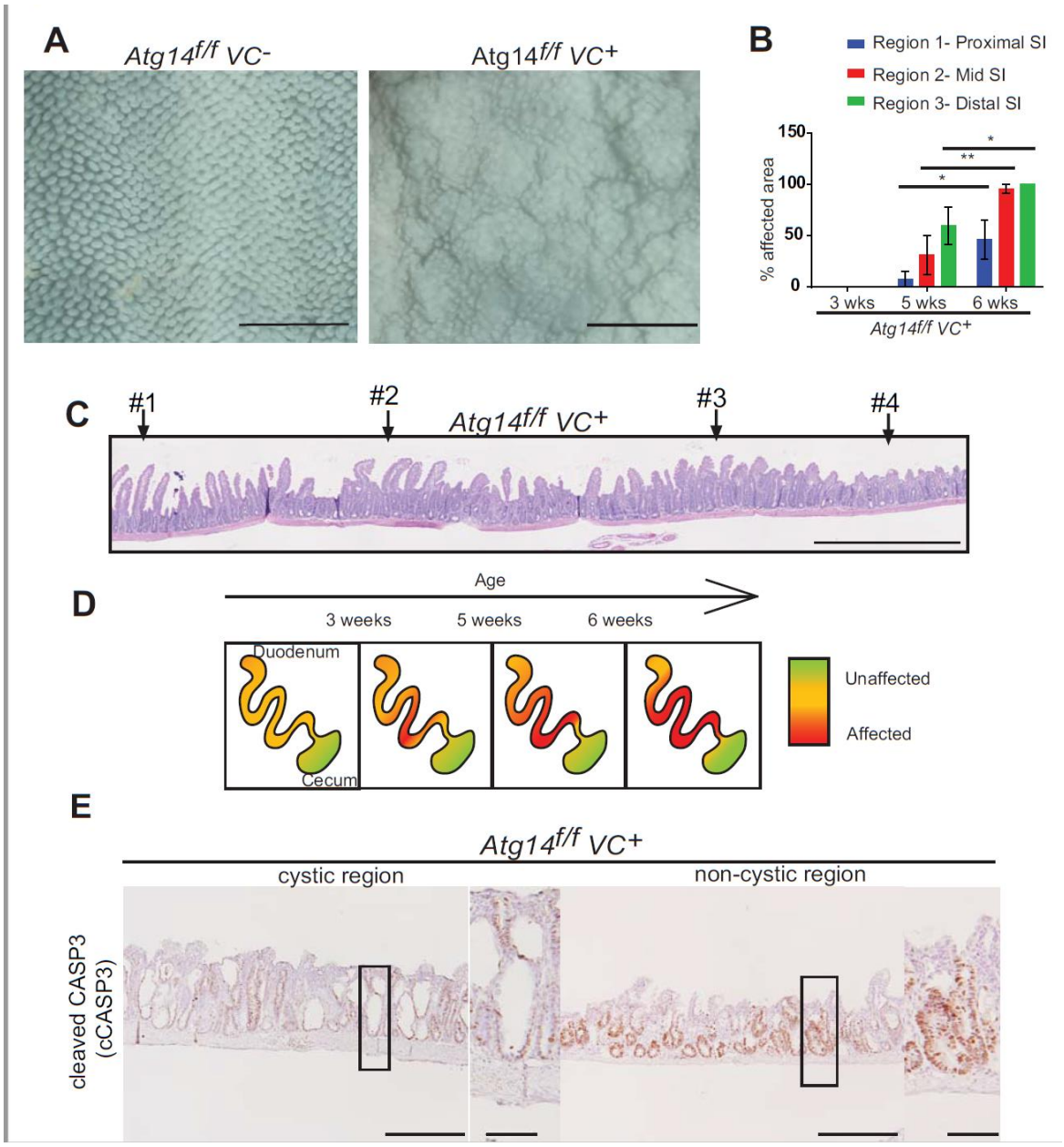

(**A**) Representative whole mount image of *Atg14*$^{f/f}$ *VC*$^{+}$ and *Atg14*$^{f/+}$ *VC*$^{-}$ mouse intestine at 5 weeks of age, bar: 100 mm. (**B**) Percent affected area ± SEM of 3-, 5- and 6-week-old *Atg14*$^{f/f}$ *VC*$^{+}$ mouse small intestine measured from H&E images in three different regions: proximal, middle and distal small intestine. Two-way ANOVA with Tukey's multiple comparisons test. (**C**) Representative H&E stitched images of *Atg14*$^{f/f}$ *VC*$^{+}$ mouse jejunal sections at 5 weeks of age to demonstrate the demarcated transition between affected and

unaffected small intestinal regions, bar: 1 mm. Image indicates 4 distinct areas: #1-Normal villi, #2-Crypt hypertrophy, #3-Villus blunting, #4-Villus loss. (**D**) Schematic of affected area of *Atg14$^{f/f}$ VC^{+}* mice over time across different regions of small intestine; n=3 mice per group. (**E**) Jejunal sections of *Atg14$^{f/f}$ VC^{+}* mouse cystic regions (left) as compared to non-cystic (right) regions with cCASP3 immunohistochemistry stain; bar: 200 μm. Insets show higher power images of crypts; bar: 50 μm. All statistically significant pairwise comparisons are displayed *p<0.05, **p<0.005.

Figure 7 Serum analysis show no serum metabolite differences in *Atg14$^{f/f}$ VC^{+}* mice versus controls

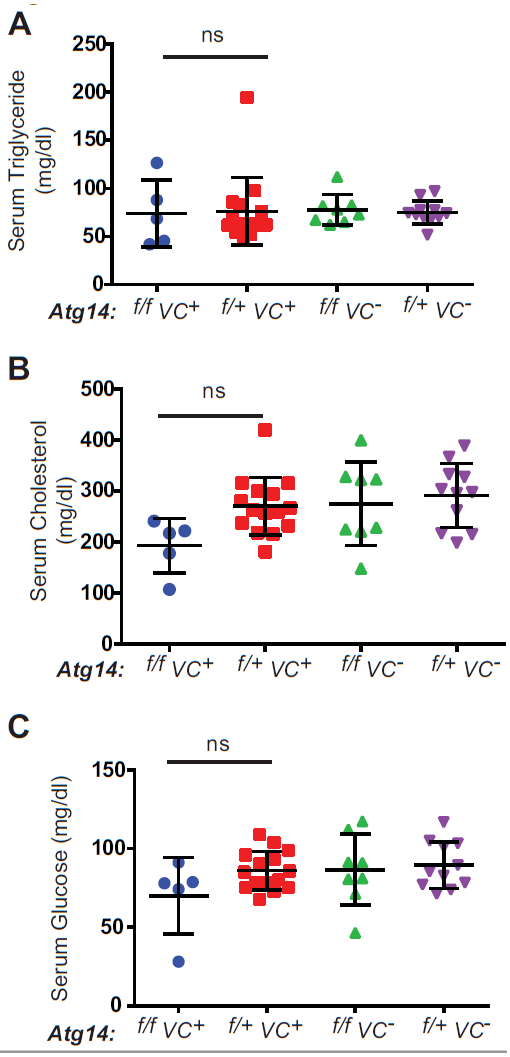

(**A**) Mean serum triglycerides, (**B**) cholesterol and (**C**) glucose levels ± SEM at 5 to 6 weeks of age of indicated genotypes; n=5-12 mice per genotype. One-way ANOVA with Tukey's multiple comparisons test.

Figure 8 Deletion of *Atg14* within the mouse intestinal epithelium results in increased programmed cell death within crypts and villi

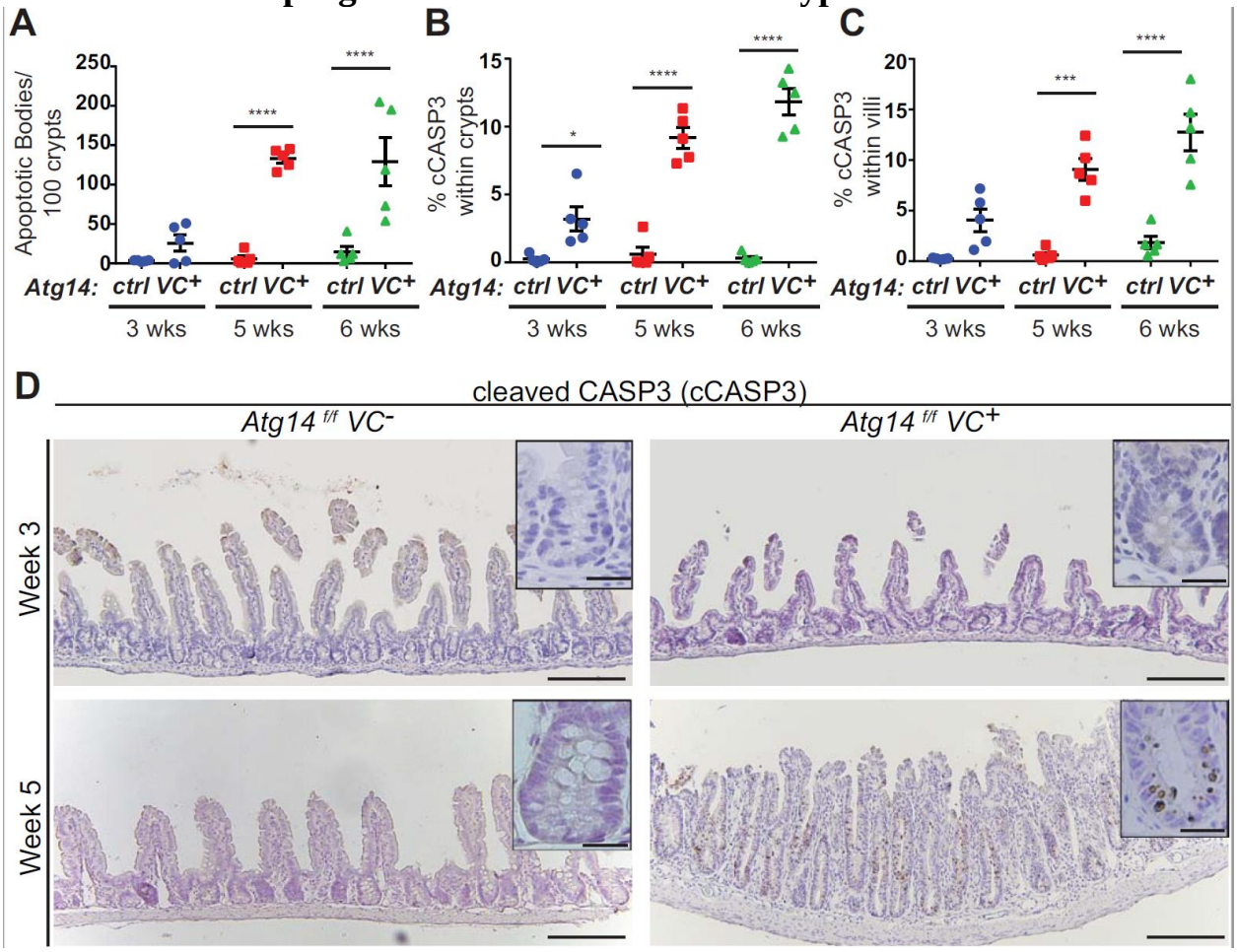

(**A-D**) Histological analysis of H&E and immune-stained small intestine sections from *Atg14*$^{f/f}$ *VC*$^{+}$ and littermate control mice at 3, 5, and 6 weeks of age; n=5 mice/group, >100 crypt-villus units/mouse; two-way ANOVA with Sidak's multiple comparisons test (variable=genotype). (**A**) Mean apoptotic bodies ± SEM. (**B-C**) Percent cleaved CASP3 (cCASP3) positive cells (**B**) within crypts ± SEM, and (**C**) within villi ± SEM. (**D**) Representative immunohistochemical staining for cleaved CASP3 (cCASP3) from 3- and 5-week-old *Atg14*$^{f/f}$ *VC*$^{+}$ and control mice; bars: 100 μm. Insets show one crypt unit at higher power; bars: 25 μm. All statistically significant pairwise comparisons are displayed *P<0.05, ***P<0.001, ****P<0.0001.

Figure 9 *Atg14*-deficient intestinal epithelial cells are sensitized to TNF-induced apoptosis

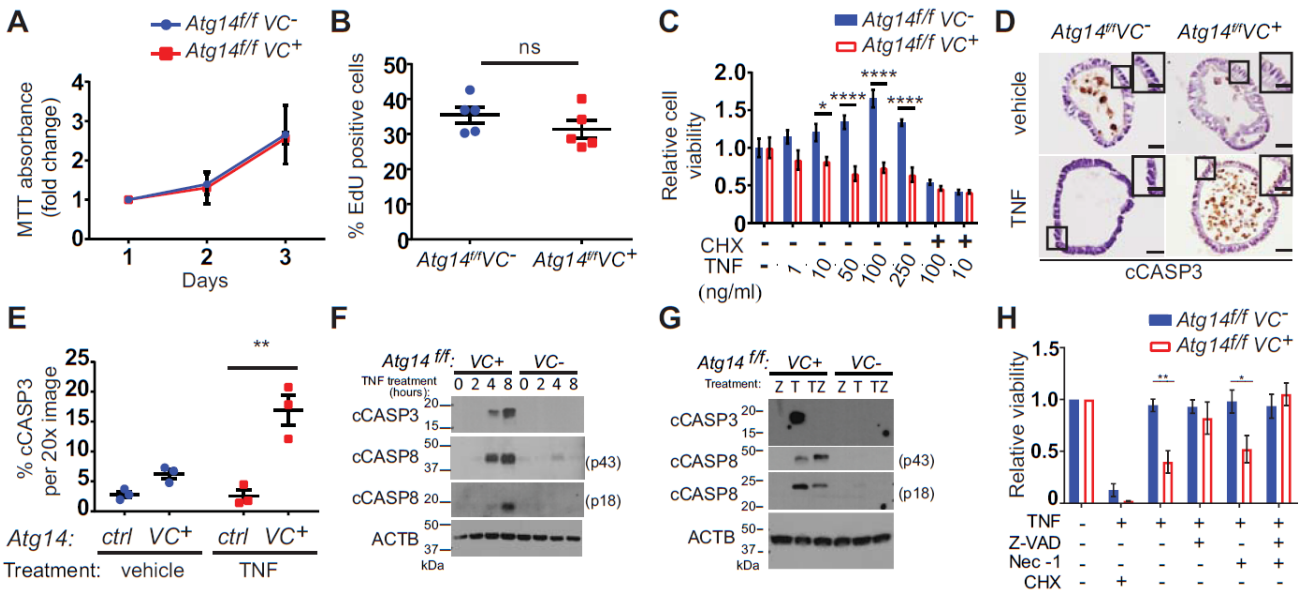

(**A-H**) Mouse jejunal spheroids from *Atg14*$^{f/f}$ *VC*$^{+}$ and *Atg14*$^{f/f}$ *VC*$^{-}$ control mice maintained as stem cells (**A and B**) or differentiated to enterocytes (**C-H**) n=3-6 independent experiments. (**A**) Cellular metabolic activity ± SEM determined by MTT assay on day 1, 2 and 3 after passage (normalized by genotype to day 1); Repeated measures two-way ANOVA with Sidak's post-test. (**B**) Cellular proliferation ± SEM determined by EdU assay on day 2; Unpaired Student's t-test. (**C**) Relative ATP cell viability ± SEM in cells treated for 12 hours with indicated dose of mouse TNF; luminescence normalized to untreated cells. Unpaired Student's t-test. (**D**) Representative immunohistochemical stained section and (**E**) quantitation of cCASP3 positive cells within the wall of spheroids treated with TNF or vehicle; n=8-10 spheroids/sample; bars: 20 μm. Insets show higher power image of cells; bars: 5 μm. (**F**) Representative immunoblot for cleaved CASP3 (cCASP3), cleaved CASP8 (cCASP8), and ACTB/β-ACTIN in cells treated with 10 ng/ml mouse TNF for indicated duration. (**G**) Representative immunoblot for cCASP3 and cCASP8 in cells treated with 10 ng/ml mouse TNF and/or 20 μg/ml Z-VAD-FMK for 12 h; Z=Z-VAD-FMK, T= TNF, TZ= TNF + Z-VAD-FMK. (**H**) Relative ATP cell viability ± SEM after 12 h treatment 1 ng/ml mouse TNF, 20 μg/ml Z-VAD-FMK, 10 μM nec-1, and/or 50 μg/ml CHX; two-way ANOVA, Sidak post-test. *P<0.05, **P<0.01, ****P<0.0001.

Figure 10 *Atg14$^{f/f}$ VC^{+}* jejunal enterocytes are specifically sensitive to death upon TNF stimulation in vitro

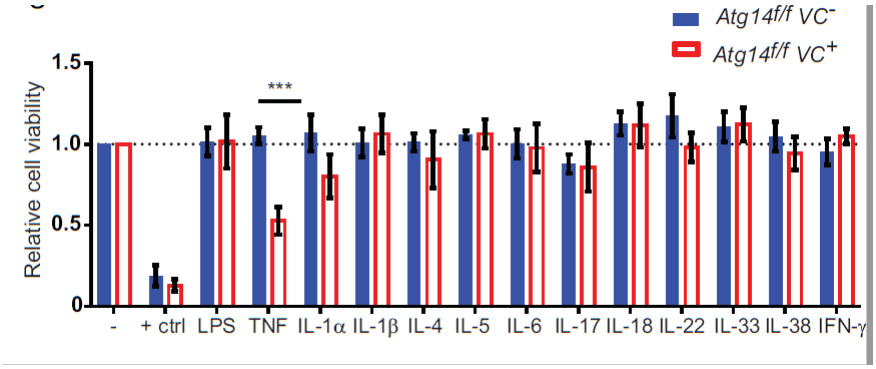

Relative cell viability determined by Cell Titer Glo ATP viability assay on primary intestinal enterocytes treated with 100 ng/ml of indicated cytokine for 12 hours; luminescence is normalized to vehicle treated cells. +Ctrl: TNF+CHX (cycloheximide) to induce lethality. ***p<0.001.

Figure 11 *Atg14$^{f/f}$ VC^{+}* jejunal enterocytes do not express markers of necroptotic cell death upon exposure to TNF and Z-VAD-FMK

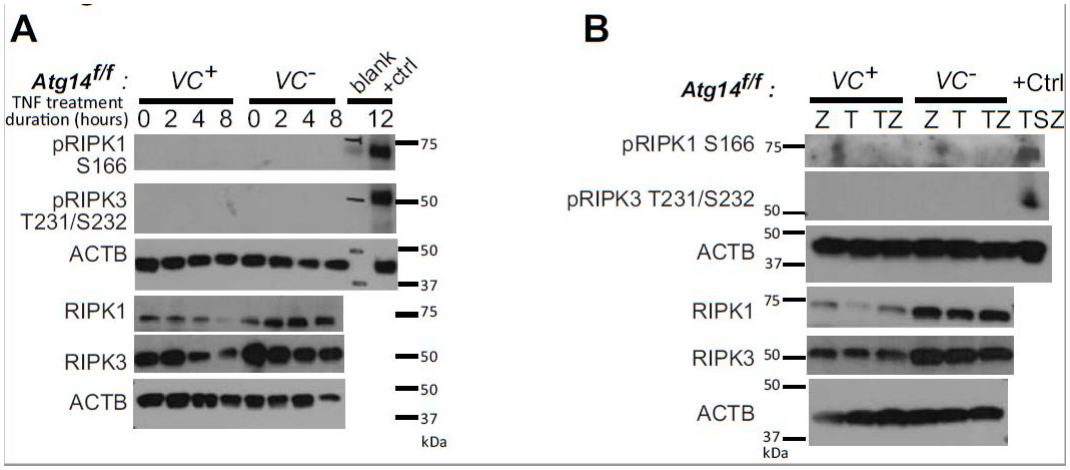

(**A and B**) Representative immunoblots for RIPK1, Phospho-RIPK1 S166, RIPK3, Phospho-RIPK3 T231/S232, and ACTB/β-Actin in cells treated with (**A**) 10 ng/ml mouse TNF for indicated duration or (**B**) 10 ng/ml mouse TNF and/or 20 µg/ml Z-VAD-FMK for 12 hours. Blank lane in (**A**) represents a lane containing a molecular weight marker for size determination. Z=Z-VAD-FMK, T=TNF, TZ=TNF + Z-VAD-FMK. +Ctrl lane (TSZ) represents control enterocyte-differentiated jejunal cells treated for 12 hours with 100 ng/ml TNF, 20 µM GDC-0152, and 20 µg/ml Z-VAD-FMK. n=3-4 experiments.

Figure 12 TNF neutralization rescues the *Atg14*-deficient mouse intestinal epithelium from intestinal pathology

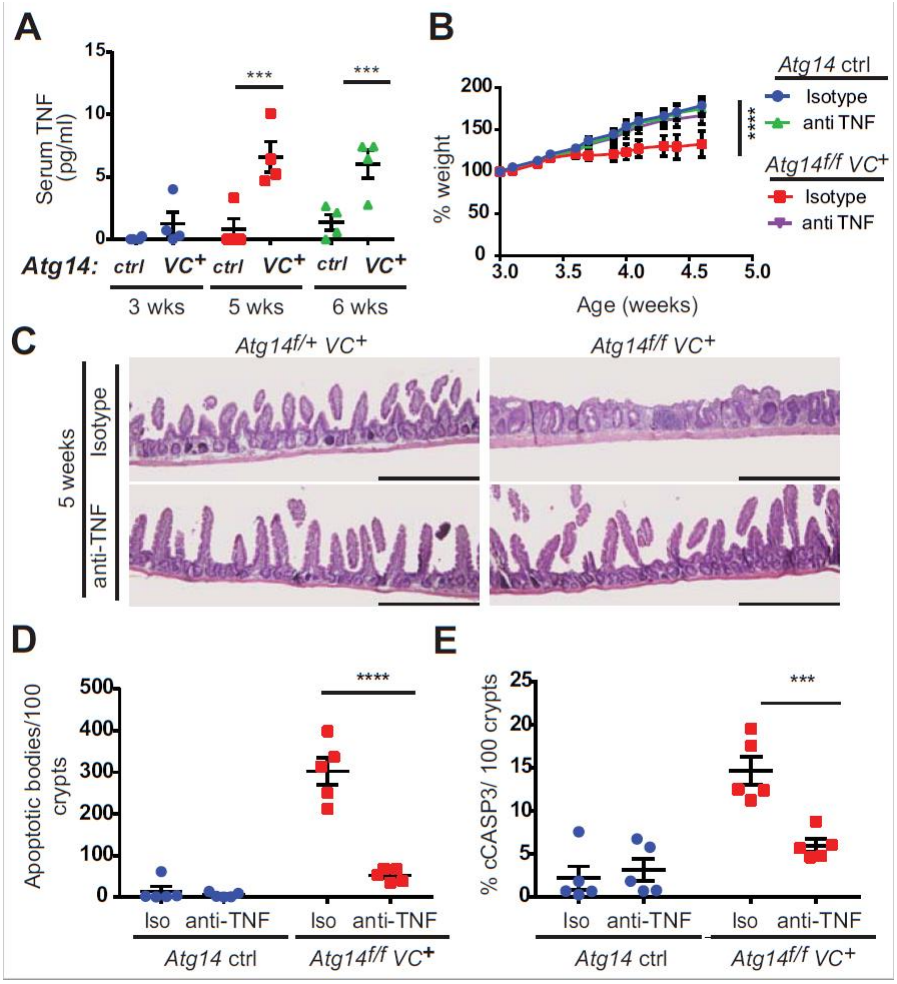

(**A**) Serum TNF levels ± SEM of *Atg14*$^{f/f}$ *VC*$^{+}$ and control mice at 3, 5, and 6 weeks; n=4 mice/group; Two-way ANOVA with Sidak's multiple comparisons test. (**B-F**) *Atg14*$^{f/f}$ *VC*$^{+}$ and control mice administered intraperitoneal TNF blocking or IgG isotype control antibody; n>5 mice/group from n=2 independent experiments. (**B**) Percent weight gain from 3 to 4.5 weeks of age; repeated measures three-way ANOVA. (**C**) Representative H&E-stained jejunal sections from 5-week-old littermates; bars: 500 μm. (**D and E**) >100 crypt-villus units analyzed/mouse; two-way ANOVA with Sidak's multiple comparisons test (variable=genotype). (**D**) Mean apoptotic bodies ± SEM within crypts. (**E**) Percent cCASP3 positive cells ± SEM. All statistically significant pairwise comparisons are displayed; ***P<0.001, ****P<0.0001.

Figure 13 Anti-TNF protects *Atg14* deficient intestinal epithelium from intestinal pathology in vivo

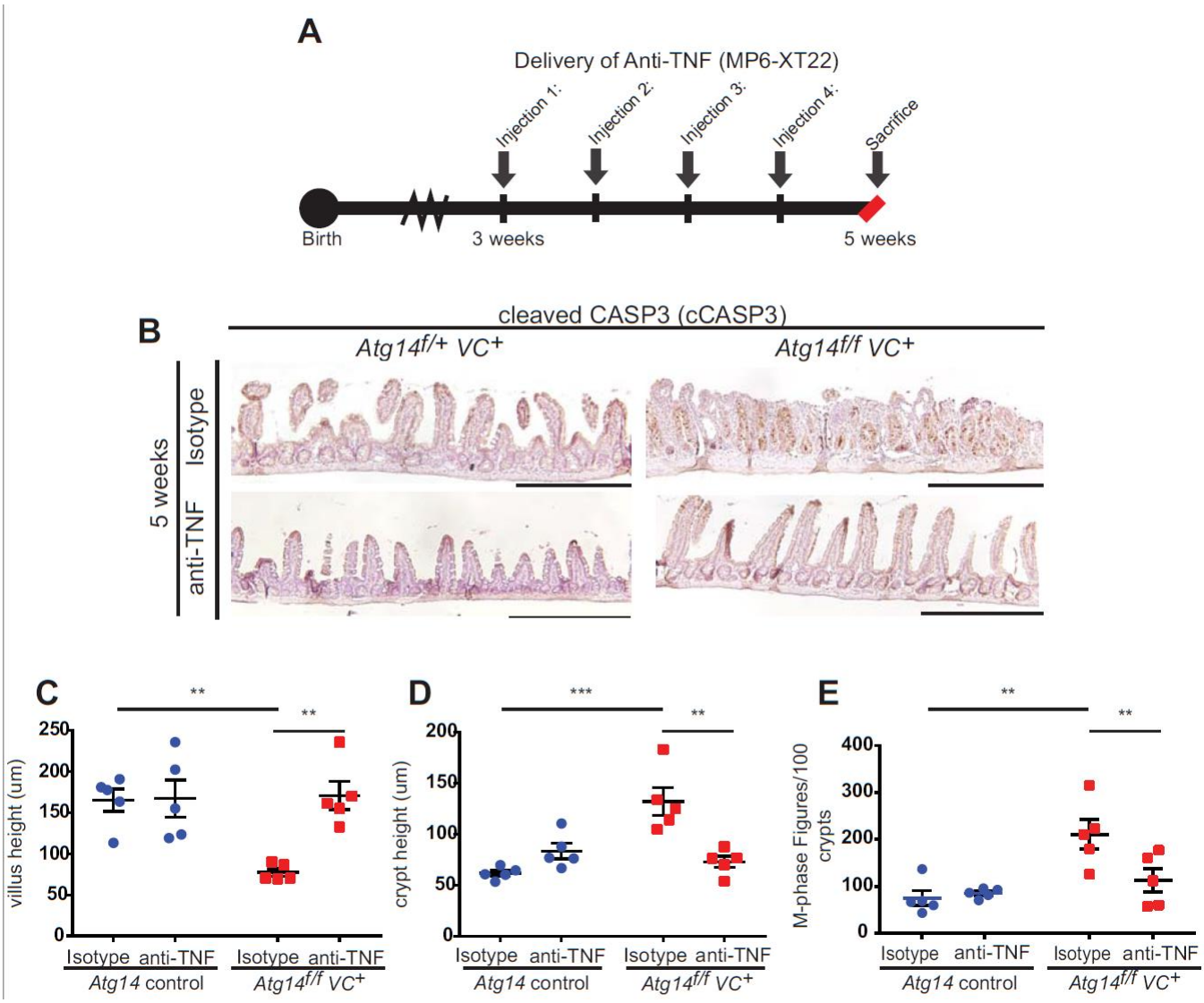

(**A**) Schematic of anti-TNF experiment set-up. (**B**) Representative images of cCASP3 immunohistochemistry staining of jejunal sections from 5-week-old mice of indicated genotype and treatment; bars: 500 µm. (**C**) Mean villus and (**D**) crypt height ± SEM of *Atg14*$^{f/f}$ *VC*$^{+}$ and littermate controls treated with anti-TNF or isotype control. Three independent experiments combined; n=5 per genotype. (**E**) Mean M-phase bodies ± SEM; Two-way ANOVA with Sidak's multiple comparisons test. All statistically significant pairwise comparisons are displayed **p<0.005.

Figure 14 TNF Receptor 1 deletion in *Atg14*-deficient mice rescues intestinal pathology

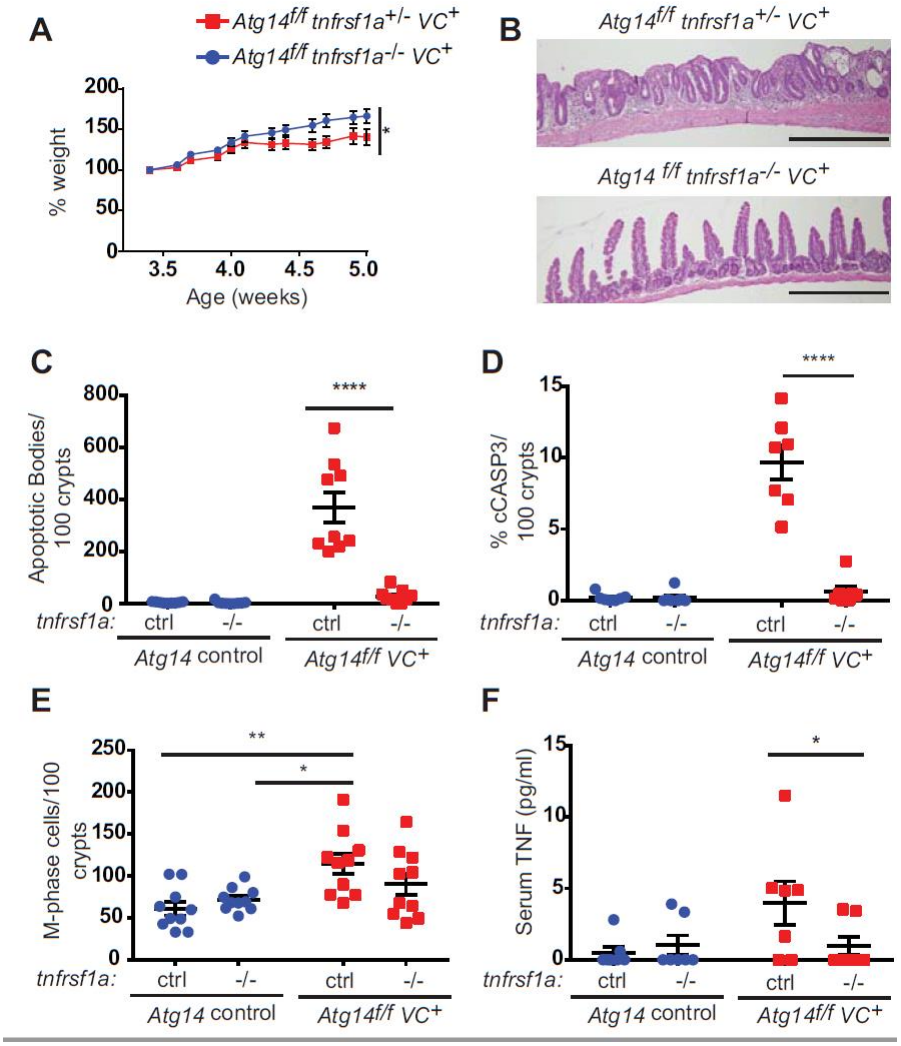

(**A**) Percent weight gain between 3 to 5 weeks of age; Repeated measures two-way ANOVA. (**B-F**) Histological analysis in H&E stained small intestine sections from *Atg14*$^{f/f}$ *VC*$^{+}$ *tnfrsf1a*$^{-/-}$ and control mice (all littermates) among 5-week-old mice; n=6-10 mice/group, >100 crypt-villus units quantified/mouse; two-way ANOVA with Sidak's multiple comparisons test. (**B**) Representative H&E stained jejunal sections from 5-week-old mice; bars: 500 μm. (**C**) Mean apoptotic bodies ± SEM. (**D**) Percent cCASP3 positive cells ± SEM. (**E**) Mean M-phase figures ± SEM. (**F**) Serum TNF levels ± SEM from indicated genotypes at 5 and 6-weeks. All statistically significant pairwise comparisons are displayed, *P<0.05, **P<0.01, ***P<0.001, ****P<0.0001.

Figure 15 TNF Receptor 1 deletion rescues *Atg14* deficient small intestine pathology

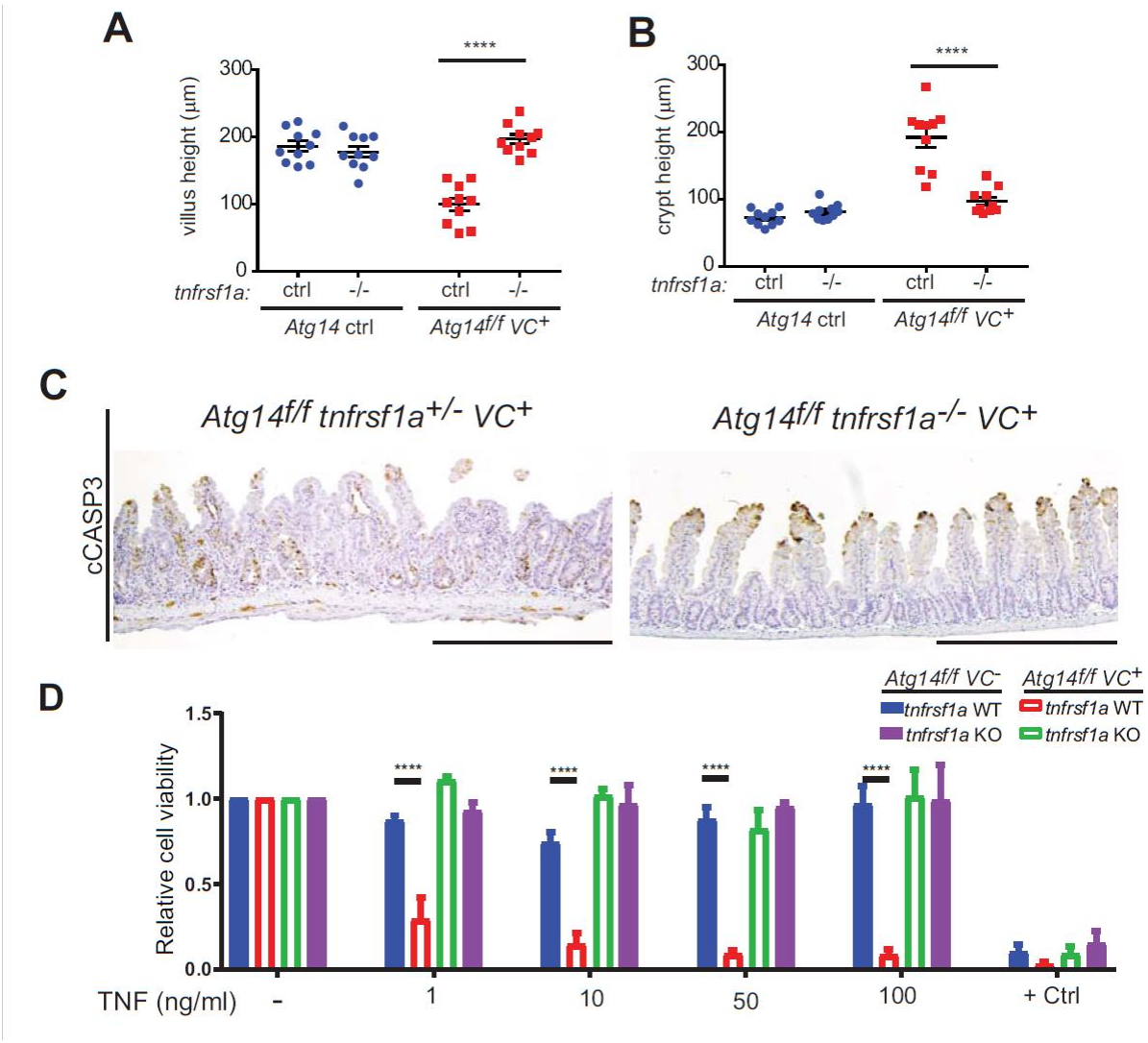

(**A and B**) values displayed as mean ± SEM by two-way ANOVA with Sidak's multiple comparisons test (variable=genotype) (**A**) villus and (**B**) crypt height of *Atg14$^{f/f}$ VC^{+}tnfrsf1a$^{-/-}$* and control mice (all littermates) at 5 weeks of age. n=9-10 per genotype. (**C**) Representative immunohistochemical staining of cCASP3 positive cells from 5-week old mice of indicated genotypes, bars: 500 µm. (**D**) Relative cell viability determined by Cell Titer Glo ATP viability assay of indicated genotypes treated with indicated doses of 12 hour TNF treatment or staurosporine positive control. +ctrl: staurosporine. All statistically significant pairwise comparisons are displayed ****p<0.0001.

Figure 16 $Atg14^{f/f}$ VC^{+} and $Atg14^{f/f}$ VC^{-} intestinal epithelial cells demonstrate comparable mRNA expression of Tnfrsf1a

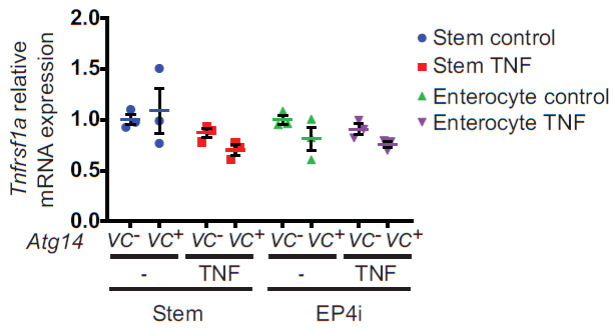

Mean Tnfrsf1a mRNA expression ± SEM in $Atg14^{f/f}$ VC^{+} and $Atg14^{f/f}$ VC^{-} stem cells or differentiated intestinal epithelial enterocytes treated with or without 100 μg/ml TNF for 24 hours. n=3 independent experiments. Two-way ANOVA Sidak's multiple comparisons test.

Figure 17 Deletion of *Rb1cc1*/*Fip200* in the mouse intestinal epithelium results in increased programmed cell death

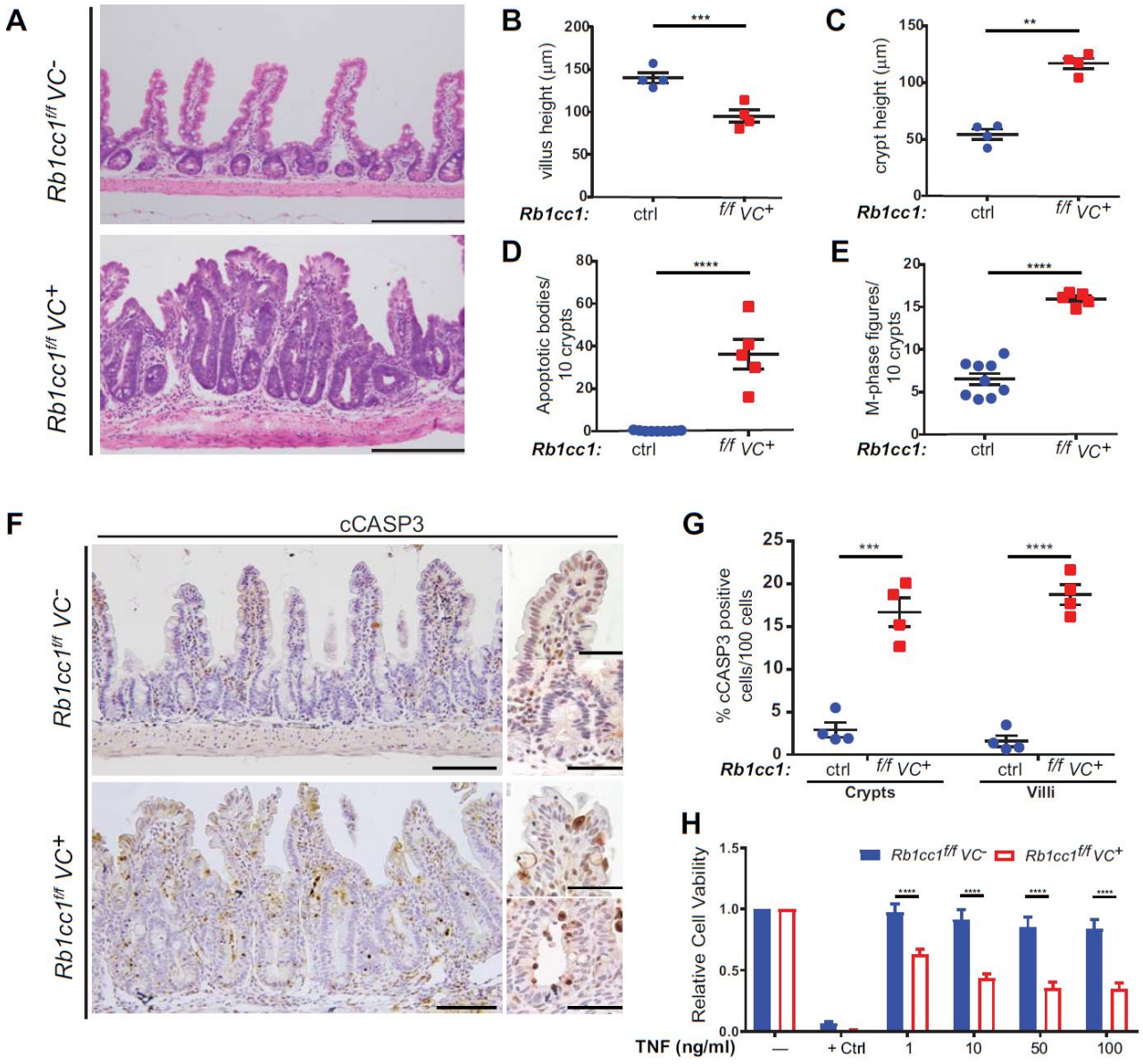

(**A-E**) Histological analysis of H&E stained small intestine sections from *Rb1cc1*$^{f/f}$ *VC*$^{+}$ and littermate control mice between 5 and 9 weeks of age; n≥4 mice/group, bar: 100 µm; (**B-G**) Two-tailed Student's t-test**.** (**A**) Representative images. (**B**) Villus height ±SEM. (**C**) Crypt height ±SEM. (**D**) Quantification of pyknotic and karyorrhexic nuclei ±SEM within crypts. (**E**) Quantification of M-phase nuclei ±SEM within crypts. **(F and G)** Immunohistochemical analysis of cCASP3-stained intestine sections from *Rb1cc1*$^{f/f}$ *VC*$^{+}$ and littermate

control mice between 5 and 9 weeks of age; n≥4 mice/group, bar: 100 µm (high power inset: bar: 50 µm). (**F**) Representative images. (**G**) Percent of cells positive for cCASP3 ±SEM within crypts and villi, mean of 10 crypts or villi/mouse. (**H**) Relative cell viability determined by Cell Titer Glo ATP viability assay of indicated genotypes treated with indicated doses of 12 hour TNF treatment. TNF+CHX: 100 ng/ml TNF + 50 µg/ml Cycloheximide; n=6 assays; 2-way ANOVA with Dunnett's post-test. **P<0.01, ***P<0.001, ****P<0.0001.

Figure 18 *Atg5$^{f/f}$ VC^{+}* mice do not undergo spontaneous villous atrophy

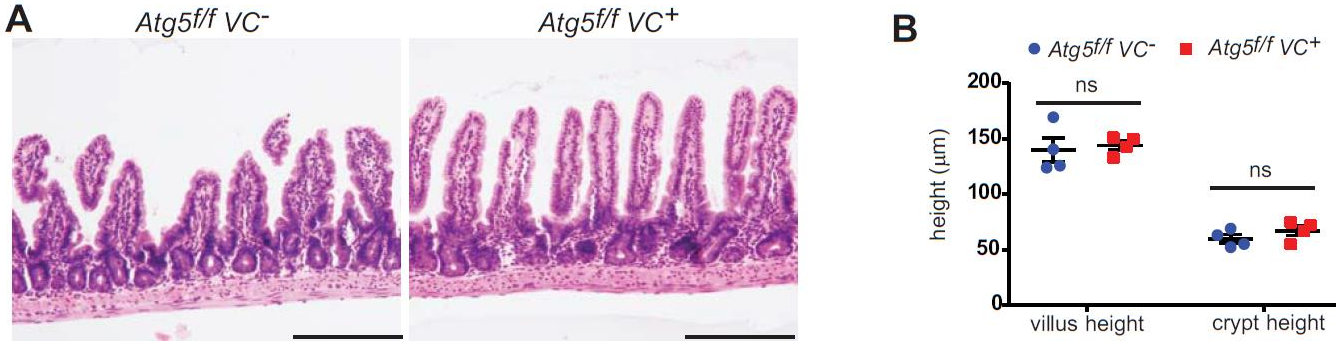

(**A**) Representative H&E images of small intestine jejunal sections of *Atg5$^{f/f}$ VC^{+}* and littermate controls, bars: 200 µm. (**B**) Mean villus and crypt height ± SEM of *Atg5$^{f/f}$ VC^{+}* and littermate control mice. n=4 mice per genotype. Two-way ANOVA with Sidak's multiple comparisons test. ns: not significant.

Chapter 3:

Sqstm1/p62 potentiates the formation of a Caspase-8 Death Induced Signaling Complex

In this chapter I present data to link an autophagy factor, Sqstm1/p62, to caspases and cell death. My overarching hypothesis is that stalled autophagy complexes containing SQSTM1/p62 cytoplasmic puncta promote TNF-triggered caspase activation. This work addresses two unanswered questions: "Why does deletion of autophagy *initiation (eg. Atg14)* lead to more severe TNF triggered death and intestinal damage than deletion of autophagy *termination (eg Atg5)*?" Data here suggest that puncta of Sqstm1/p62 in the intestinal surface epithelium differentiate these knockout models. It also addresses the question: "What is the link between autophagy and activation of caspases?" Data suggest that puncta of Sqstm1/p62 within the intestinal surface epithelium colocalize with and potentiate the activation of caspases.

3.1 Abstract

Intestinal autophagy is protective against TNF-triggered injury and cell death. However, the molecular mechanisms that link the TNF cell death pathway to the autophagy pathway are not fully understood. Furthermore, significant phenotypic differences exist between *Atg16L1* or Atg5 conditional KO (cKO) mice and that of *Atg14* or *Rb1cc1/Fip200* cKO mice with respect to their relative sensitivities to TNF triggered cell death. While *Atg16L1* and Atg5 cKO mice demonstrate cell death upon a two-factor challenge through combined injury (such as DSS colitis) and infection model (such as MNV or Helicobacter Hepaticus), *Atg14* and *Rb1cc1/Fip200* cKO mice demonstrate spontaneous death shortly after weaning. Here we demonstrate a role for the autophagy signal adaptor Sqstm1/p62 in modulating the sensitivity of the enterocyte to TNF triggered apoptosis. Sqstm1/p62 forms large cytoplasmic punctate structures within cells most sensitive to TNF triggered apoptosis: the crypt-base cells of *Atg5* and *Atg16L1* cKO mice, and the surface epithelium of *Atg14* or *Rb1cc1/Fip200* cKO mice. Puncta are not found in the surface epithelium of *Atg5* or *Atg16L1* cKO mice, in spite of their autophagy defect. Furthermore, these structures are activated for selective autophagy and colocalize with cleaved caspase-8. Knockout of *Sqstm1/p62* in the *Atg14* KO background rescues cell death within the intestinal epithelium, despite yielding an incomplete rescue of intestinal morphology. Primary spheroids derived from these mice had reduced cytotoxicity after challenge with TNF in culture. Together these findings implicate p62 puncta as structures in the *Atg14* deficient cell that link caspases and autophagy at the molecular level.

3.2 Introduction

Autophagy, as described in this dissertation previously, is a stepwise pathway of several distinct enzymatic and structural complexes working in concert to achieve the endpoint of sequestering,

trafficking, and degrading cytoplasmic cargo within the acidic lysosome. This pathway is termed 'canonical degradative autophagy' and this document will use this term as cited by Codogno et. al. for a degradative process that utilizes the four commonly accepted stepwise processes: Initiation (achieved by the Ulk1 complex), Nucleation (Beclin1– PtdIns3KC3–Atg14L complex), elongation (Atg5-Atg12-Atg16L1), and lysosomal fusion [136]. Canonical autophagy can degrade cargo in bulk (best illustrated through starvation induced yeast vacuole formation) or in a targeted fashion where cargos are specifically marked for autophagic sequestration and degradation [137, 138].

However, additional autophagic factors are required for the process of targeted autophagic degradation, common referred to as selective autophagy. One such factor is Sqstm1/p62. p62 is an autophagy cargo receptor and functions to tether cellular debris (proteins, organelles, etc…) to the autophagosome for degradation. As a substrate for autophagy it is critical to note that autophagy-deficient cells cannot clear p62 and therefore have increased levels of this protein [33] [34] along with increased abundance of the cellular autophagic cargo [38].

There are two related properties of p62 pertinent for this study: its function as a signaling scaffold and its ability to form punctate cytoplasmic structures or microdomains. The formation of p62 puncta is incompletely understood, but it is associated with deletion of the *initiation factors* of autophagy [40] [41] [42]. The puncta often contain high local concentrations of ubiquitin and ubiquitinated proteins. P62 can directly bind polyubiquitinated proteins (through its UBA ubiquitin binding domain) and shuttle them to an LC3-coated autophagosomal vesicle (through its LIR LC3 Interacting Region domain) for degradation [32].

Secondly, p62 can mediate signaling outcomes. The initial discovery of p62 identified its role as an interacting factor of RIPK1, facilitating TNF-triggered NF-kB stimulation [35].

Subsequent findings demonstrated a broader function of this protein as a scaffold to mediate signaling of several other fundamental processes and pathways such as cancer, cell death, and metabolism [44] [43] [45]. Specifically of interest to this work is its contribution to TNF triggered cell death signaling through its interaction with both RIPK1 (which is now recognized as a master regulator of cell fate) and with CASP8/Caspase-8 [36] [37]. In each of these reports, the respective authors identified, within the context of TRAIL-stimulated, autophagy mutant cancer cells, that SQSTM/p62 can form a scaffold to activate cell death pathways. Despite each of these reports, there remains the open question as to how generalizable these findings are in the context of homoeostatic tissue function, or even within the context of TNF, rather than TRAIL signaling. Overexpression studies using tagged protein has been used to identify the binding partners of p62 and its role in signaling pathways, while puncta formation has been broadly studied in cell lines under autophagy deficient, starvation conditions. It is critical to address the extent to which p62 plays a role as a scaffold and as a caspase signal transducer in-vivo, specifically within autophagy deficient intestinal epithelium.

3.3 Materials and Methods

Mice:

To functionally test the role of p62 within the context of the *Atg14* $^{f/f\,VC+}$ mouse model of intestinal cell death and villous atrophy, we crossed the *Atg14* conditional KO mouse to the *Sqstm1/p62* full body KO mouse model (Sqstm1^{tm1Keta}).

The breeding strategy generated Atg14 $^{F/F}$; VC+; Sqstm1 $^{-/-}$ double knockout animals, along with Atg14 $^{F/F}$; VC-; Sqstm1 $^{-/-}$ and Atg14 $^{F/F}$; VC+; Sqstm1 $^{+/-}$ controls. Because Atg14 F/F VC+ animals cannot act as breeders, expected frequency of double KO animals is only 1/8. Double KO mice were born as expected in approximately Mendelian ratios, but due to the breeding strategy, proper littermate controls were not obtained for each litter.

Figure 19 Breeding strategy for Atg14; Sqstm1/p62 double KO mice

Breeders: **Atg14 $^{F/F}$; VC-; Sqstm1 $^{-/-}$** X **Atg14 $^{F/+}$; VC+; Sqstm1 $^{+/-}$**	
	Expected frequency:
Atg14 $^{F/F}$; VC+; Sqstm1 $^{-/-}$	1/8
Atg14 $^{F/F}$; VC-; Sqstm1 $^{-/-}$	1/8
Atg14 $^{F/F}$; VC+; Sqstm1 $^{+/-}$	1/8
Atg14 $^{F/F}$; VC-; Sqstm1 $^{+/-}$	1/8
Atg14 $^{F/+}$; VC+; Sqstm1 $^{-/-}$	1/8
Atg14 $^{F/+}$; VC-; Sqstm1 $^{-/-}$	1/8
Atg14 $^{F/+}$; VC+; Sqstm1 $^{+/-}$	1/8
Atg14 $^{F/+}$; VC-; Sqstm1 $^{+/-}$	1/8

Atg14 $^{F/+}$; VC-; Sqstm1 $^{-/-}$, Atg14 $^{F/+}$; VC+; Sqstm1 $^{-/-}$, Atg14 $^{F/+}$; VC-; Sqstm1 $^{+/-}$ and Atg14 $^{F/+}$; VC+; Sqstm1 $^{+/-}$ were also generated out of this breeding strategy, unless cited specifically, these animals were not used in my analysis.

Out of this breeding strategy, I hypothesized that Atg14 $^{F/F}$; VC-; Sqstm1 $^{-/-}$ mice would represent my negative control. These mice, I hypothesized would behave in a similar manner to that of p62KO mice, which according to conversations with members of Skip Virgin's lab (from whom I

obtained the animals) and literature reports, had no known intestinal phenotype within the age range of interest (3-8 weeks).

I also hypothesized that the mice would not be haploinsufficient for p62 and that Atg14 $^{F/F}$; VC+; Sqstm1 $^{+/-}$ animals would behave similar to that of Atg14 $^{F/F}$; VC+; animals and demonstrate spontaneous intestinal epithelial cell death. This assumption was borne out in the data.

Mouse strains were genotyped by Transnetyx.

Antibodies and reagents

Immunohistochemistry was performed using guinea pig polyclonal anti- C-terminal Sqstm1/p62 (Progen GP62-C), Mouse monoclonal anti-Sqstm1/p62 clone 2C11 (Novus, H00008878-M01), rabbit monoclonal anti-cleaved CASP3 Asp175 (Cell Signaling Technologies, 9664), rabbit monoclonal anti-cleaved CASP8 Asp387 (Cell Signaling Technologies, 8592), rabbit monoclonal anti-cleaved PARP Asp214 (Cell Signaling Technologies, 94885), mouse monoclonal anti-ACTB HRP conjugated (Ptglab, HRP-60008) and corresponding species-specific secondary antibodies.

3.4 Results

3.4.1 Punctate accumulation of Sqstm1/p62 is a defining factor of TNF-sensitive autophagy KO mice

Autophagy factors involved in multiple steps of the canonical degradative autophagy pathway demonstrate sensitivity to cell death by TNF, suggesting a shared mechanism. However, there is significant variance when comparing the intestinal epithelial specific knockouts of different autophagy pathway genes with respect to cell death and damage. Furthermore, the molecular mechanisms that define the threshold of sensitivity to TNF remain undefined. Therefore, in this study we sought to address these unanswered questions to understand more precisely how autophagy intersects with TNF-triggered activation of caspases.

Previous reports have identified that, at steady state, accumulation of Sqstm1/p62 is a marker for the degree of autophagy inhibition. Sqstm1/p62 is an autophagy cargo receptor that functions to bind selected proteins, organelles, and aggregates, and tether them to an autophagic vesicle for degradation via the autophagy lysosome system. P62 is a molecule that is itself degraded by autophagy: therefore loss of autophagy results in increased cellular abundance of p62 [33]. Immunoblot analysis of small intestinal tissue from *Atg14* $^{F/F}$ *VC+* mice revealed increased levels of p62 protein (**Figure 20**)

Across multiple cell types, deletion of autophagy factors that catalyze the entry steps of the autophagy pathway (e.g. Atg9, Ulk1/2, Fip200, Beclin-1, Atg14) demonstrate an increased abundance of this protein relative to that of factors later in the pathway (Atg5, Atg16L1) [40-42]. We hypothesized that intestinal epithelial p62 levels may represent a biomarker for TNF-triggered sensitivity to cell death. We observed a striking burden of Sqstm1/p62 puncta within *Atg14* $^{F/F}$ *VC+* mouse small intestinal villus epithelium relative to the virtual absence of staining seen in the enterocytes of littermate controls *Atg14* $^{F/+}$ *VC+* and *Atg14* $^{F/F}$ *VC-* mice) (**Figure 21**).

We next defined the role of p62 puncta among other intestinal epithelial deficient autophagy deficient mice (*Atg16L1* $^{F/F}$ *VC+*, *Atg5* $^{F/F}$ *VC+*, *Rubicon -/-*, *Sqstm1 -/-*, and *Rb1cc1* $^{F/F}$ *VC+).*

By immunoblot, tissue derived from *Atg5* $^{F/F}$ *VC+* and *Atg16L1* $^{F/F}$ *VC+* mice had increased levels of p62 compared to littermate controls, but these animals did not demonstrate the presence of p62 puncta throughout the villus epithelium; rather diffuse staining was visualized **(Figure 22**). Similar to that of *Atg14* $^{F/F}$ *VC+* tissue, *Rb1cc1* $^{F/F}$ *VC+* demonstrated a high burden of p62 punctate staining throughout the villus epithelium (**Figure 22**).

Upon closer inspection, there was a small region of distinct punctate staining for p62 within the crypt base of *Atg16L1* $^{F/F}$ *VC+* mice (**Figure 22** Consistent with reports in the literature, Paneth

cells are exquisitely sensitive to TNF triggered cell death in these two lipid ligase autophagy deficient models [68, 108]. Therefore, the formation of p62 puncta once again correlated with cells that are sensitive to TNF-triggered death. Taken together, these results suggest that Sqstm1/p62 marks cells that are sensitive to death.

3.4.2 Isolation and validation of a TNF-sensitive mouse immortalized cell line

Spheroid culture derived from primary mouse tissue plays a critical role in validating and recapitulating phenotypic observations under controlled conditions. Our previous work has shown that spheroids derived from *Atg14* $^{F/F}$ *VC+* mice are sensitive to TNF-triggered apoptosis, similar to that of intestinal tissue [70]. However, further biochemical approaches to look at protein-protein interactions require a more amenable cell type that can be expanded in large quantities, while still maintaining the properties of primary mouse intestinal spheroids. In collaboration with a postdoc (Qiuhe Lu), jejunal spheroids from an *Atg14* $^{F/F}$ *VC-* mouse were immortalized using the SV40 antigen Transformed cells no longer required matrigel for growth, but could be maintained as an adherent monolayer on a standard tissue culture treated plastic vessel. Transformed cells were transduced with either Ad5-Cre GFP to generate knockout lines or Ad5-GFP vector to generate controls (**Figure 23**). Clonal populations were isolated on the basis of transient nuclear GFP expression and screened by PCR for excision of the floxed exon with verification through Sanger sequencing.

Both *Atg14* $^{f/f}$ *VC+* spheroids and the *Atg14* KO SV40 immortalized cells modeled the autophagy defect that was seen in mouse villus epithelial tissue: developing large, discrete punctate structures of p62 in the cytoplasm. Punctate structures were visualized within histological sections of spheroids and within fixed, mounted monolayers of *Atg14* KO SV40 immortalized cells (**Figure 24** . Virtually no punctate structures were visualized within sections of control spheroids or in control

immortalized cells.

To functionally test the responsiveness of this cell line, I treated immortalized cells (both control and KO lines) for 36 hours with 100ng/ml recombinant Mouse TNFα. Cellular viability was assessed through phase contrast microscopy **(Figure 25).** TNF-treatedAtg14 KO cells demonstrated cell death, while untreated KO controls and TNF-treated control cells both did not show any detectable evidence of cell death. As a measure of confidence, cells were treated for 24 hours with increasing dosages of TNF and viability was measured by Cell Titer Glo assay (**Figure 26).** Similar to the image-based assay, and similar to that of primary spheroids, immortalized intestinal cells demonstrated dose-dependent loss of cellular viability. Together, these results demonstrate that immortalized mouse jejunal cells represent a viable model for studying the molecular mechanism of cell death.

3.4.3 Sqstm1/p62 puncta are associated with ubiquitinated protein, suggesting a defect in selective autophagy

Given our novel histological findings and the development of a new tractable cellular model for testing cytotoxicity, we wished to define the functional role of Sqstm1/p62 within autophagy deficient cells. Previous reports identify a role for p62 as a scaffold and a signaling platform, promoting NF-kB responses through interaction with Ripk1, or directly interacting with Caspase-8 [35, 37]. To define the extent to which p62 directly interacts with signaling pathways or cell death factors we performed mass spectroscopy on immunoprecipitated cell lysates from immortalized cells using a rabbit monoclonal antibody against p62. Immortalized cells from either *Atg14* $^{F/F}$ *VC-* or *Atg14* $^{F/F}$ *VC+* cells were treated with vehicle or TNF and ~5mg protein was isolated per condition.

While binding partners of p62 were not detected due to low efficiency of co-IP, markers of p62 phosphorylation were detected. One such marker was phosphorylation of Serine 405 (S403 in

human cells), a marker suggesting a role of p62 in a process called selective autophagy [139, 140]. Selective autophagy is the term to described the application of the canonical degradative autophagy pathway towards the specific sequestration and degradation of target proteins, rather than bulk sequestration and catabolism of cytoplasmic contents as under starvation conditions. Such target proteins often are 'flagged' for selective autophagy degradation by the autophagy-lysosome system upon polyubiquitination [141]. P62 binds such proteins by binding polyubiquitin via its UBA domain and can tether cargo to the LC3 labeled autophagosome via its LIR domain[138]. Under these circumstances, p62 acts as an intermediary to tether specific cargo to a nascent autophagosome for degradation.

We observed that phosphorylation of Serine 405 was enriched in *Atg14* KO cells compared to *Atg14 F/F* controls, and that S405 was equally abundant in TNF or vehicle treated cells (Figure 27). To validate these results, we immunoblotted for S405 in spheroids treated with an acute time course of TNF. Consistent with the mass spectroscopy results, we observed a striking abundance of S405 phosphorylated p62 in KO cells relative to that of controls. Phosphorylation was independent of TNF treatment. Immunoblots for ubiquitin also demonstrated enrichment among *Atg14* KO cells relative to controls (Figure 27). Together, these data are consistent with the model that p62 is participating in the process of selective autophagy. Observations thus far demonstrate that p62 accumulates within "stalled" punctate inclusion bodies. We hypothesize that these punctate bodies are in close association or in complex with as of yet undefined ubiquitinated protein factors in the *Atg14* deficient cell. We further propose that the interaction of p62 with ubiquitinated cargo in a selective fashion, meets the criteria for selective autophagy.

3.4.4 Activated Caspase-8 accumulates within punctate structures and colocalizes with Sqstm1/p62 puncta within the intestinal epithelium

We observed increased abundance of ubiquitin and SQSTM1/p62 aggregates within the

intestine and within our apoptosis sensitive cells. Such accumulation suggest a defect in proteostasis, and we hypothesize, based upon numerous examples in the literature, that the proteostatic defects include the accumulation of factors that promote TNF-triggered cell death [140]. Identification of molecular factors from the TNF pathways or the cell death cascade that intersect with the autophagy pathway is of utmost importance and significance. The ability to modulate or block the activity of these factors may represent a new avenue for therapeutically treating cell death and tissue dysfunction.

Caspase-8 is well characterized in the context of the TNF-triggered apoptotic cascade. Caspase-8 is termed the initiator caspase, because it is a proximal catalytic protein of a family of Cysteine-Aspartic acid proteases that mediate cytotoxicity downstream of TNF [20, 142, 143]). By interfacing with the proximal components of the TNF signaling complex (including Rip kinase, Fadd, Tradd and cFLIP) and acting as a master activator of the death cascade. Pro-caspase-8 is constitutively synthesized and so its total abundance does not inform its activity. As illustrated in **Figure 3**, pro-caspase-8 is self-processed into a p43 form. p43 cleaved caspase-8 is partially active, but is spatially restricted **(Figure 4)**[1]. It is still localized to the Death Induced Signaling Complex (DISC) by means of its interactions with other Death Effector Domain containing proteins, namely Tradd. Complete autocatalysis, results in the generation of cytoplasmic p10/p18 dimers that subsequently cleave downstream effector caspases such as caspase-3 and caspase-7 that, in turn, mediate apoptosis[144].

Accordingly, we performed immunofluorescence on small intestinal tissues using an antibody against cleaved Caspase-8, the initiator caspase that was cleaved to its active forms upon TNF addition. We hypothesized that similar to the staining pattern of cleaved Caspase-3, a large proportion of dead and dying cells from *Atg14* $^{f/f}$ *VC+* would demonstrate cytoplasmic staining

positive for caspase-8, providing a secondary validation of cell death. Immunofluorescence for cleaved caspase-8 was performed using an antibody that detects the p43 and p10/p18 cleavage forms. In a unexpected result, a punctate staining pattern was observed in the enterocytes of *Atg14* $^{F/F}$ *VC+* mice, while no such staining was present in *Atg14* $^{F/F}$ *VC-* mice (**Figure 29** . Most cells of the *Atg14* $^{F/F}$ *VC+* surface epithelium demonstrated positive punctate staining. Cells with this staining pattern were not displaying hallmarks of cell death, including karyorrhexis, pyknosis and cell shrinkage/cytoplasmic blebbing. As expected, there was also a second pattern of cytoplasmic staining in a population of cells consistent with cells undergoing apoptosis. These cells were smaller and were in the process of extrusion (**Figure 29** . Taken together, immunofluorescence for cleaved caspase 8 revealed two distinct populations of positive cells: actively apoptotic cells, and cells primed for apoptosis.

The punctate staining pattern of cleaved caspase-8 was similar to that of p62. Therefore, we hypothesized that puncta of p62 and caspase-8 colocalize. Dual staining was consistent with this hypothesis, revealing a significant population of each puncta that share the same spatial position (**Figure 30** . As a measure of confidence, dual staining between ubiquitin and cleaved caspase-8 was also performed. Evidence of co-staining between the two groups was also observed (**Figure 30**) together, these findings suggest a role for the direct interaction between p62 and the initiator caspase of the TNF-triggered apoptotic cascade.

Literature suggests a role for vesicles in the compartmentalization of the TNF-induced cell death factors (the TNF receptosome) as the TNF signaling complex is trafficked for the cell membrane to endosomes to the lysosome for degradation[59] [145]. Transmission Electron Microscopy (TEM) of intestinal tissue from *Atg14* $^{F/F}$ *VC+* mice revealed an increased number of large vacuolated structures in the apical cytoplasm relative to controls suggesting a vesicular

trafficking defect relative to littermate control *Atg14* $^{F/F}$ *VC*- mice (**Figure 28** Extending these observations, a subset of p62 was identified by immunogold staining in association with these structures, and in close proximity to another Caspase-8-associated cell death factor, Fadd [Fas-Associated via Death Domain] (**Figure 28** Immunofluorescence of intestinal tissue demonstrated that p62 co-localized with a subset of early endosomal markers (**Figure 31**). Further experiments are needed to conclusively define the extent to which p62 colocalize with TNF receptosomes and to define the functional significance of this co-localization.

3.4.5 Sqstm1/p62 accumulation correlates with loss of function of the coiled-coil domain of Atg14 and with sensitivity of enterocytes to cell death

Atg14 is recognized to act at two distinct steps of the autophagy pathway. It functions proximally as part of the Atg14-Becn1-Vps34-Vps15 lipid ligase to nucleate assembly of the autophagosomal membrane. In this context, Atg14 heterodimerizes with Beclin-1 through a conserved motif called a coiled-coil domain[24]. The coiled-coil domain of Atg14 is indispensable for the initiation of autophagy[146]. Atg14 also functions at the terminal step of the pathway in conjunction with STX17 to mediate fusion of the autophagosomal vesicle with the lysosome. This second role is mediated through the N-terminal cysteines (C43, C46, C55, and C58) of Atg14 [146].

I hypothesize that the process of autophagosomal biogenesis (autophagy initiation) is the rate-limiting step to modulate the outcome of TNF triggered apoptosis. An experimental approach that has been used by other groups to decipher these two functions is through a complementation experiment, complementing *Atg14* deficient cells with deletion mutants of *Atg14*. To address this question, I generated expression constructs to complement *Atg14* deficient cells with either: Full length *Atg14*, Δ Coiled-coil *Atg14*, C43A/C46A *Atg14* or, as a control, *GFP* **(Figure 32).** I hypothesized that full length Atg14 should rescue autophagy and TNF-triggered apoptosis, that Atg14 Δ Coiled-coil should not rescue autophagy initiation and TNF-triggered apoptosis and that

Atg14 C43A/C46A should rescue autophagy initiation, and TNF-triggered apoptosis. Constructs were delivered to *Atg14* F/F and *Atg14* KO immortalized cells via lentiviral transduction and puromycin was used to enrich for a positive population. Cells were challenged with increasing doses of TNF and viability was measured 24 hours later via Cell Titer Glo assay. Consistent with my hypothesis, *Atg14* KO transduced with *GFP* construct remained sensitive to TNF in a dose dependent manner while transduction of full length *Atg14* construct fully rescued cell death. Transduction of *Δ coiled-coil Atg14* did not rescue the cell death phenotype, while C43A/C46A *Atg14* did rescue, consistent with my hypothesis that the coiled-coil domain (nucleation domain) of the autophagy complex is necessary for protection against TNF triggered cell death (**Figure 33**).

No changes in TNF-triggered viability were measured among control *Atg14* $^{F/F}$ cells transduced with any of the constructs. As a measure of confidence, phase contrast images were captured of immortalized cells treated at 24 hours with TNF or TNF-CHX , demonstrating visually the pattern of cell death seen under Cell Titer Glo viability assay **(Figure 34).**

3.4.6 *Atg14* $^{F/F}$*; VC*$^{+}$ *Sqstm1* $^{-/-}$ mice have reduced cell death within the intestinal epithelium, despite defects in epithelial architecture

The data thus far demonstrates an association between the formation of p62 puncta and surface epithelial cells that are sensitive to TNF-triggered death. It also demonstrates a spatial association of p62 with caspase-8 within cytoplasmic puncta. Therefore, we next wanted to functionally test the role of p62 in the Atg14 null background through genetic loss of function studies. We hypothesized that deletion of p62 would block TNF-triggered caspase activation. Our approach is to generate a double knockout mouse model. A commonly used model is the *Sqstm1/p62* full body KO mouse (Sqstm1^{tm1Keta}). Previous publications using this model, report that the delivery of cargo to the autophagosome for degradation is impaired [147-149]. Two notable

phenotypes that are found in this mouse model include osteolysis and obesity. The bone phenotype emerges at 9 months of age and includes lytic lesions with decalcification similar to Paget's Disease. [150] As these mice approach one year of age, they also demonstrate increased weight gain compared to controls. The currently accepted model is that these mice experience hyperphagia, and have metabolic changes to glucose and insulin tolerance [151, 152] These phenotypes are expected to have minimal bearing on the studies presented here as the timescales of interest for this study include animals 3-6 weeks of age.

To functionally test the role of p62 within the context of the *Atg14* $^{f/f\,VC+}$ mouse model of intestinal cell death and villous atrophy, we crossed the *Atg14* conditional KO mouse to the *Sqstm1/p62* full body KO mouse (Sqstm1^{tm1Keta}) to generate *Atg14* $^{F/F}$*; VC+; Sqstm1* $^{-/-}$ (dKO) and littermates. Double knockout mice were born in expected ratios and when possible, appropriate littermate controls were obtained (both VC- animals to test the contribution of Atg14, and p62+/- animals to test the role of p62).

Mice were sacrificed at 6 weeks of age and intestinal tissue was collected for histology. Similar to experiments with *Atg14* $^{F/F}$ *VC+* crossed to TNFR1 -/- mice, the primary readout was the rescue of intestinal architecture, namely villous atrophy and crypt elongation. The secondary readout was epithelial cell death.

Whole mount imaging of *Atg14* $^{F/F}$*; VC+; Sqstm1* $^{-/-}$ mice compared to littermate control *Atg14* $^{F/F}$*; VC+* mice demonstrated an reduction in regions of confluent villus blunting, with increased numbers of discrete villi visualized. (**Figure 35**). Histological (H&E) sections were obtained to compare the histological structure of tissues from *Atg14* $^{F/F}$*; VC+; Sqstm1* $^{-/-}$, *Atg14* $^{F/F}$*; VC+; Sqstm1* $^{+/-}$, *Atg14* $^{F/F}$*; VC-; Sqstm1* $^{-/-}$ and *Atg14* $^{F/F}$*; VC-; Sqstm1* $^{+/-}$ (**Figure 35**).

Villin-cre – mice (both p62 +/- and -/-) (left panels) retain repeating units of villus-crypt

architecture. *Atg14* deficient mice heterozygous for p62 (upper right) demonstrate villus loss, crypt elongation, and features of crypt dropout. *Atg14 f/f VC+; p62 -/-* mice (lower right) demonstrate villus retention with columnar surface epithelium. Villi are abnormal and crypts are elongated, but there is reduced evidence of crypt dropout. (**Figure 35**). Together, these findings suggest a partial rescue of histological structure due to genetic loss of function of p62. To define the extent to which dKO mice are rescued from our secondary metric: cell death, we measured Cleaved caspase-3 and cleaved-PARP (a caspase substrate) through immunohistochemistry of small intestinal tissue sections. We hypothesized that dKO tissues would show reduced caspase activation. As demonstrated in **Figure 36** both readouts of caspase activation were decreased in dKO mice relative to single *Atg14* $^{F/F}$ *VC+* tissues. Defects resulting from loss of autophagy (large goblet cells, elongated crypts, suggesting that cell death has been uncoupled from defects in tissue morphology (**Figure 36**). The DKO relative to *Atg14* $^{F/F}$ *VC+* tissues demonstrated rescue of cell death, rescue of crypt and villus loss, but retains tissue architectural abnormalities.

3.4.7 *Atg14* $^{F/F}$*; VC*$^{+}$ *Sqstm1* $^{-/-}$ spheroids are protected from apoptotic death after TNF stimulation

Crossing the *Sqstm1 -/-* mouse to the *Atg14* $^{F/F}$*; VC+* background demonstrated a reduction in cell death compared to control mice. However, in this mouse model, p62 is deleted in in every mouse tissue, not just the intestinal epithelium. Therefore, we must test the hypothesis that deletion of p62 plays a non-cell autonomous role in the mouse to protect the intestinal epithelium against TNF-triggered cell death. To test this hypothesis, we isolated primary intestinal epithelial cells from 2 dKO mice (*Atg14* $^{F/F}$*; VC+; Sqstm1* $^{-/-}$) in comparison to cells derived from littermate control mice (both *Atg14* $^{F/F}$*; VC+* single KO and *Atg14* $^{F/F}$*; VC-*) We compared the response of cells to a range of dosages of TNF administered for a period of 15 hours (**Figure 37**). While *Atg14* single KO cells

displayed dose dependent loss of viability compared to VC- controls, double KO cells were protected from cell death (**Figure 37**). By immunoblot, cleaved PARP, a marker of apoptotic cell death, was decreased in these cells compared to *Atg14* single KO cells (**Figure 37**). These findings are consistent with the hypothesis that p62 acts within the intestinal epithelial cell (in a cell autonomous fashion) to protect in the intestinal epithelium from death.

3.5 Discussion

The cellular and tissue data reveal a strong correlation between the presence of cells expressing punctate p62 and those that are sensitive to TNF triggered cell death. This correlation is demonstrated in the comparative analysis of *Atg14* and the *Rb1cc1/Fip200* conditional knockout relative to *Atg5 and Atg16L1* conditional knockout mice. Furthermore, the coiled coil domain, was shown to be necessary to prevent TNF-triggered cell death, providing additional confirmation that canonical degradative autophagy is required to control TNF sensitivity.

p62 plays more than just a passive role as a biomarker, indicating the degree to which autophagy is impaired. Data in this chapter suggest that p62 plays a role in selective autophagy, a pathway though which specific proteinaceous targets are aggregated and sequestered for degradation by canonical degradative autophagy. One candidate target for selective autophagy is the DISC (Death Inducing Signaling Complex). Caspase-8 is a core member of this complex, and data in this chapter indicates co-localization between Casp8 and p62. Lastly generation of the Atg14; p62 double knockout mouse revealed a functional role for p62 in the context of the intestinal epithelium. Deletion of p62 attenuates cell death in the intestinal epithelium, and spheroids derived from these animals are protected from TNF triggered death. Together these findings support the hypothesis that stalled autophagy complexes containing SQSTM1/p62 cytoplasmic puncta promote TNF-triggered caspase activation. It identifies a specific molecular factor (p62) that intersects with caspase-8, the

initiator caspase of the TNF-apoptotic pathway. These findings have broad implications for understanding the basic mechanisms through which cell death and autophagy interact.

3.6 Figures

Figure 20 Increased abundance of p62 protein by immunoblot from jejunal tissue and primary jejunal spheroids

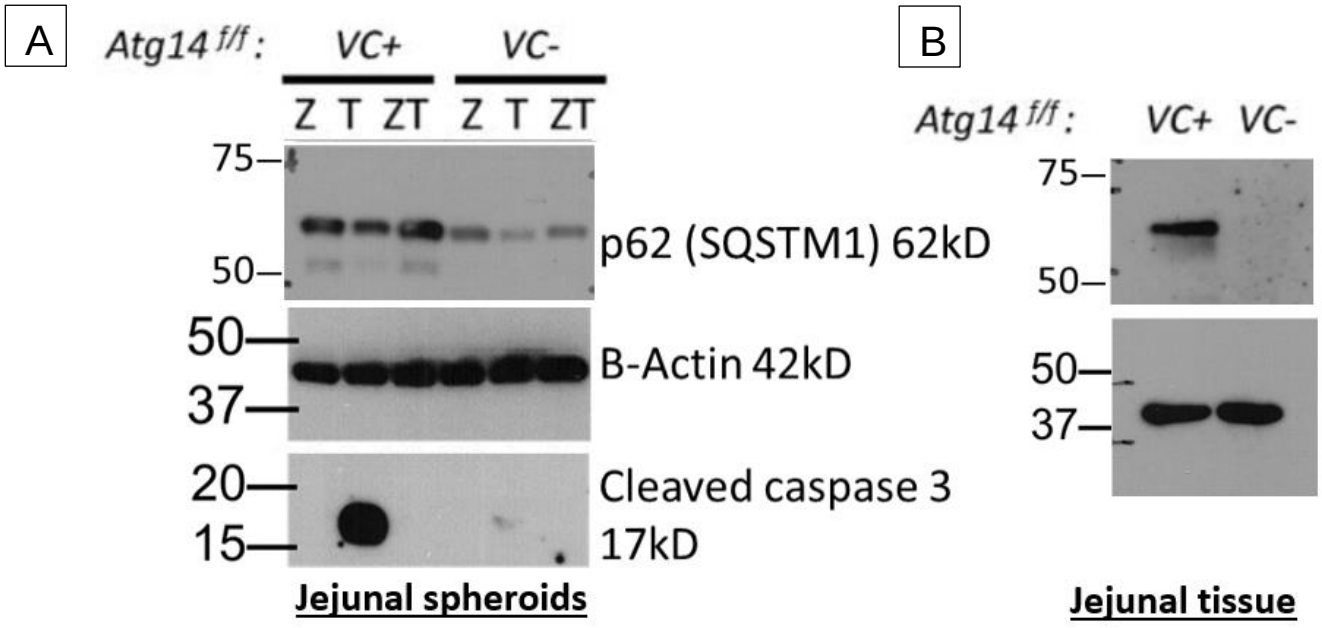

A) Enterocyte differentiate spheroids were isolated from the jejunum of Atg14 $^{F/F}$; VC+ mice and Atg14 $^{F/F}$; VC- mice, respectively and treated with treated with 10 ng/ml mouse TNF and/or 20 µg/ml Z-VAD-FMK for 12 h ; Z=Z-VAD-FMK, T= TNF, TZ= TNF + Z-VAD-FMK. B) Tissue from the midpoint of the small intestine was homogenized from Atg14 $^{F/F}$; VC+ mice and Atg14 $^{F/F}$; VC- mice.

Figure 21 Discrete punctate staining pattern of Sqstm1/p62 by immunofluorescence within the crypt and villus epithelium of Atg14 $^{f/f}$ VC^{+} mice

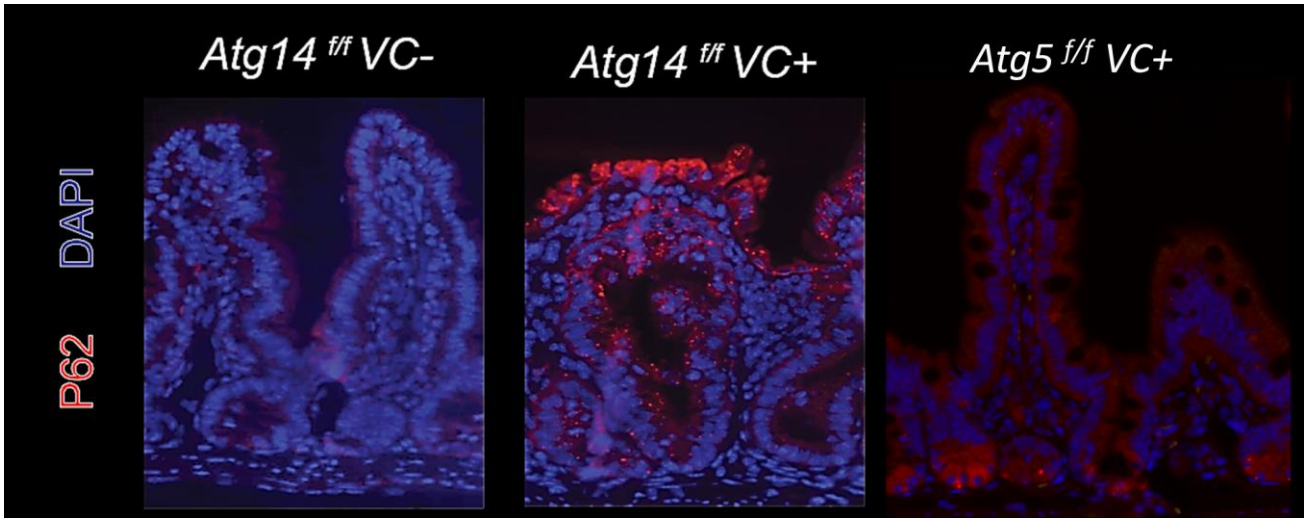

Representative immunofluorescence staining of Sqstm1/p62 within small intestinal tissue sections from Atg14 $^{f/f}$ VC+ mice Atg14 $^{f/f}$ VC- and Atg5 $^{f/f}$ VC+ mice N>10 mice per group. Representative images demonstrate the accumulation of red puncta within the surface epithelium of Atg14 $^{f/f}$ VC- mice, and accumulation of red puncta within the crypt bases for Atg5 $^{f/f}$ VC+ mice.

Figure 22 Epithelial puncta of Sqstm1/p62 by immunohistochemistry within the crypt and villus differentiates autophagy KO mice and correlates with cell death

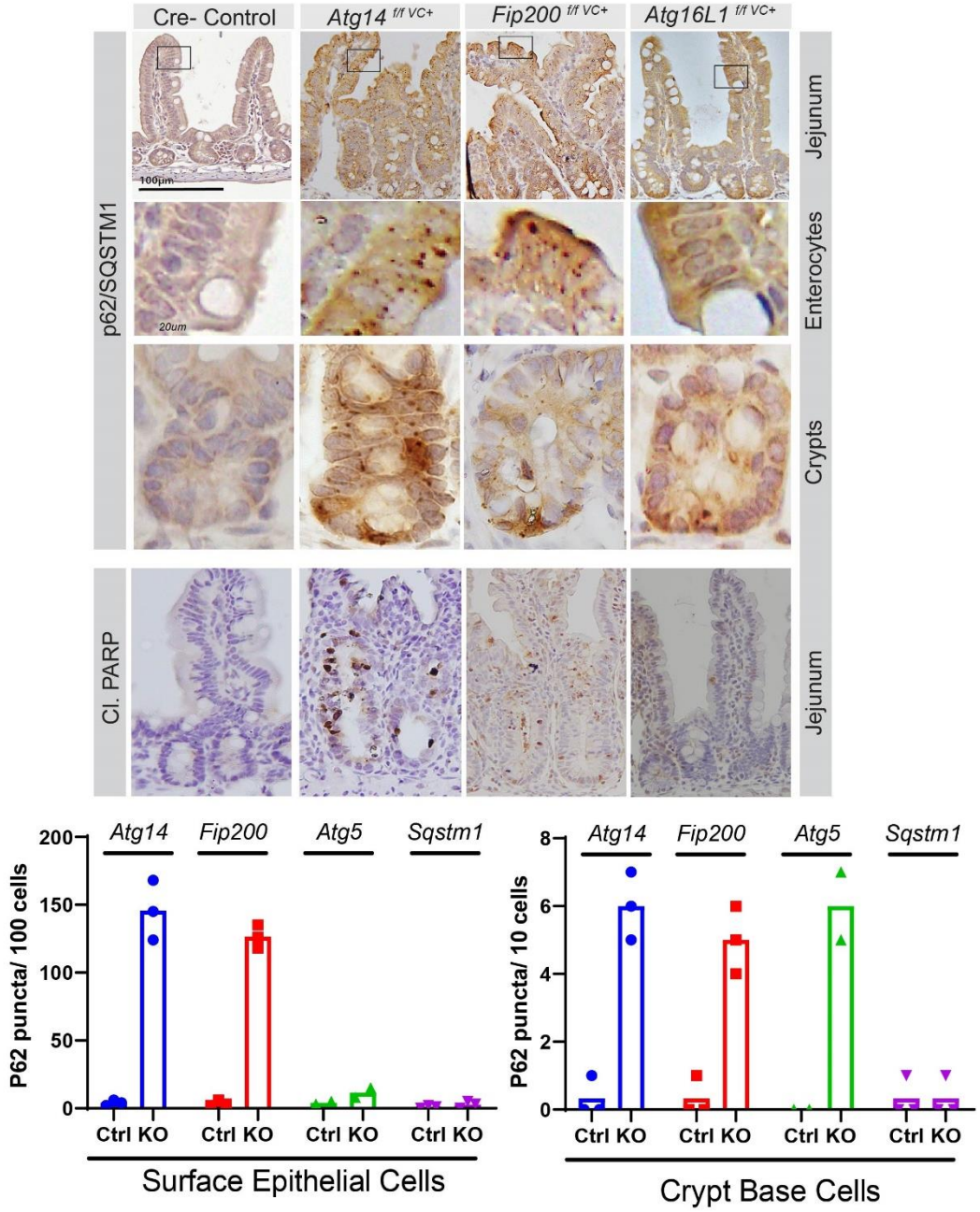

Representative immunohistochemistry for Sqstm1/p62 in small intestine of indicated autophagy KO mice. Genotypes with p62 accumulation in the surface epithelium correlate with genotypes sensitive to cleaved PARP+ cell death in the surface epithelium. *Fip200*, *Atg16L1*, and *Atg14* images each represent distinct autophagy core complexes for canonical degradative autophagy.

Representative images demonstrate the presence of punctate structures within the surface epithelium of

Atg14 and *Fip200*, but not *Atg16L1* conditional KO nor control mice. N>5 mice per genotype

Representative images demonstrate the presence of punctate structures within the crypt base of *Atg14*, *Fip200*, and *Atg16L1* conditional KO, but not control mice. N>5 mice per genotype

Representative images demonstrate the presence of cell death via cleaved PARP staining of the surface epithelium of *Atg14* and *Fip200*, but not *Atg16L1* conditional KO nor control mice. N>5 mice per genotype. Quantification of p62 puncta within the surface epithelium or the crypt base. N=3 mice,

Figure 23 Schematic for the generation of a novel immortalized mouse jejunal epithelial cell line

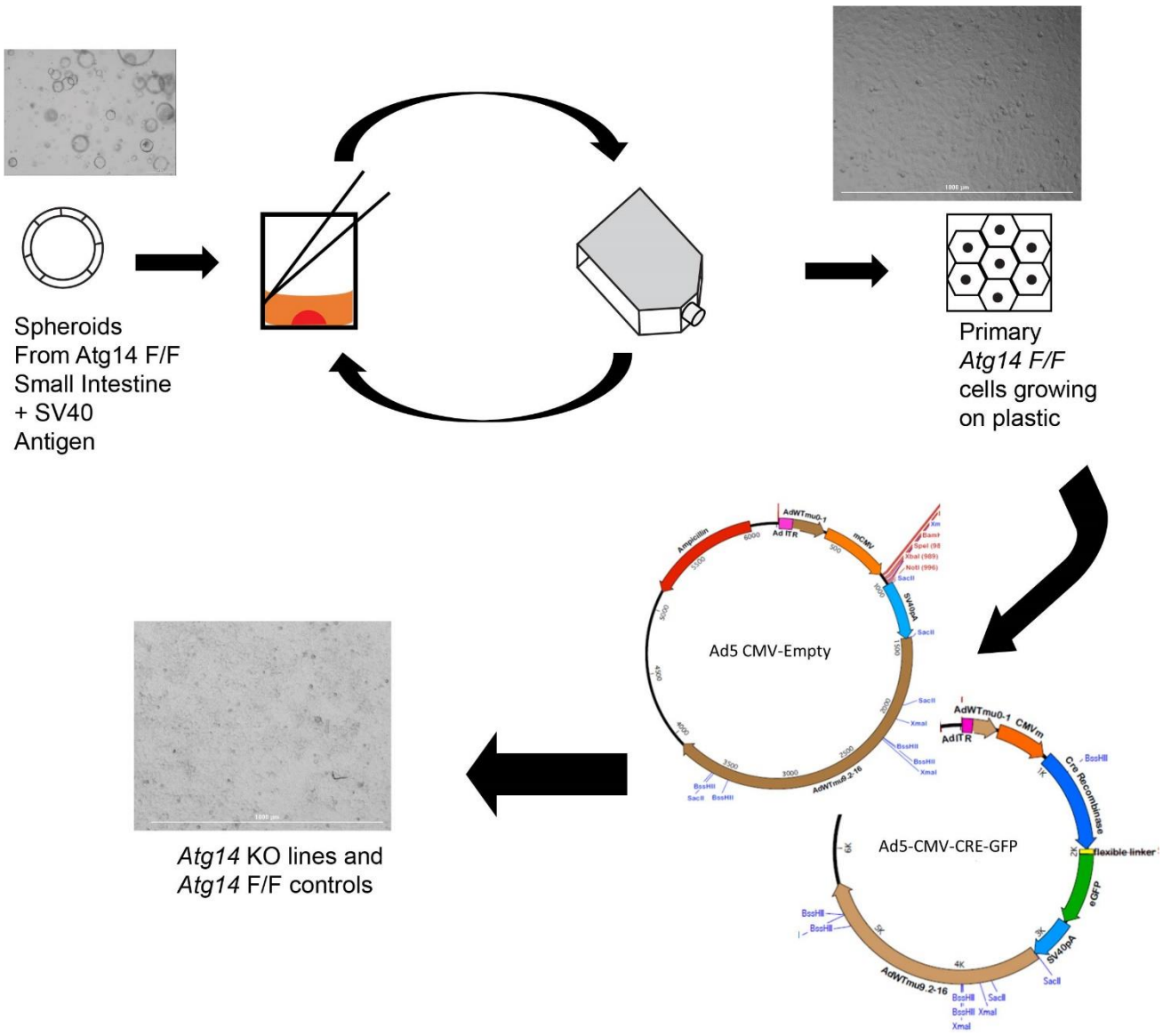

Cells amenable to biochemical analysis are generated from jejunal spheroids of *Atg14* $^{f/f}$ mice. Cells were transduced with a lentivector encoding the SV40 antigen. Positive clones were selected and grown under alternating cycles of culture in matrigel or tissue-culture treated plastic dishes. Clones were selected on the basis of preferential monolayer growth. Transduction by Ad5-CMV-empty or Ad5-CMV-CRE-GFP was performed to excise the floxed *Atg14* allele. Validation by sequencing and immunoblot.

Figure 24 P62 accumulates as puncta within spheroids and immortalized cells

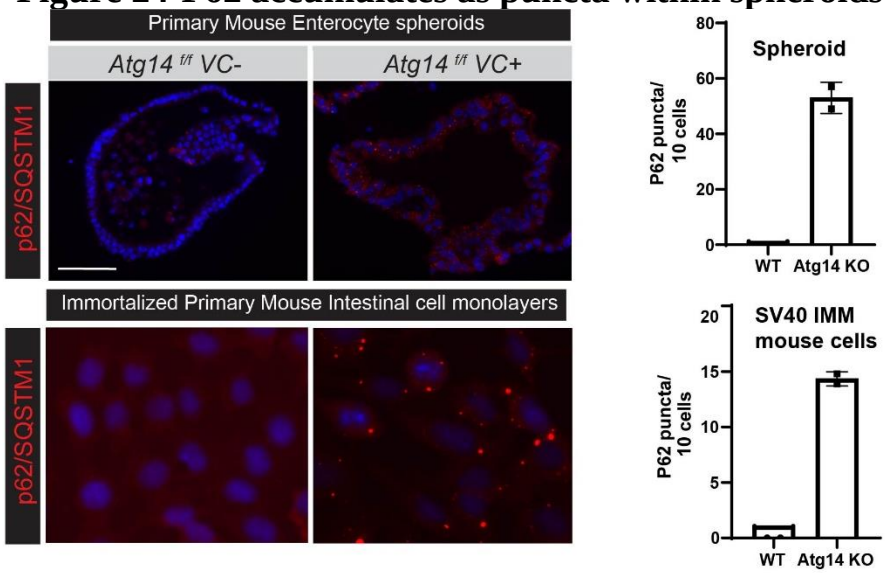

Both Spheroids and immortalized mouse cells accumulate large puncta of p62 upon deletion of *Atg14*. Representative images (left) 5um sections of enterocyte differentiated spheroids (upper) and of monolayers of SV40 immortalized jejunal cells grown on a glass chamber slide (lower). Quantification (right) of the number of puncta per 10 cells data point indicate mean number of puncta +/- SD.

Figure 25 Immortalized mouse cells phenocopy spheroids with respect to TNF-triggered cell death

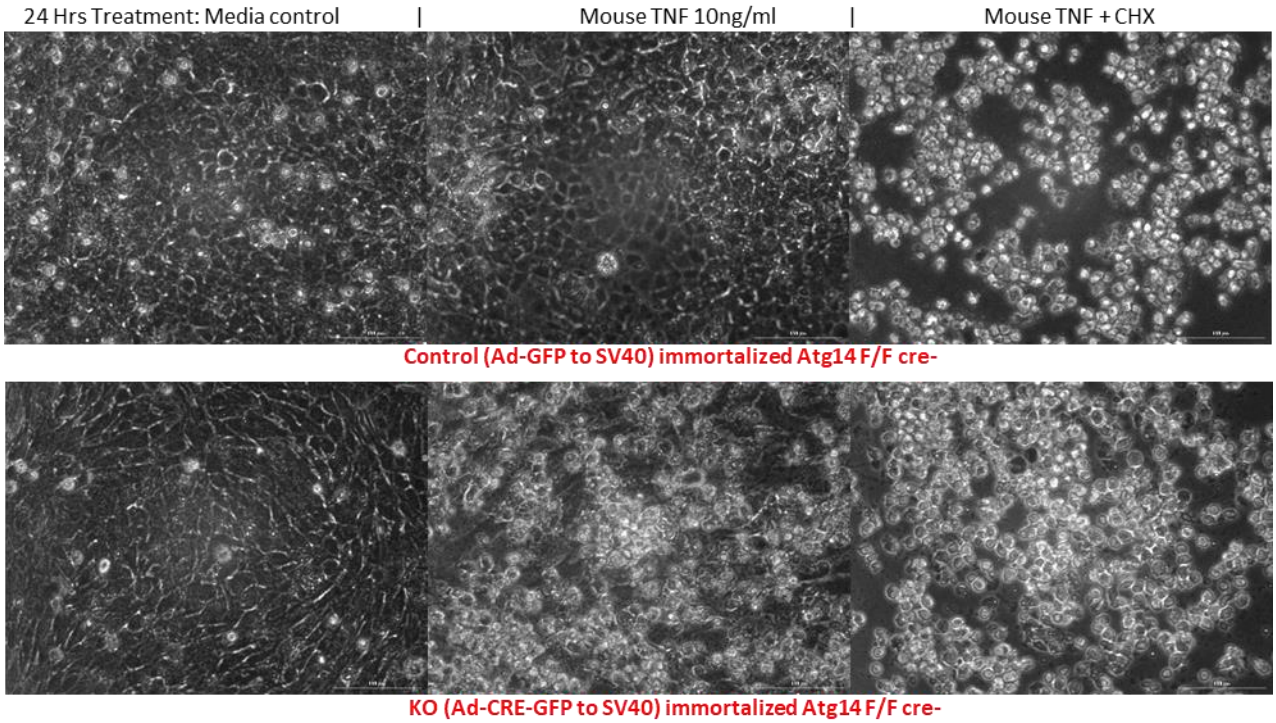

SV40 immortalized jejunal cells were grown to 90% confluency and treated for 24 hours with either 10ng/ml Mouse TNF, 10ng/ml mouse TNF with 50ug/ml CHX, or media control. Cells were imaged under a 20x phase contrast objective. White colored objects indicates cells that are dead or dying and are being extued into the media. Mouse TNF induces a qualitative increase dead cells within the KO group treeated with TNF, relative to controls and control cells administered TNF. Similar to mouse spheroids, minimal cell death is visualized in cells in the absence of TNF. TNF+ CHX represents positive control for cell death. Scale bar: 100um.

Figure 26 Immortalized mouse cells phenocopy spheroids with respect to TNF-dose dependent loss of viability

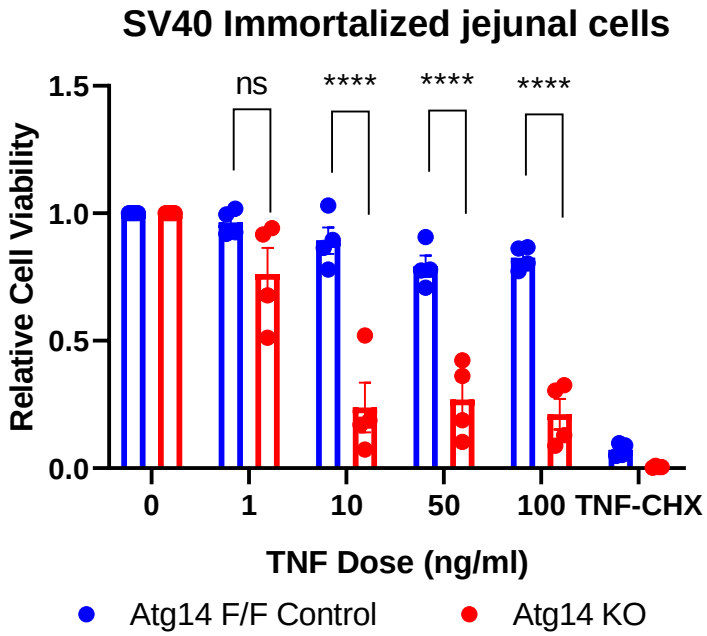

SV40 immortalized jejunal cells demonstate a dose dependend decreas in cell viability relative to controls. Cells were treated for 24 hours with the indicated dose of mouse TNF or with 10ng/ml mouse TNF with 50ug/ml CHX. Cell Viability was measured by Cell Titer Glo Assay. N=4 experiments.

Figure 27 P62 is activated to bind polyubiquitin and mediate selective autophagy

A

[M+H]	m/z	z	Δm ppm	Ret Time Min	Site	Sequence	Xcorr Score			
							Sample 1	Sample 2	Sample 3	Sample 4
2537.1	846.387	3	0.14	104.3	S405	LIESLSQMLpSMGFSDEGGWLTR	-	-	-	3.04
2553.14	851.7203	3	2.48	101.0948	S405	LIESLSQMLpSMoGFSDEGGWLTR	-	-	4.71	5.32

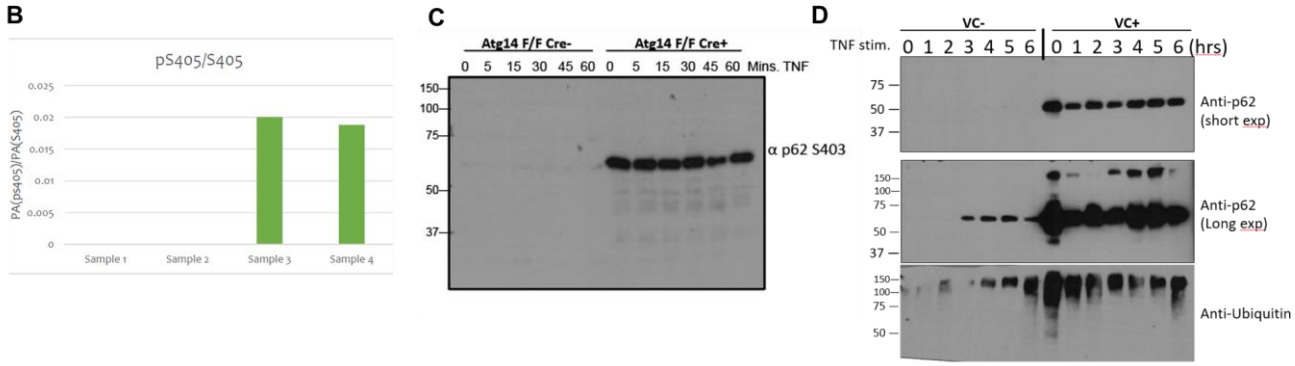

A-B) Mass spectroscopy data identifying the presence of a phospho-peptide in p62 corresponding to S405 (equivalent to human S403) in Atg14 KO cells. Sample 1: control cells, no TNF; Sample 2: control cells, + TNF; Sample 3: *Atg14* KO cells, no TNF; Sample 4: *Atg14* KO cells, + TNF C) immunoblot validation of phospho p62 S403/S405 D) increased abundance of p62 and ubiquitin in *Atg14* deficient cells relative to controls

Figure 28 Localization of p62 by TEM within vesicles adjacent to cell death factors

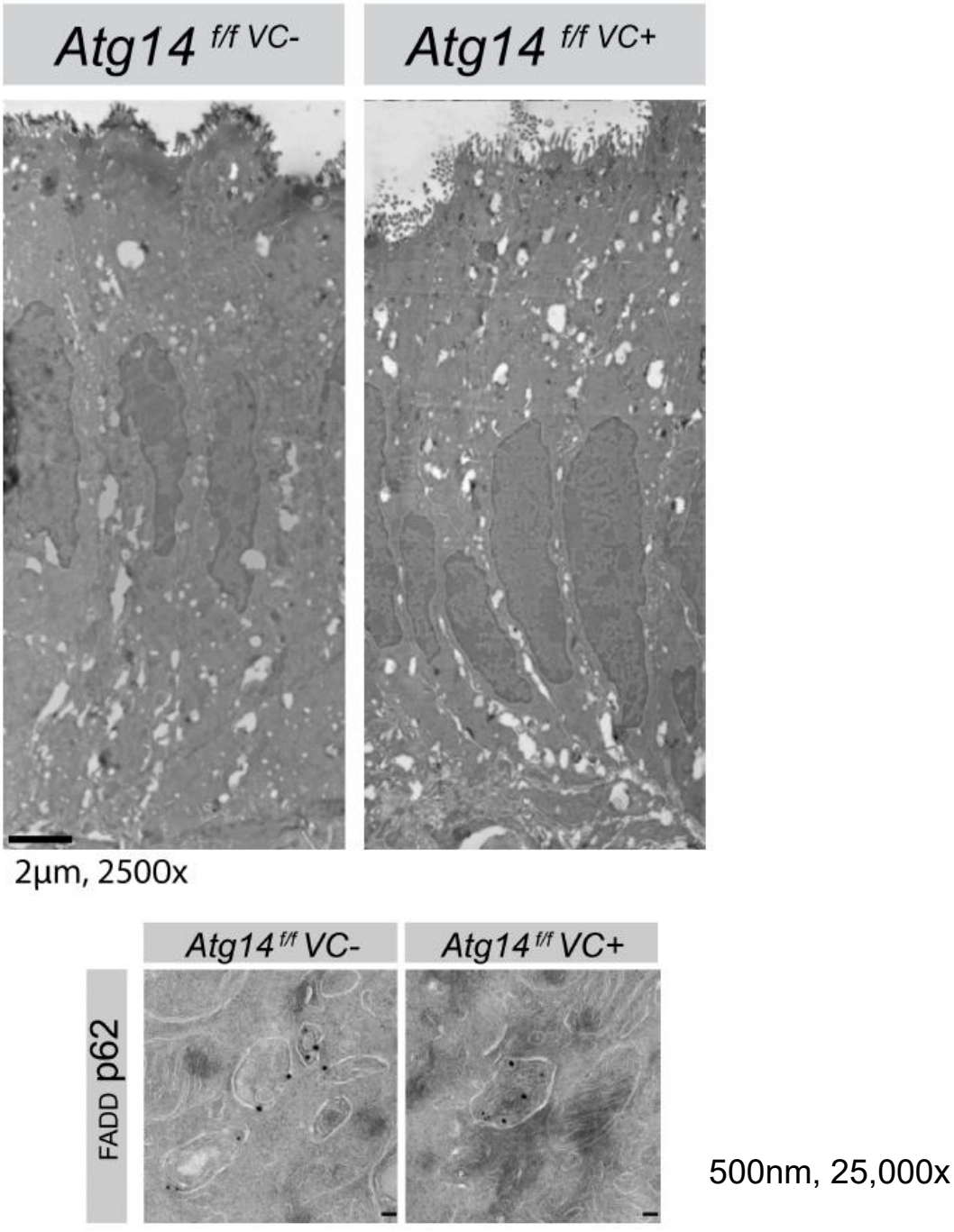

Representative transmission electron micrographs from fixed frozen mouse jejunal tissue. Upper images demonstrate increases in electron lucent vacuolar/vesicular structures in Atg14 KO tissue relative to that of control. Lower panel indicates association of p62 and a cell-death factor in a common vesicular structure 12nm: FADD, 18mm: p62. Magnification and scale bar length listed.

Figure 29 Identification of caspase-8 puncta within enterocytes

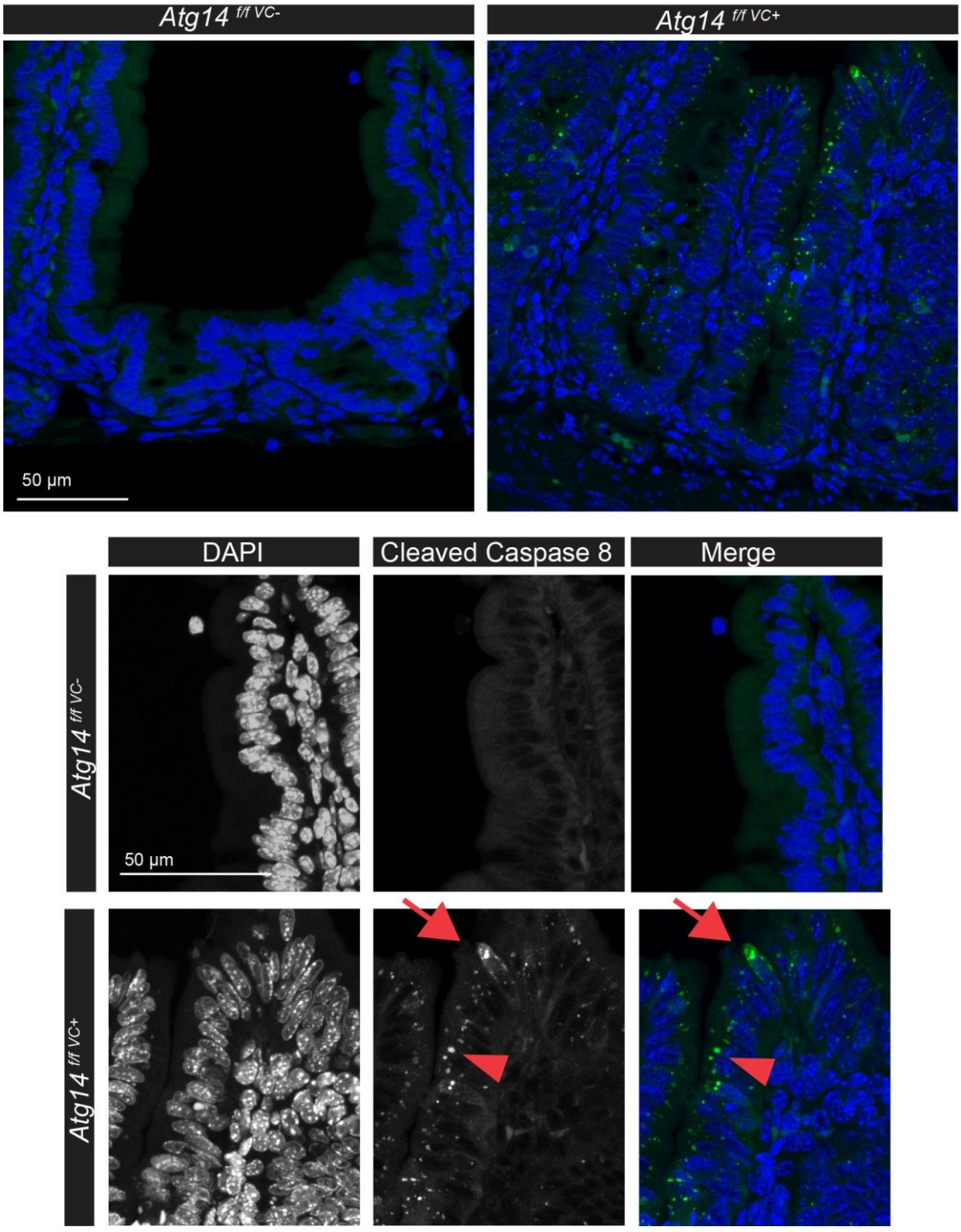

Representative confocal images of jejunal tissue from indicated mice. Arrowheads show discrete punctate staining for CASP8 without cytoplasmic staining, consistent with self-processing of CASP8 to the p43 primed spatially restricted isoform. Arrows indicate cells with cytoplasmic CASP8 indicative of p18/p10 processing and activation of the caspase cascade. No puncta were observed within the littermate control tissue. N>5 mice, with 8 fields captured per mouse.

Figure 30 Caspase-8 co-localizes with both p62 and ubiquitin

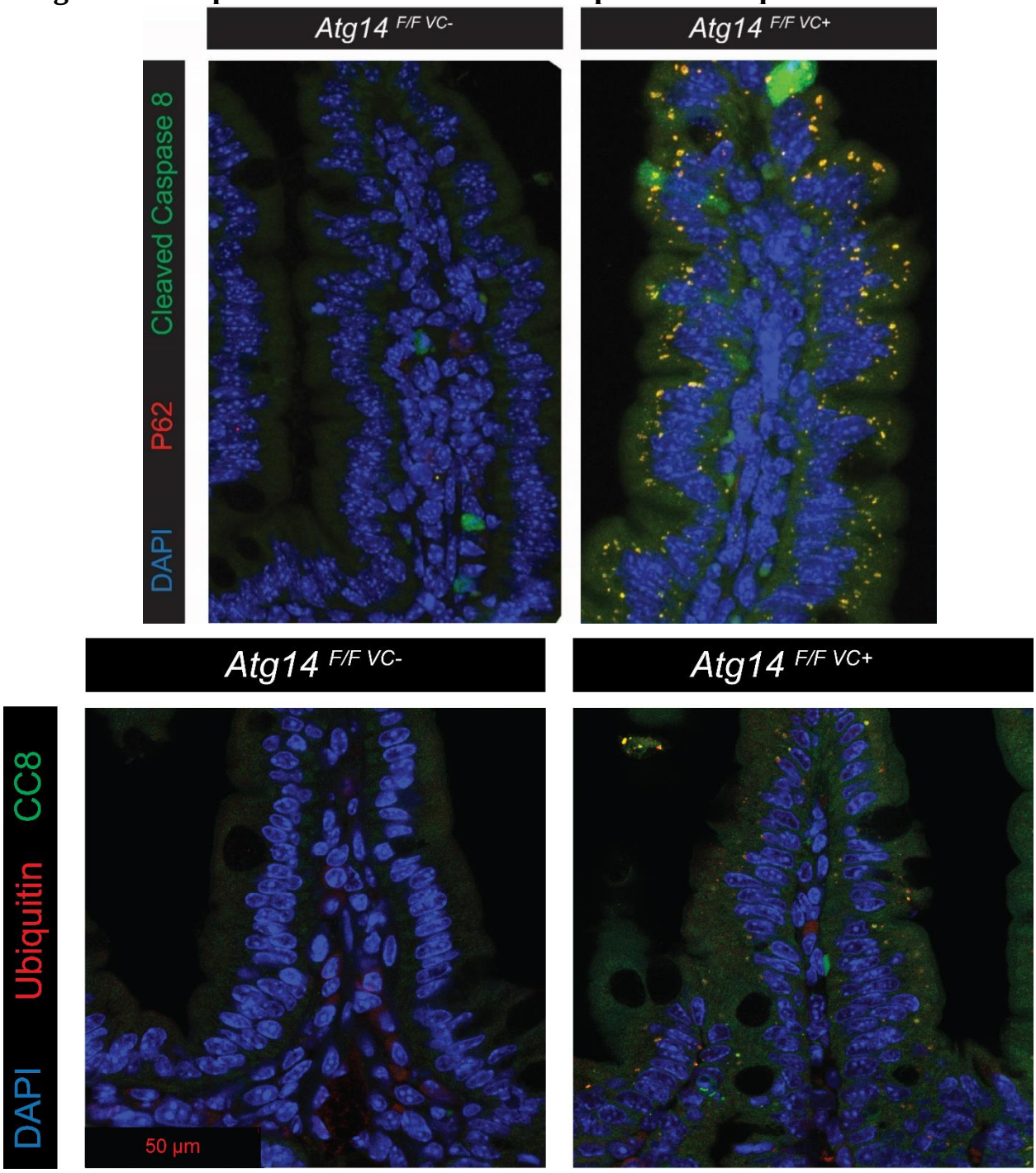

Representative confocal images of jejunal tissue from indicated mouse genotypes to assess co-localization of markers of cell death with markers of autophagy or ubiquitin. Punctate structures are observed among *Atg14* deficient tissue sections, but not in control tissues. N>5 mice, with >5 fields captured per mouse.

Figure 31 Differences in endosomal markers, but not lysosomal markers in tissue by immunofluorescence

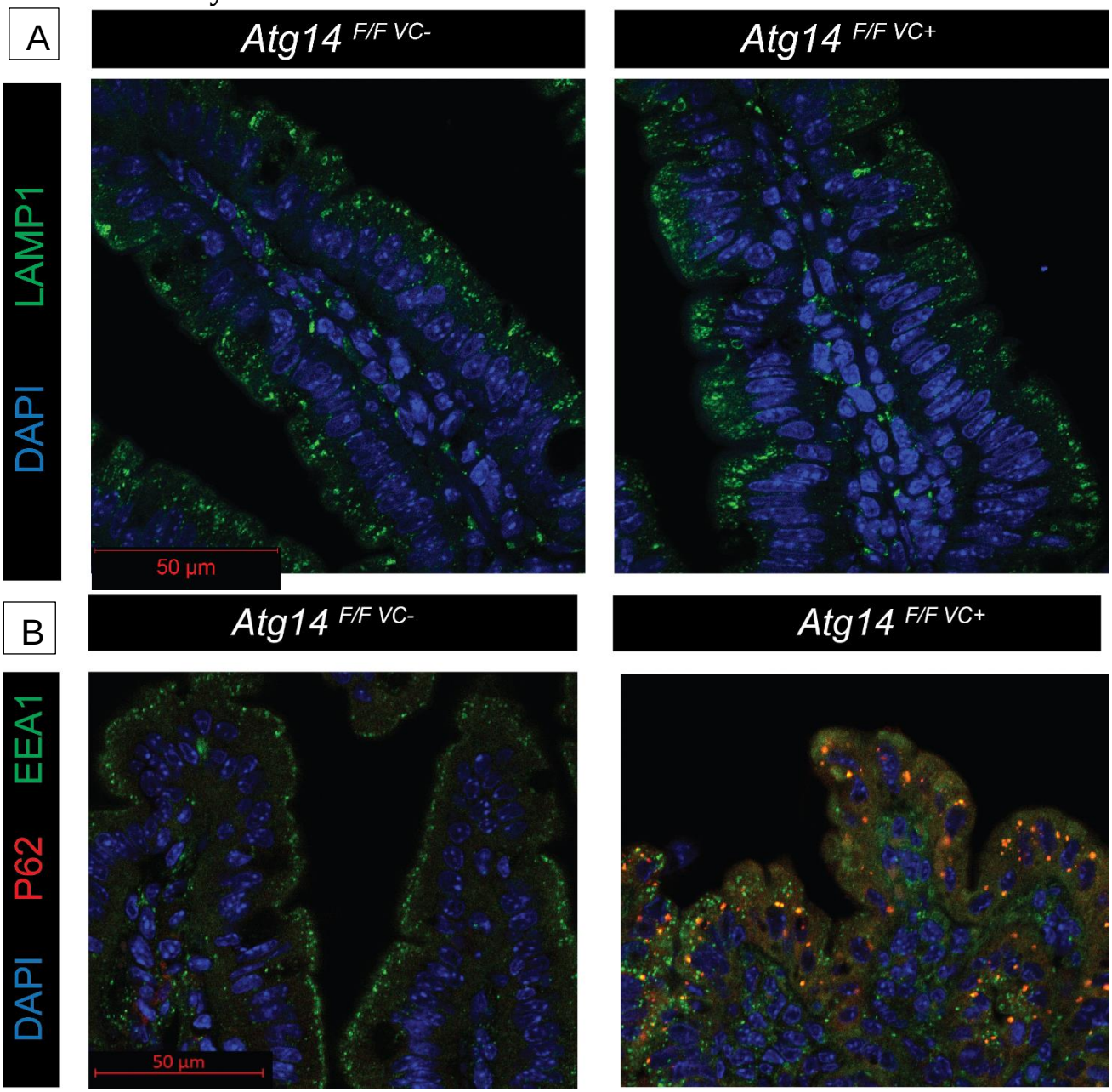

A) Representative confocal images of jejunal tissue from indicated mice from indicated mouse genotypes to assess A) relative abundance of lysosomes, the terminal vesicles of the autophagic cascade. No qualitative changes in lysosome abundance is observed between Atg14 deficient and control tissue sections.
B) Representative image to assess co-localization of the autophagy receptor p62 with an early endosomal marker, EEA1. Partially colocalization is observed N>5 mice, with >5 fields captured per mouse.

Figure 32 Schematic of *Atg14* full-length and truncation complementation constructs

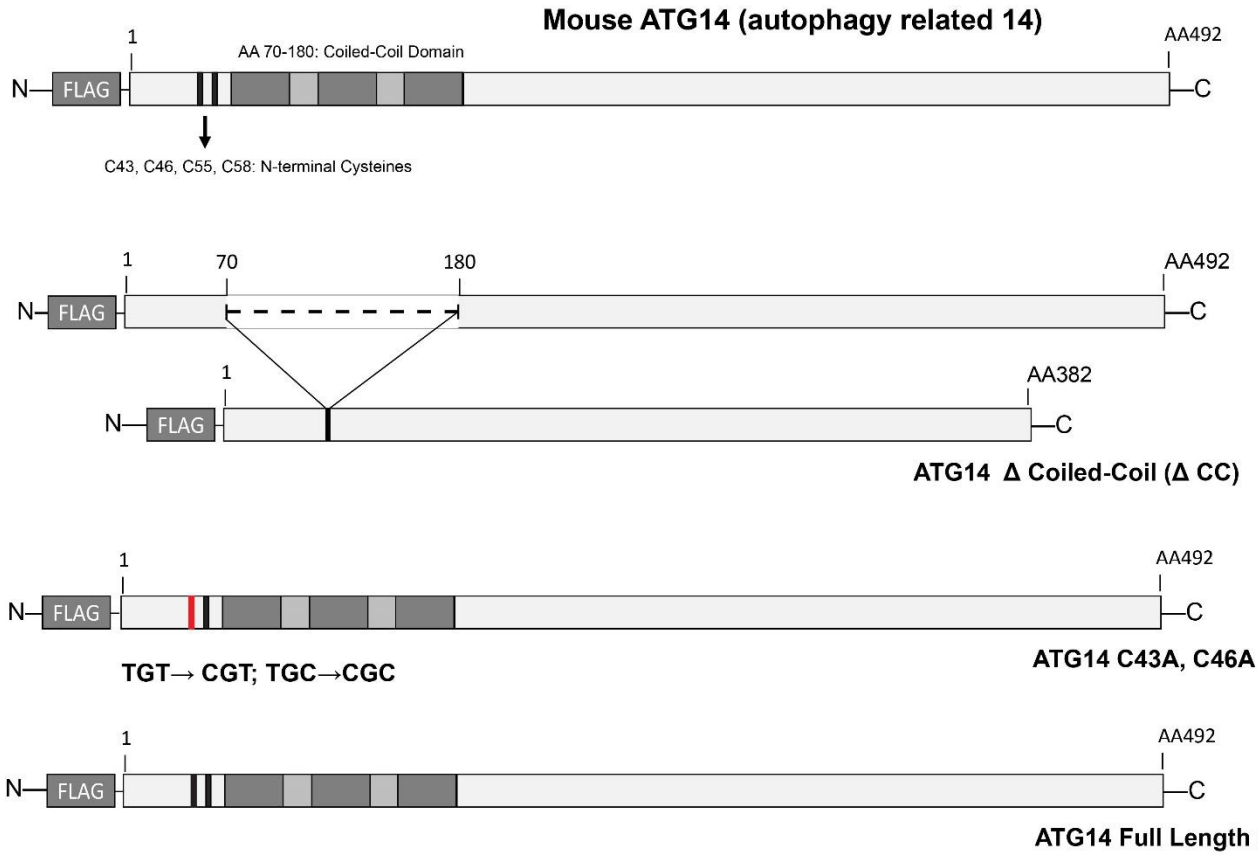

Schematic of the expression constructs to used complement *Atg14* deficient cells. Full-length mouse Atg14 contains two pertinent domains: 4 N-terminal cysteine residues that promote a role for Atg14 in the fusion of vesicles with the lysosome. Of these 4 residues, C43 and C46 are required, while C55 and C58 are dispensable. The coiled coil domain is the conserved domain required for heterodimerization with Beclin-1 to direct the activity of the lipid kinase that is require for the initiation (nucleation step) of autophagy. Full length Atg14 was also used as a rescue control.

Figure 33 Response of *Atg14* complementation mutants to TNF dose curve

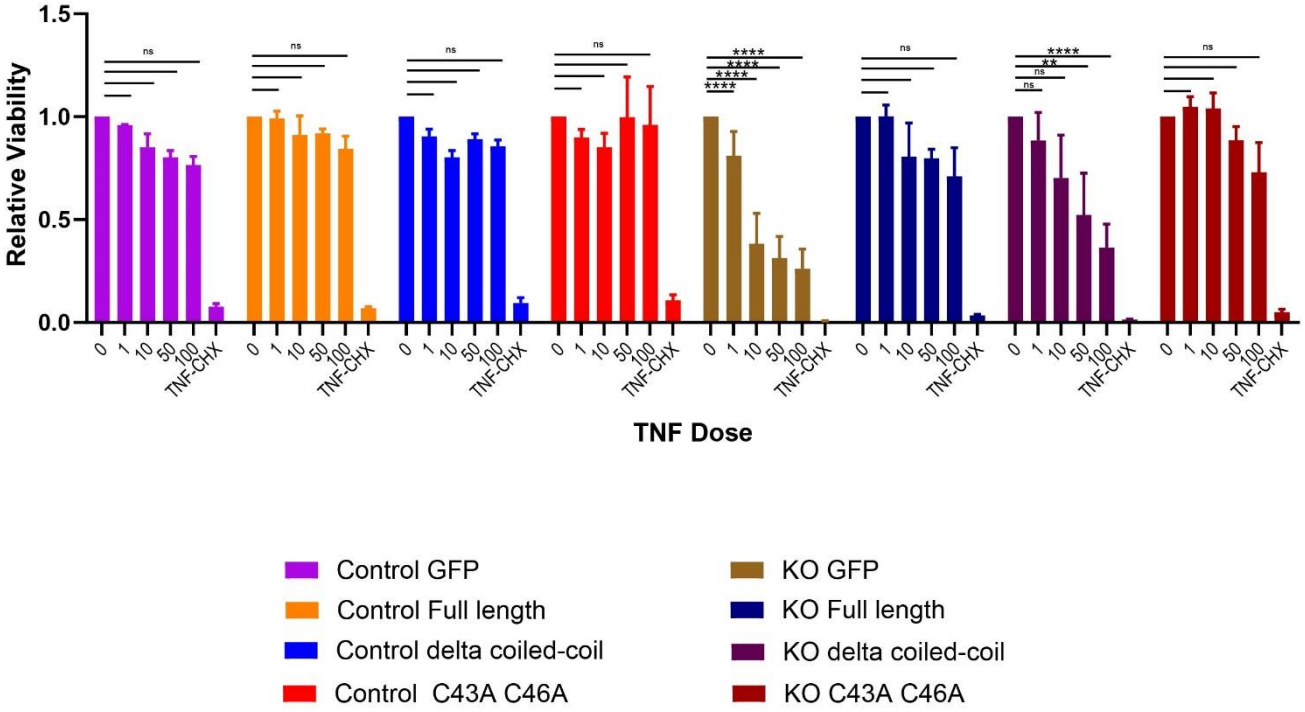

Functional test of the rescue of *Atg14* KO cells by full-length *Atg14*, delta-coiled-coil *Atg14*, and C43A, C46A *Atg14* or *GFP* control. Expression constricts were transduced and a stable population was selected by puromycin. Cells were treated in indicated doses of mouse TNF for 24 hours or with 10ng/ml mouse TNF with 50ug/ml CHX. Cell Viability was measured by Cell Titer Glo Assay. N=4 experiments.

Figure 34 Response of Atg14 complementation mutants to TNF

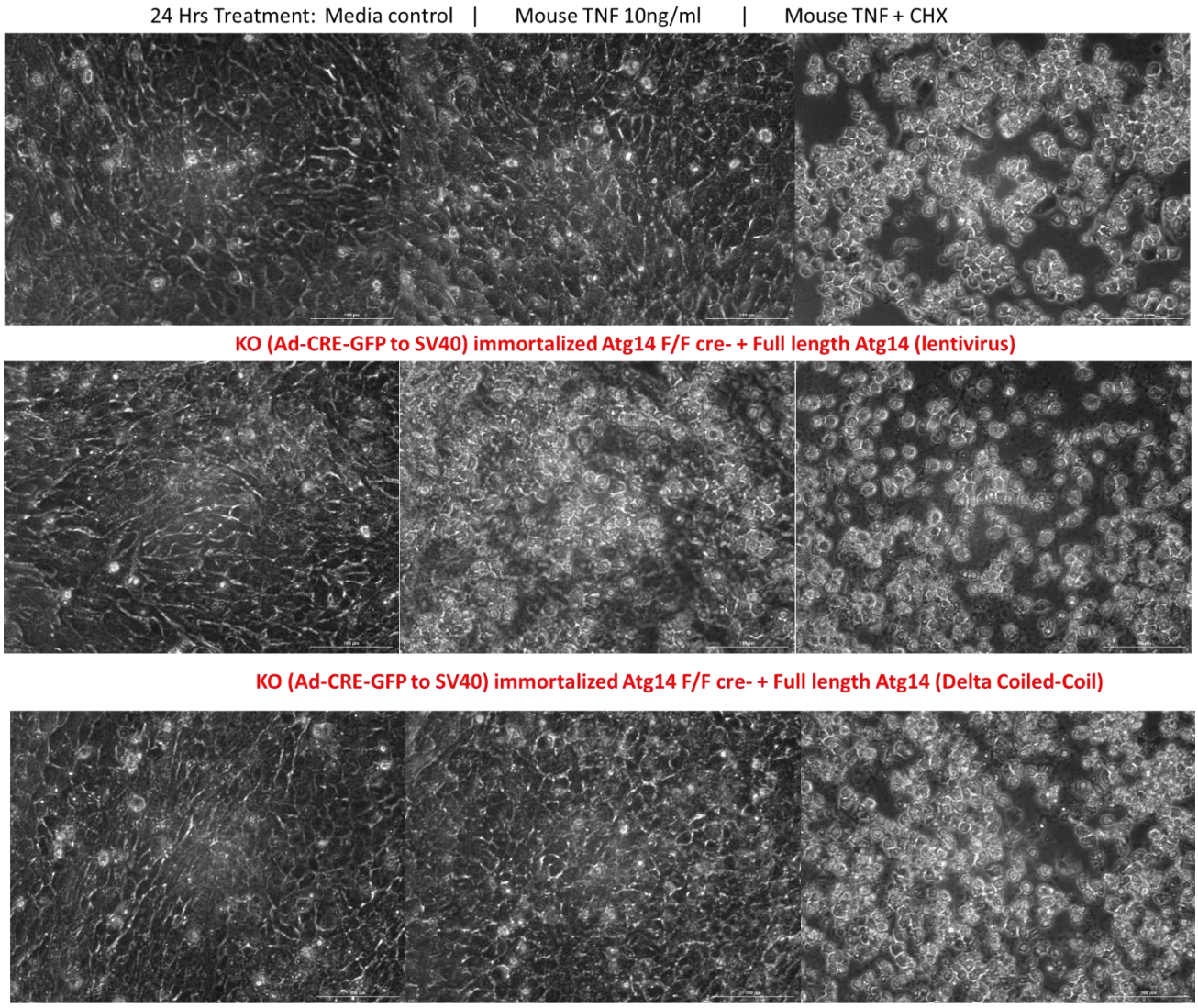

SV40 immortalized jejunal cells were grown to 90% confluency and treated for 24 hours with either 10ng/ml Mouse TNF, 10ng/ml mouse TNF with 50ug/ml CHX, or media control. Cells were imaged under a 20x phase contrast objective. White colored objects indicates cells that are dead or dying and are being extued into the media.. TNF+ CHX represents positive control for cell death. Scale bar: 100um.

Cell lines shown here include *Atg14* Ko cells transduced with either A) full length Atg14 (upper) B) Delta Coiled-Coil Atg14 (middle) or C43A, C46A Atg14 (lower) . Mouse TNF induces a qualitative increase in cell death within the Delta Coiled-Coil complementation group [no rescue], but not among the full length or the C43A, C46A complementation groups [rescue].

Figure 35 Generation of Atg14 $^{F/F}$; VC+; Sqstm1 $^{-/-}$ mice and controls

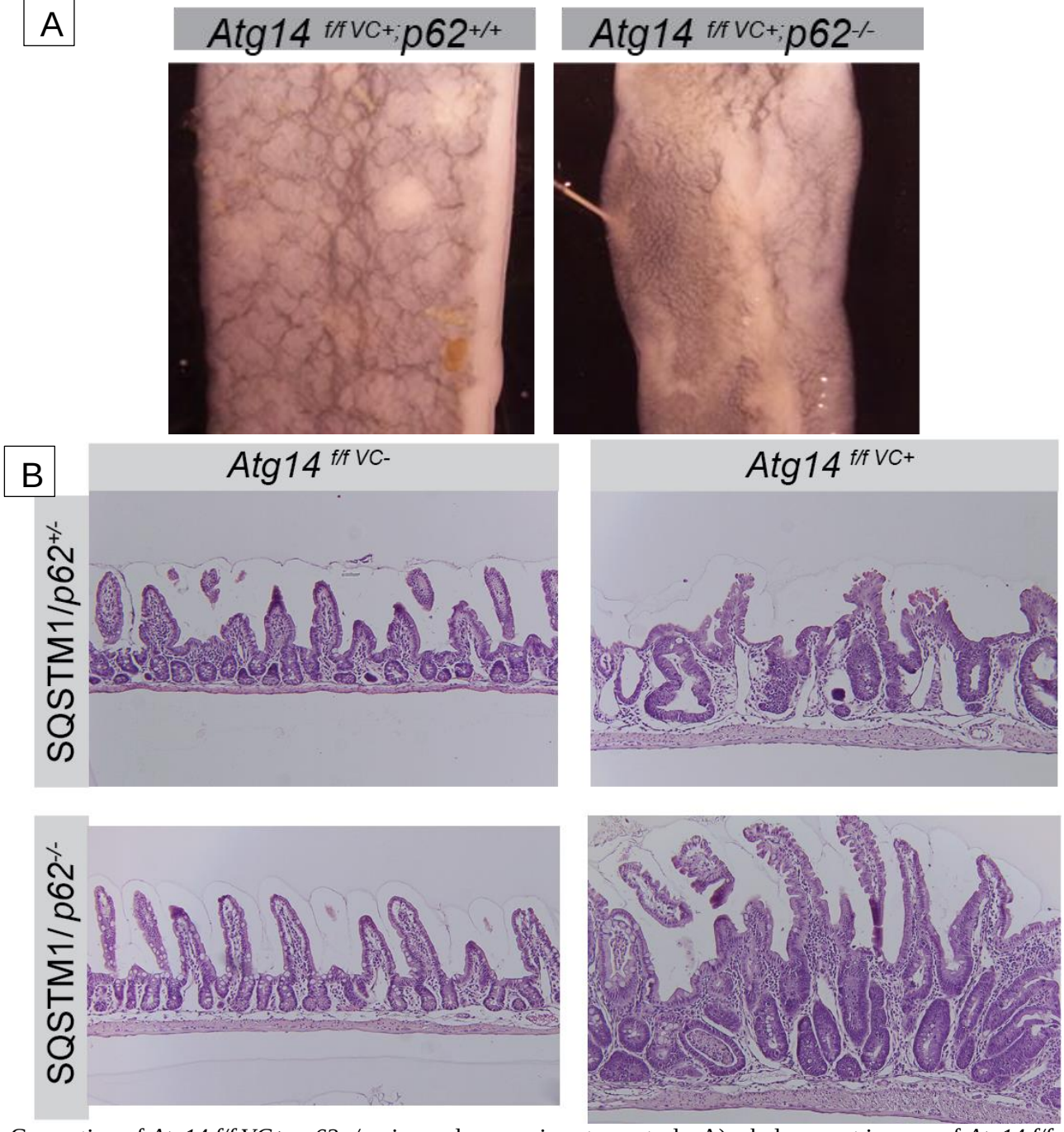

Generation of *Atg14 f/f VC+; p62 -/-* mice and comparison to controls. A) whole mount images of *Atg14 f/f VC+* (left) demonstrating patchy regions of confluent villus loss; images of *Atg14 f/f VC+; p62 -/-* mice (right) with increased abundance of villus rescue and limited regions of villus loss
B) Histological (H&E) sections taken from the mid-small intestine from mice with the indicated genotypes. *Atg14* sufficient mice with loss of p62 (left) retain repeating units of villus-crypt architecture. *Atg14* deficient mice (upper right) demonstrate villus loss, crypt elongations, and features of crypt dropout. *Atg14 f/f VC+; p62 -/-* mice (lower right) demonstrate villus retention with columnar surface epithelium. Villi are abnormal and crypts are elongated, but there is reduced evidence of crypt dropout.

Figure 36 Cell death in Atg14 F/F; VC+; Sqstm1 -/- mice and controls

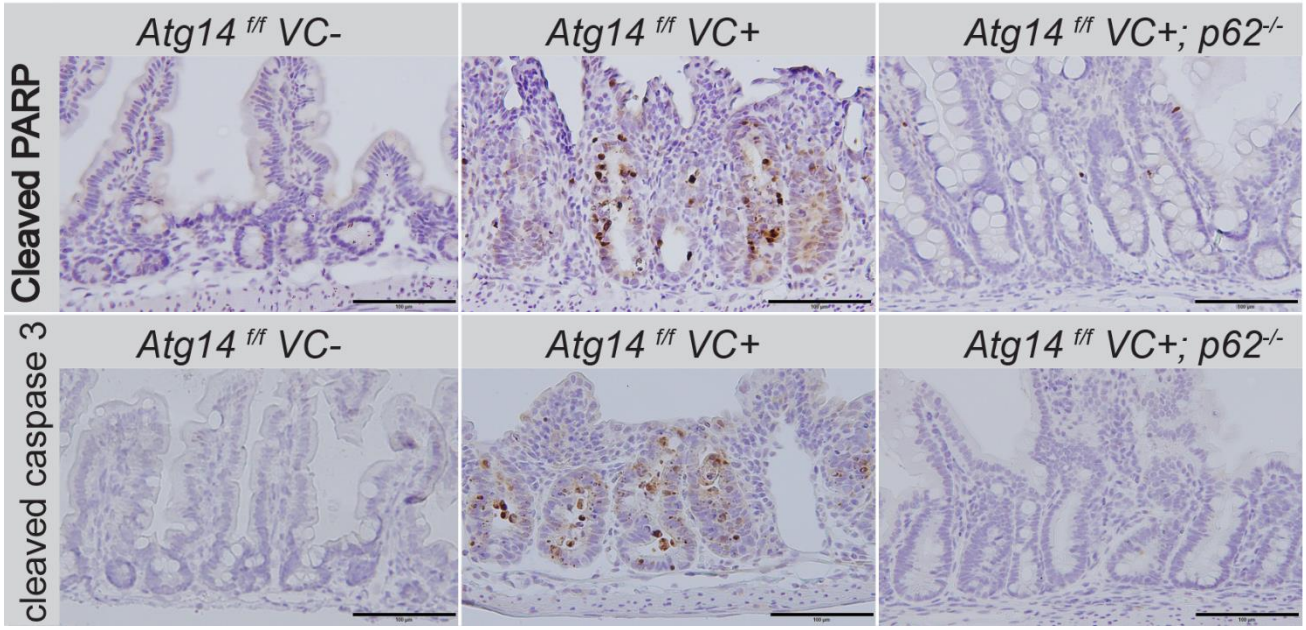

Representative histological sections of control, *Atg14* deficient, and *Atg14 f/f VC+; p62 -/-* mice from the midpoint of the small intestine. Section were immunohistochemically stained for 2 markers of cell death: Cleaved PARP (upper) and Cleaved Caspase-3 (lower). A reduction in epithelial cell death markers are visible among double knockout animals relative to single knockout animals, despite retained defects in crypt and villus architecture. Bar=100um

Figure 37 Cell death in Atg14 F/F; VC+; Sqstm1 -/- Spheroids and controls

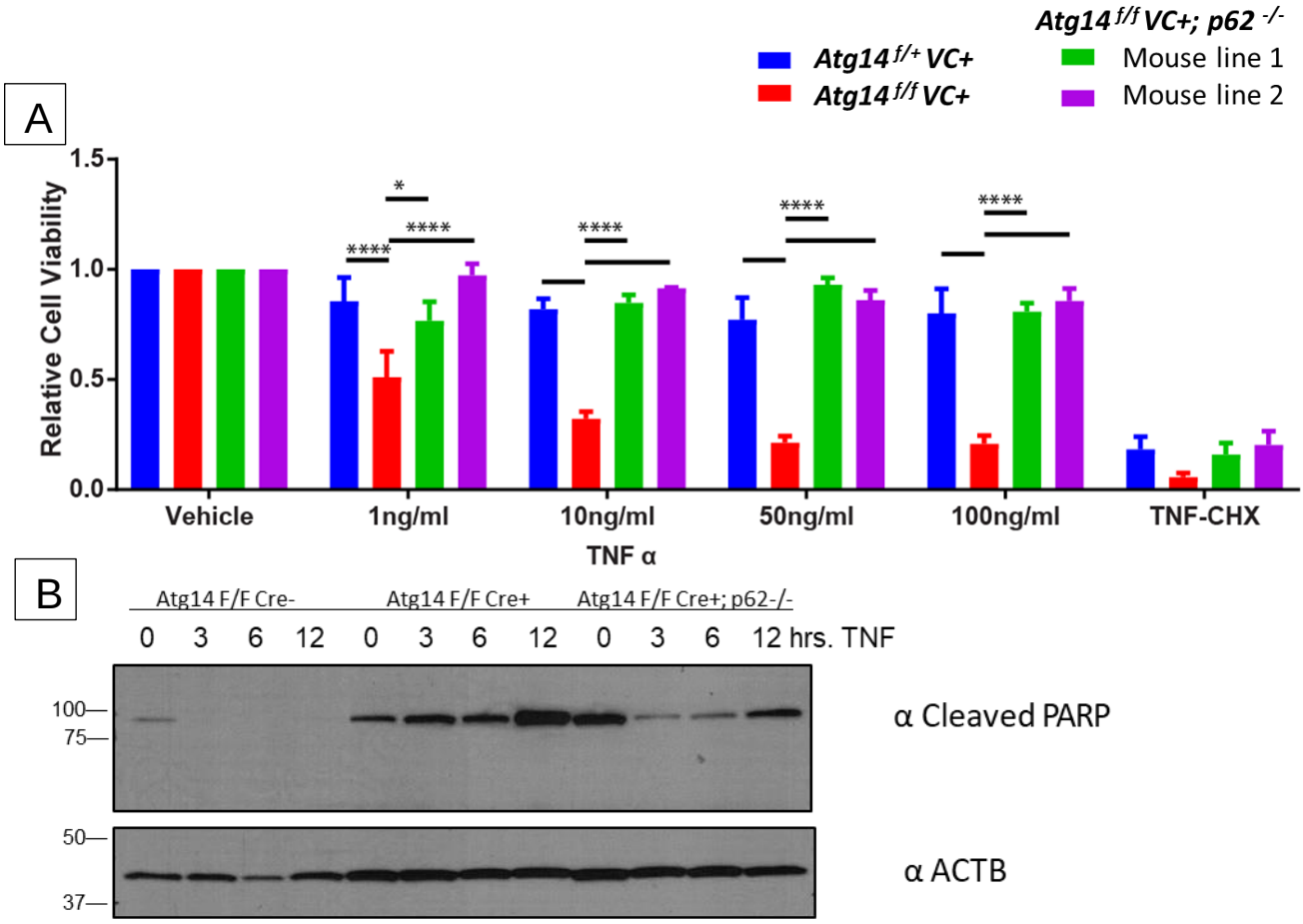

Spheroids isolated from *Atg14 f/f VC+; p62 -/-* mice demonstrate reduced cytotoxicity after TNF treatment relative to *Atg14 f/f VC+* cells. A) Spheroids isolated from the mid-small intestine from two separate *Atg14 f/f VC+; p62 -/-* mice were maintained alongside small intestinal spheroids from *Atg14 f/f VC+* and *Atg14 f/f VC-* mice. Cells were treated with indicated dosages of mouse TNF for 12 hours or with 10ng/ml mouse TNF with 50ug/ml CHX. Cell Viability was measured by Cell Titer Glo Assay. N=3 experiments. two-way ANOVA, Sidak post-test. *P<0.05, **P<0.01, ****P<0.0001. B) representative immunoblot for Cleaved PARP, substrate of caspase activation, demonstrating rescue of cell death after p62 deletion.

Figure 38 Model for the interaction between p62 and the cell death machinery

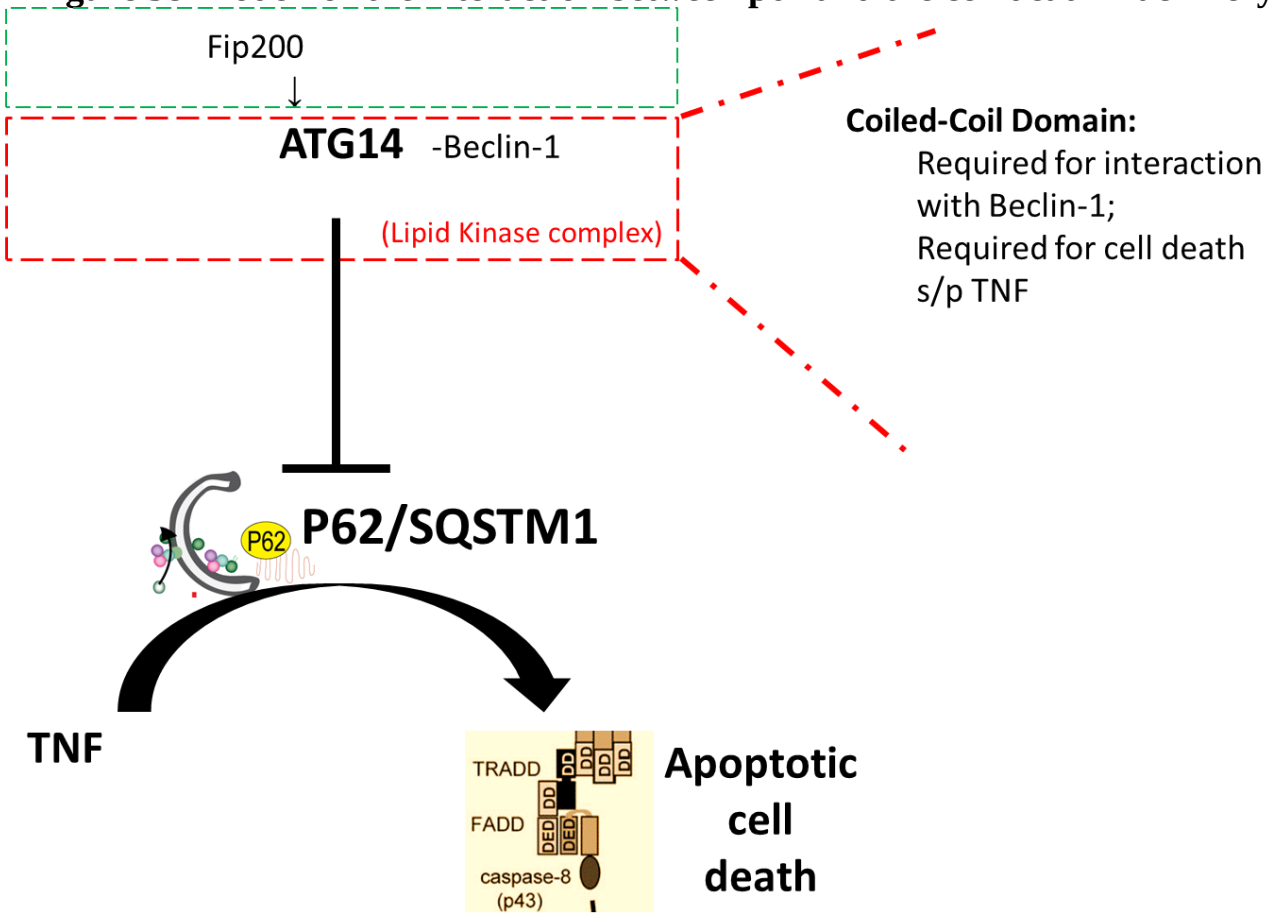

Atg14 and Fip200 are required for protection from cell death. Atg14 requires its Beclin-1 canonical autophagy interaction domain to protect the intestinal cell from TNF triggered death. P62 is a factor that is preferentially abundant in TNF sensitive cells, therefore, the working hypothesis is that p62 puncta potentiates the activation of caspase-8 upon TNF stimulation.

Chapter 4:

Future directions: Divergence of the cell death response among autophagy-deficient human and mouse cells

In this chapter I present work in progress that ATG14 deficient human cells, unlike mouse cells, are not sensitive to TNF-triggered death. My overarching hypothesis is that the master caspase regulator, CFLAR/CFLIP drives the differences in sensitivity between human and mouse cells. This work addresses the questions, "What is the significance of autophagy deletion to cell death within the human intestinal epithelium?" Data in this chapter outlines the generation and validation of new ATG14 deficient human cell lines. It also demonstrate that wild-type mouse cells, *Atg14* deficient mouse cells, and *ATG14* deficient human cells each express different forms of cFLIP upon TNF stimulation. Taken together, I proposed a model hypothesize that stalled autophagy scaffolds containing Sqstm1/p62 are necessary for the formation of a death complex, but that human cell expression of a protective splice isoform of CFLIP, represent an evasion mechanism to constrain the DISC and prevent inappropriate activation of the cell death pathway.

4.1 Abstract

Models of intestinal injury seek to recapitulate the pertinent features seen within human physiology and pathophysiology. The pathology of the intestine during inflammatory bowel disease is noted for a small, but significant increase in cell death, a phenotype which is rescued through neutralization of signaling through the cytokine TNFα [51] . Meanwhile, loss of function mouse models for intestinal autophagy, a pathway associated with Crohn's disease, demonstrate that autophagy controls the switch between survival and death pathways downstream of TNF signaling [9, 50, 70]. However, it remains unclear the degree to which human cell death, TNF, and autophagic pathways are sufficiently conserved to facilitate the same degree of inter-pathway crosstalk that causes mouse cells to be sensitive to TNF-triggered apoptosis. Here, we generate *ATG14* deficient human cell lines: HeLa, Caco-2, HEK 293T, and primary human ileal lines, and characterize their response to TNF triggered apoptosis. Results from HeLa cells are presented. In contrast to both mouse primary untransformed and immortalized intestinal epithelial cells, HeLa cells did not demonstrate a significant increase in cell death in response to TNF treatment. These cells were defective in autophagy, as measured by increases in Sqstm1/p62 puncta formation, but loss of autophagy was insufficient to induce cell death. To define the point of divergence between mouse and human, a candidate approach was taken to assess the TNF and cell death pathways in human and mouse cells. From this study we identified a unique post-transcriptionally modified form of Cflar/Cflip, expressed only in autophagy deficient mouse cells, not in wild-type controls. Furthermore, human cells express yet a different isoform of CFLAR that is associated with protection from cell death. Further work is needed to functionally test these correlations through both loss of function and gain of function experiments with cFLIP in human and mouse cells. The implication of these findings are broad: autophagy intersects with TNF in a very precise manner, and the crosstalk between pathways have a strong dependence

upon the cell type and species under investigation.

4.2 Introduction

Cell death is observed within the intestine of patients with inflammatory bowel disease, and treatment of such patients with anti-TNFα antibody therapy reduces cell death [153]. These findings are consistent with the hypothesis that TNF triggers apoptotic cell death in the context of intestinal disease. It is still unclear the extent to which the human intestinal epithelium is susceptible to death during health and disease, what mode of cell death occurs, and what factors provoke and palliate cellular turnover.

Multiple mouse models of colitis also induce epithelial cell death and barrier dysfunction, leading to translocation of luminal contents across the epithelial barrier, and induction of inflammation [154]. Likewise, single nucleotide polymorphisms in autophagy factors, namely *ATG16L1* T300A have been modeled in mouse and have successfully recapitulated the morphological and functional defects seen in human Paneth cells, antimicrobial defense cells localized to the crypts of Lieberkühn. [155]

Defects in autophagy have been shown by multiple groups, including ours, to enhance the sensitivity of the intestinal epithelium to TNF triggered death [67-70, 108]. These mouse loss-of-function models provide compelling genetic evidence that this conserved pathway is required for the selective clearance of the Death Induced Signaling Complex. However, multiple variables exist between human and mouse biology, including differentially expressed variants of the cell death effector proteins [156].

An open question in the field is the extent to which reductionist mouse models contribute to our knowledge of human pathways of TNF, cell death, and autophagy, and the extent to which our findings in mouse can improve our understanding of human disease and spur the development

of beneficial therapeutics. A candidate molecule that diverges between mouse and human is CFLAR/CFLIP, a master caspase regulatory protein that is differentially expressed between human and mouse cells [1]. CFLAR variants in human include full length (cFLIP-L, 55kDa), and a caspase-inhibitory/protective splice isoform (cFLIP-S, 23kda). Cflar variants in mouse include full length (cFLIP-L, 55kDa), a form that is cleaved by Caspase-8 (cFLIP-p43, 43kDa), and a caspase-protective that predominates in mouse strains other than C57BL/6 (cFLIP-R, 25kDa). Human CFLAR does not carry the caspase-cleavage motif that allows for catalytic processing to the cFLIP-p43 form [95].

In order to address these issues, we report the generation of multiple human *ATG14* deficient cell lines generated by CRISPR-CAS9 genomic editing. We report the results from the first of these cell lines, HeLa cells, which do not recapitulate the phenotype that is seen within mouse primary intestinal epithelial cells. While these cells are defective in autophagy and accumulate punctate structures of Sqstm1/p62, they express different splice isoforms of cFLIP in response to TNF stimulation. We provide characterization of Cflip protein abundance between human and mouse cells after TNF stimulation. Lastly, work-in-progress include experiments to functionally test the role of cFLIP splice isoforms by cross expressing human CFLIP-S (caspase-inhibitory) in mouse cells, and expressing mouse cFLIP-L (caspase permissive) in human cells.

Together, this work aims to define how autophagy, TNF signaling, and cell death are linked at the molecular level. Identification of the variances between human and mouse will inform future work to develop molecular-oriented therapies to modulate autophagy and cell death.

4.3 Materials and Methods

Cells:

Hela cell (CCL2, Wild-type) HEK 293T and Caco-2 (C2BBe1 clone, CRL-2102) were purchased from ATCC. To model the phenotype of the *Atg14* deficient jejunal enterocyte within a human cell, a postdoctoral fellow in the lab generated an *ATG14* knockout HeLa cell line utilizing the CRISPR-CAS9 approach. Wild-type HeLa cells were purchased from ATCC (Clone CCL2) and a gRNA Cloning Vector (addgene 41824) and a CRISPR Cas9-D10A Nickase Plasmid were transfected. Cutting was validated through A T7 Endonuclease I assay and single clones were isolated through limiting dilution plating. Clones were expanded and genetic knockout lines were screened by PCR and verified by sanger sequencing. Lines were validated for knockout by immunoblot against ATG14 antisera and secondarily validated for autophagic disfunction through Immunoblot against SQSTM1 antisera.

Additional HeLa clones, Caco-2 cells, and were generated by lentiviral transduction. Wild-type CCL2 HeLa cells were transduced with pLentiCRISPR v2 vector expressing one of three gRNA sequences. Positive selection was performed for 7 days under 1.5ug/ml Puromycin.

Protein BLAST analysis: Amino Acid sequences were obtained from UNIPROT and submitted as pairwise comparison to pBLAST in May 2020.

4.4 Results

4.4.1 Atg14 KO primary intestinal cells are uniquely sensitive to TNF-triggered death relative to ATG14 KO human transformed and cancer cell lines

Polymorphisms or mutations in the initiation and nucleation steps of autophagy (eg. ATG14 and RB1CC1/FIP200) have, to date, not been identified as risk factors for human Inflammatory Bowel Disease. Neither are these genes commonly associated with other manifestations of intestinal disease. However, in the mouse they are, of the genes tested, the most potent regulators of autophagic flux [27]. Their loss of function leads to the most potent sensitization to TNF-triggered apoptosis [70]. Therefore, we sought to define the contribution of autophagy initiation on human cell turnover and the cellular response to TNF.

In order to model the effect of the *ATG14* loss of function mutation in human cells we generated HeLa knockout lines through two approaches. In the first approach, CCL2 WT HeLa cells were transfected with both gRNA plasmid and a CAS9 D10A nickase plasmid. Knockout clones were isolated and one clone was sequence verified to carry a homozygous mutation within exon 3. In order to generate additional clones, a lentiviral approach was taken. Lentivirus was generated to express wild-type Cas9 and 1of either 3 different guide RNAs targeting regions of exon 1 or exon 3 of ATG14 (**Figure 39** .

Cell death and viability were previously tested in *Atg14* $^{F/F}$ *VC+* spheroids through Cell Titer Glo assay and immunoblot, respectively. When HeLa cells were challenged by TNF alpha treatment for up to 36 hours, loss of cell viability by Cell Titer Glo Assay was also not observed **(Figure 40** In each experiment, TNF+ CHX represented a positive control for cell death. To extend the observation we immunoblotted against markers of cell death. No cleavage of Caspase-8 or Caspase-3 was observed except under positive control conditions (TNF+CHX) (**Figure 40**)

4.4.2 Sqstm1 puncta and defects in selective autophagy are conserved among human and mouse *Atg14* KO cells

A hallmark of autophagy deficient cells include increases in the protein abundance of autophagy scaffolding proteins such as p62. HeLa cells deficient for *ATG14*, demonstrated an increase in SQSTM1/p62 abundance by immunoblot, phenocopying the results seen in mouse cells, and suggesting a defect in autophagic flux as a result of ATG14 protein loss (**Figure 41**). Likewise, *Atg14* knockout in mouse intestinal epithelia and primary cells derived from mouse epithelia causes formation of pathogenic puncta of Sqstm1/p62 [33]. To define the extent to which puncta are found within *ATG14* deficient Hela cells, we performed immunofluorescence of cultured HeLa cells against p62. Similar to that of *Atg14* deficient spheroids and immortalized cells, cytoplasmic p62 puncta were observed (**Figure 41**). Further colocalization and co-IP experiments are required to determine the extent to which p62 in human cells represents a platform for caspase activation.

4.4.3 The master Caspase-8 regulator *Cflar/Cflip* is differentially expressed between mouse intestinal cells and human cells

Numerous genetic and functional differences exist between that of human and mouse cells. However, we hypothesized that a critical factor differentiating the apoptotic response would be a known factor within either the TNF, cell death, or autophagic pathways. We also hypothesized that the defect would manifest at the protein level through either differential protein expression or through divergence in peptide sequence. Taking a candidate approach, we used protein BLAST to compare the amino acid sequences of autophagy candidate genes and TNF-associated signaling factors to measure conservation at the amino acid level. While autophagic pathway factors are highly conserved (>90%) at the amino acid level between that of human and mouse, there is less

conservation among several key factors of the TNF-triggered cell death pathway such as CASP8 and CFLAR **(Figure 42)**. These differences we hypothesized are sufficient to drive significant differences in the cell death response of the epithelium.

To validate these findings, we immunoblotted for multiple members of the TNF-triggered cell death pathway in Atg14 KO or control cells (**Figure 44 Figure 45 Figure 46).** We hypothesized that a candidate factor, would be differentially expressed between Atg14 KO and control cells. It would also be changed (increased, decreased, or cleaved) upon TNF stimulation. Lastly, it would be differentially expressed between mouse and the non-responsive HeLa cells. We observed changes in protein abundance among some candidate targets (Ripk1, Tradd) between Atg14 KO and control cells (**Figure 44** . However, a striking difference was observed with immunoblotting for Cflip/Cflar. A lower molecular weight band was observed solely in the *Atg14* deficient cell, not controls, and the band was seen only after TNF treatment (**Figure 46 Figure 47** . Furthermore, a different staining pattern was seen in the HeLa cells (**Figure 48**). Therefore, Cflar/Cflip was the only protein candidate to meet all three criteria.

Among mouse cells, *Atg14* KO cells demonstrated higher basal levels of the p55 cFLIP-L protein as baseline as compared to controls. Only upon TNF treatment and only in the Atg14 KO group, cFLIP-L would be converted to a shorter (43kDa) isoform, known as cFLIP-p43 in the literature. cFLIP-p43 is detectable within 1 hour after TNF stimulation and is robustly cleaved around 3 hours after stimulation (**Figure 47** . In contrast HeLa cells generated a different splice isoform, cFLIP-S (22kDa), after TNF stimulation. (**Figure 48**). Differences among the human and mouse isoforms of cFLIP are detailed in **Figure 43** .

4.4.4 A caspase-generated cFLIP isoform is specifically expressed in Atg14 mouse, but not HeLa cells.

cFLIP-p43 is, by definition, not a splice isoform of cFLIP, but rather a post-translationally processed form of the larger p55 cFLIP-L protein that is cleaved at ASP376, by CASP8. Spatially, cFLIP-p43 is only formed within the large multimeric Death Induced Signaling Complex (DISC), through heterodimerization with CASP8 [95]. Heterodimerization allows for the mutual formation of cFLIP-p43, and the p43 active form of CASP8, allowing this complex to be poised to activated apoptotic cell death. (**Figure 43**)

Z-Vad-FMK is an irreversible small molecule inhibitor of multiple caspases. In chapter 2, Z-Vad-FMK was delivered to *Atg14* deficient mouse spheroids to block cell death, as measured by increased viability by Cell Titer Glo Assay (Figure 9 . Likewise, by immunoblot, this compound decreased the processing of CASP8 to its fully active p18 form and prevented the processing of Caspase-3 to its active pro-apoptotic form. This compound can be used to functionally test the role of CASP8 and CASP3 in the cell [157]

Therefore to validate that the 43kDa band is generated through caspase processing, We pretreated autophagy deficient and sufficient cells with Z-VAD-FMK or vehicle control before a 3 hour treatment with TNF. No changes in cFLIP processing were seen in control cells with either the compound or TNF. In *Atg14* KO cells, TNF triggered the processing of p55 cFLIP-L to cFLIP-p43, and the addition of Z-Vad-FMK blocked this conversion and restored the p55 cFLIP-L **(Figure 47).**

4.5 Discussion

Together, these results highlight a pertinent distinction between the cell death response of *Atg14* deficient mouse cells relative to that of *ATG14* deficient human (HeLa) cells: the post-translational processing of a pro-caspase TNF-associated molecule cFLIP. This work has demonstrated a divergence between mouse and human (HeLa) cells in terms of sensitivity to TNF, despite their shared autophagy defect. It has further identified that the cell death pathways diverge

between mouse and human. Immunoblot of factors downstream of TNF identify differences among several proteins including Tradd, and Ripk1 Further work needs to be done to assess the significance of these changes. However, the leading candidate is cFLIP.

It is recognized that outbred mouse strains (MSM, SPRET/Ei) are less sensitive than the common inbred C57BL/6J mouse strain to TNF-triggered apoptotic cell death [158, 159]. Linkage analysis have mapped the loci that affect this threshold for TNF sensitivity to a region that coded for *Cflar/Cflip* [95]. Literature reports of *Cflar* expression between the outbred and B6 strains demonstrated that outbred strains favor expression of the cFLIP-R splice isoform, a form of cFLIP that inhibits CASP8 cell processing and prevents apoptotic cell death [160]. In contrast, B6 mice favor the expression of cFLIP-L which were processed to the aforementioned cFLIP-p43 after TNF stimulation [1].

Expression of Cflar/Cflip differs between mouse and human, between *Atg14* KO and control, and between TNF treatment vs vehicle. Therefore, Cflip is an autophagy-labile, TNF sensitive, caspase processed, species-specific candidate protein to drive cell death downstream of *Atg14* loss. Coupled with evidence from the literature that Cflip is a known direct regulator of caspase activity and that splice isoforms of this protein drive differences in the TNF cell death response, Cflip is the top candidate for driving differential TNF sensitivity between mouse and human.

4.6 Future Directions

4.6.1 Validation and Comprehensive testing of human ileal spheroid clone for cell death sensitivity

Rationale: Differences between the *ATG14* deficient HeLa cell lines (chapter 4) and the intestinal cells utilized in chapters 2 and 3 can be attributable to genetic differences between mouse and human, or alternatively due to differences between aneuploid cancer cells and normal cells.

To reconcile this concern, we are generating an *ATG14* knockout human spheroid line derived from a healthy male ileal resection specimen (Hu292d). This line has been tested extensively by our lab and represents a model human cell line [161]. Results from this line are forthcoming.

Experiments and Expected Results: To test the hypothesis that divergence to TNF-triggered cell death occurs at the species level, individual CRISPR clones (n=3) of Hu292d will be generated and validated first by the sequencing and then my immunoblot against ATG14. To assess the extent to which the autophagy pathway is defective in these cells, we will measure flux through the autophagy cascade. In brief, we will utilize immunoblot to measure p62 abundance and the LC3 lipidation ratio at baseline, upon induction by starvation or mTOR inhibition, and with autophagy blockade through lysosomal inhibition. We hypothesize that autophagy flux will be blocked in the *ATG14* KO line.

To measure the extent to which the human *ATG14* KO cells are sensitive to TNF-triggered death we will assess their survival when challenged with recombinant mouse TNF. Cells will be treated with a range of Human TNF dosages from 1-200ng/ml and viability (normalized to media control treated cells) will be measured by the Cell Titer Glo assay. Furthermore, cells will be treated with a fixed dose of TNF (200ng/ml) and protein lysates will be harvested from cells after 0, 2, 4, 8, 12, and 24 hour time points. Immunoblots will be run and probed for cell death markers including cleaved caspase-3, cleaved caspase-8 and cleaved PARP. I hypothesize that the human spheroids will not be sensitive to TNF triggered death and will not demonstrate a dose dependent reduction in viability by

Cell Titer Glo assay. This experiment will test the degree to which the lack of cytotoxic response to TNF is attributable to differences in mouse relative to human TNF.

Alternative approaches: *ATG14* KO human intestinal spheroids may be sensitive to TNF triggered death. If this result is obtained then an alternative hypothesis is: intestinal cells, both mouse and human require *ATG14* to protect the cell from TNF-triggered apoptosis. Further work will be needed to compare the sensitivity of non-intestinal cells (eg. primary human fibroblasts and Mouse Embryonic Fibroblasts (MEF) relative to intestinal cells. A subsequent scientific question to address would be: "What drives differences in TNF sensitivity between Atg14-deficient intestinal and extra-intestinal tissues?"

4.6.2 Rescue of cell death sensitivity by overexpression of human CFLAR/CFLIP within mouse cells

Rationale: The differences between the human and mouse Cflip/Cflar isoforms have been characterized in the literature [1]. While mice express a form of Cflip that can promote CASP8 self-processing, this pro-caspase species of Cflip is not conserved in human cells: either among control or *ATG14* knockout cells. Rather the anti-apoptotic cFLIP-S species is favored in both cancer cells lines and in primary human cells. This form is protective against cell death (Figure 4) . Therefore, we propose an experiment whereby heterologous expression of human CFLIP (cFLIP-S) will rescue the mouse cells' sensitivity to TNF.

Experiments and expected results: Lentiviral expression vectors were generated to drive constitutive expression of Human CFLIP-S, under the control of the EF1α promoter. Mouse cells will be transduced with this vector, placed under positive selection, and stable clones will be isolated. Cells will be treated with a range of mouse TNF dosages from 1-100ng/ml and viability (normalized to media control treated cells) will be measured by the Cell Titer Glo assay. We

hypothesize that viability will not decline in a dose dependent manner in cells that express human cFLIP. Furthermore, cells will be treated with a fixed dose of TNF (100ng/ml) and protein lysates will be harvested from cells after 0, 2, 4, 8, 12, and 24 hour time points. Immunoblots will be run and probed for cell death markers including cleaved caspase-3, cleaved caspase-8 and cleaved PARP. We hypothesize that cell death markers will be attenuated within cells that express human cFLIP.

Alternative approaches: Overexpression of human cFLIP may not be sufficient to rescue cell death by Cell Titer Glo or Immunoblot. We observe that cFLIP cleavage is a proximal step in priming the cell for apoptosis. Mouse cell data in Figure 47 demonstrates that the autophagy deficient mouse cells processed cFLIP-L to cFLIP-p43 after TNF stimulation in a caspase-dependent manner. We wish to test if this processing is blocked in these transduced mouse cells by blotting the cells for the presence of cFLIP-p43 and Casp8 p43. We will also treat cells with Z-Vad-FMK to validate that the cleavage forms are generated by caspase processing. These results will define the extent to which the DISC is still active in the mouse *Atg14* KO cells.

4.6.3 Recapitulation of cell death sensitivity by overexpression of mouse Cflar/Cflip within human cells

Rationale: TNF is not a potent cytotoxic cytokine, but there are compounds that sensitize the cell to apoptosis. One prototypical approach to trigger cell death include the use of the protein synthesis inhibitor Cycloheximide (CHX). Both human and mouse expression of CFLIP is inducible: this gene is a classical TNF-induced gene through the transcriptional transactivation of NF-kB inducible elements. *CFLIP* is a classical "survival gene" because its protein product heterodimerizes with CASP8 and under standard conditions suppresses it autocatalysis. CHX blocks synthesis of Cflip, including the protective form, cFLIP-S. Data presented in **Figure 40** reveals that HeLa cells demonstrate a dose-dependent decrease in cell viability after CHX treatment. One hypothesis is that loss of the "protective" form of cFLIP (cFLIP-S) allows the cells to model that of the mouse TNF

response. Therefore, we propose an experiment whereby heterologous expression of mouse Cflip (cFLIP-L) will allow the HeLa cells to become sensitive to TNF.

Experiments and expected results: Lentiviral expression vectors were generated to drive constitutive expression of mouse cFLIP-L under the control of the EF1α promoter. Human cells will be transduced with this vector, placed under positive selection, and stable clones will be isolated. Cells will be treated with a range of Human TNF dosages from 1-200ng/ml and viability (normalized to media control treated cells) will be measured by the Cell Titer Glo assay. We hypothesize that viability will decline in a dose dependent manner in cells that express mouse cFLIP. Furthermore, cells will be treated with a fixed dose of TNF (200ng/ml) and protein lysates will be harvested from cells after 0, 2, 4, 8, 12, and 24 hour time points. Immunoblots will be run and probed for cell death markers including cleaved caspase-3, cleaved caspase-8 and cleaved PARP. We hypothesize that cell death markers will be present starting at 8 hours within cells that express mouse cFLIP.

Alternative approaches: Overexpression of mouse cFLIP may not be sufficient to induce cell death by Cell Titer Glo or Immunoblot. We observe that cFLIP cleavage is a proximal step in priming the cell for apoptosis. Mouse cell data in Figure 47 demonstrates that the autophagy deficient mouse cells processed cFLIP-L to cFLIP-p43 after TNF stimulation in a caspase-dependent manner. We wish to test if this processing is conserved in human cells by blotting the cells for the presence of cFLIP-p43 and Casp8 p43. We will also treat cells with Z-Vad-FMK to validate that the cleavage forms are generated by caspase processing. These results will define the extent to which the DISC is accumulating in the human *ATG14* KO cells.

Another factor which was hypothesized to play an active role in cell death is Ripk1 (Receptor Interacting Kinase 1). Data from enterocyte-differentiated spheroids (**Figure 11**) revealed a TNF dependent decrease in Ripk abundance specifically in the *Atg14* deficient cell. A smaller decrease

was seen upon shorter time points of stimulation in jejunal stem cells as presented in **Figure 44**. However, no decrease in RIPK1 was seen in Atg14 deficient HeLa cells upon TNF treatment (**Figure 46**). Similar results are observed in immortalized mouse intestinal cells treated with TNF. With the identification of the pathogenic cFLIP signature, I hypothesize that the loss of Ripk1 is secondary to cFLIP cleavage and Casp8 activation.

4.7 Figures

Figure 39 Schematic for generation and evaluation of human *Atg14* KO cells

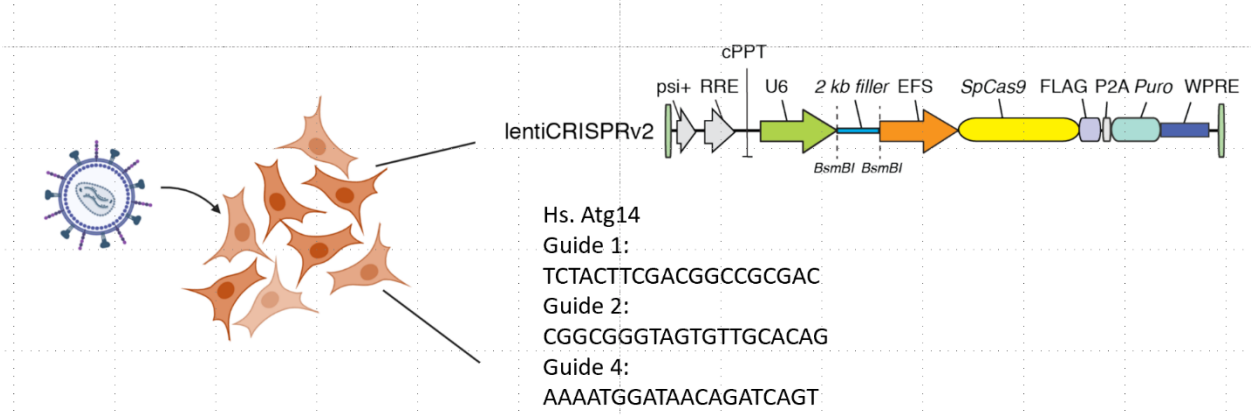

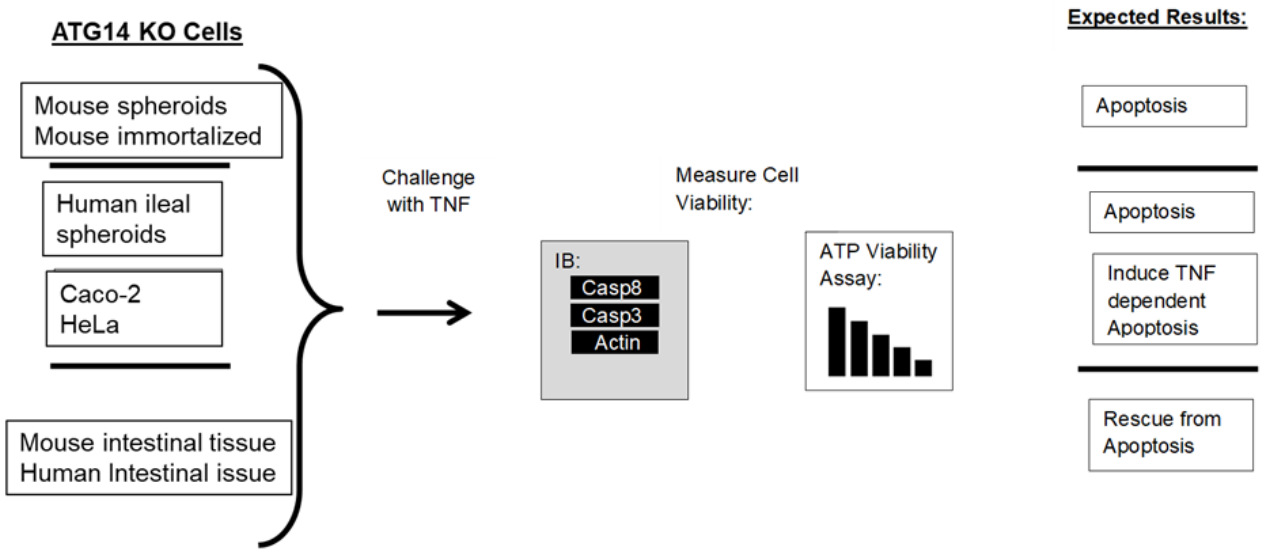

Figure 40 Measurement of HeLa cell viability in the present of an inhibitor of cFLIP-S

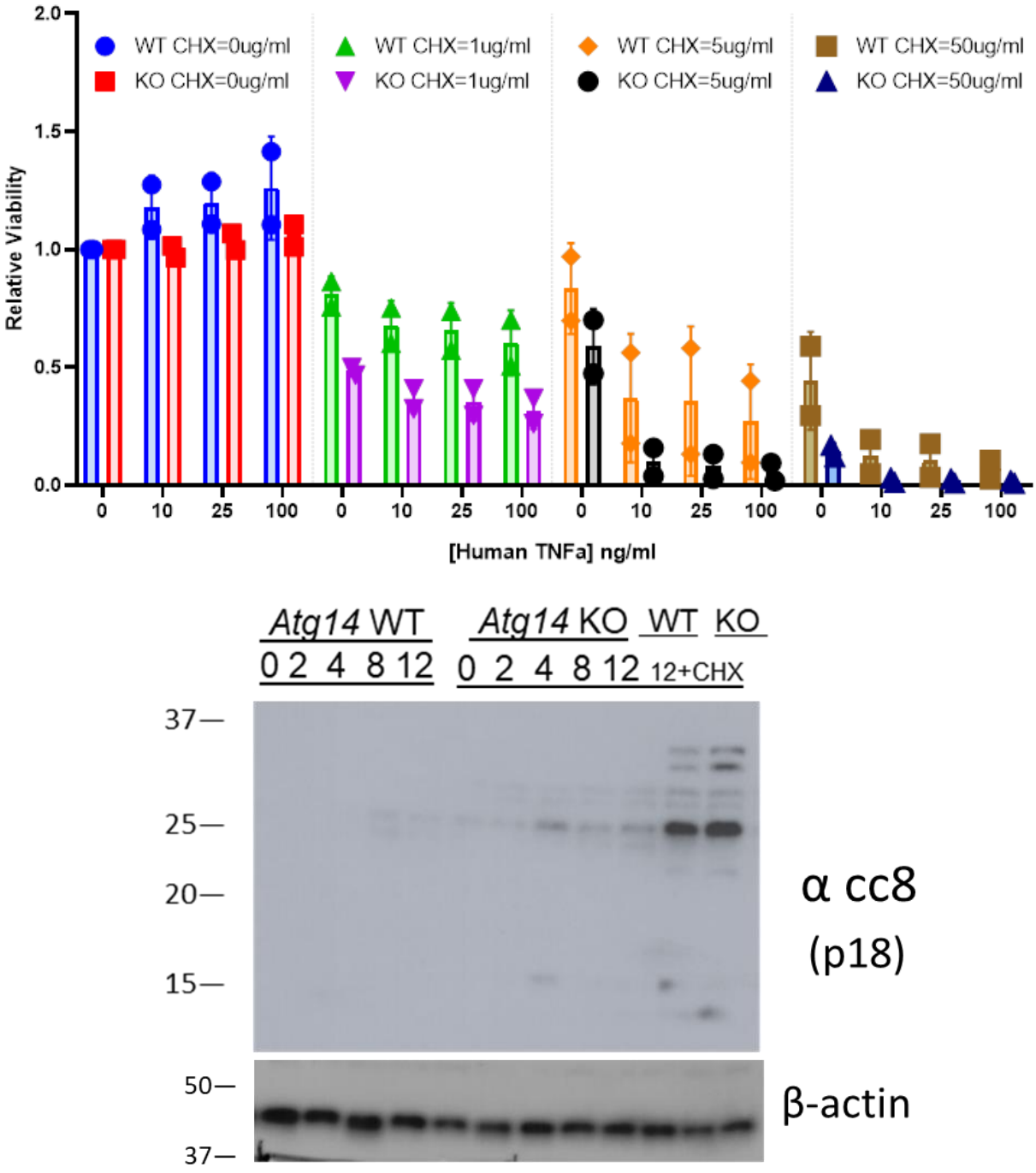

[Upper] HeLa cells were treated with the indicated dosages of human TNF or cycloheximide (CHX) for 24 hours and cell viability was measure by Cell Titer Glo assay N=2 independent experiments. [Lower] HeLa cells were treated with 200ng/ml Human TNF for the indicated number of hours. Lysates were probed for the cleavage of CASP8.

Figure 41 An autophagy defect is conserved in *ATG14* deficient HeLa cells

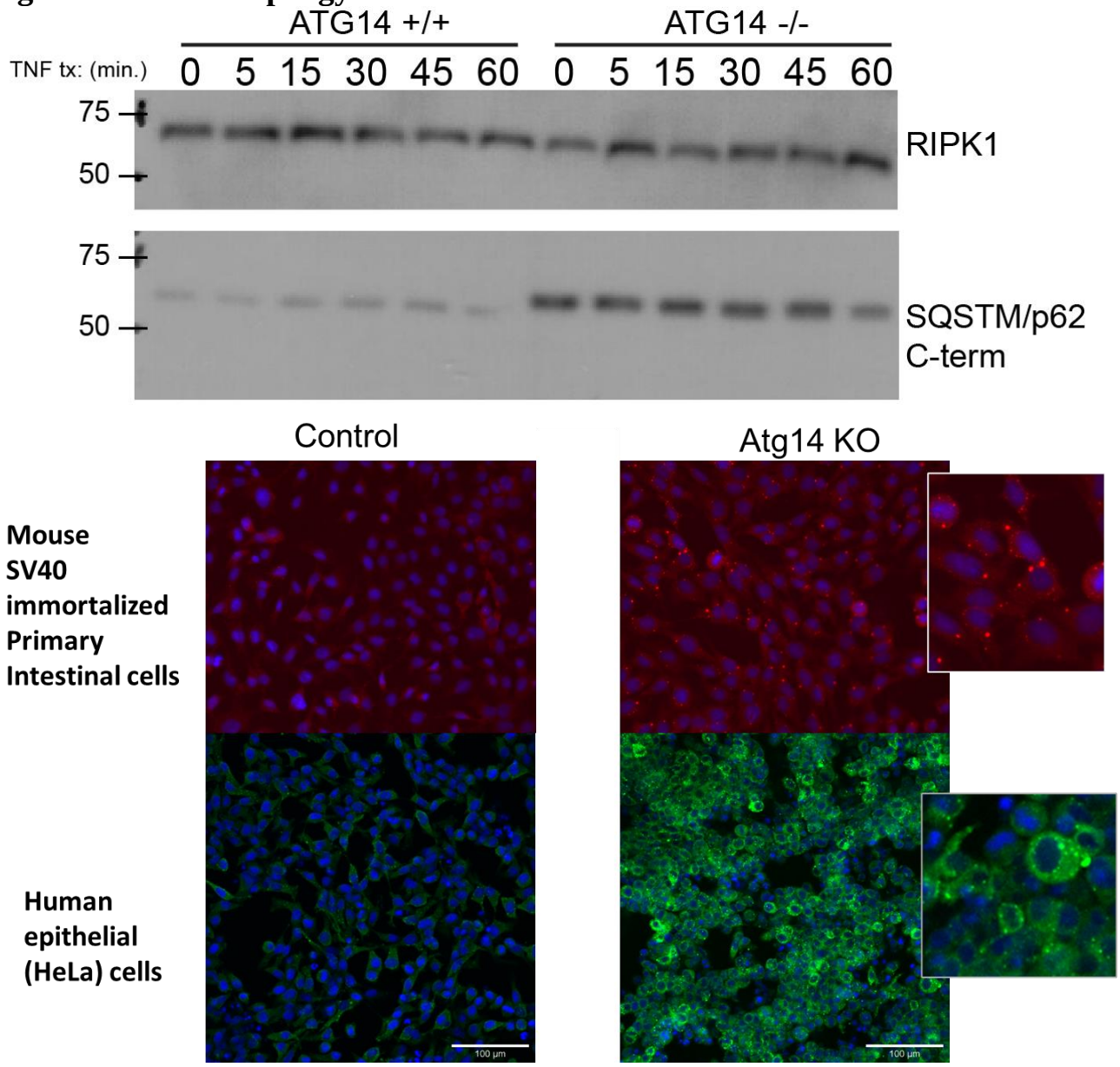

Figure 42 Conservation of Autophagy and TNF signaling factors between mouse and human

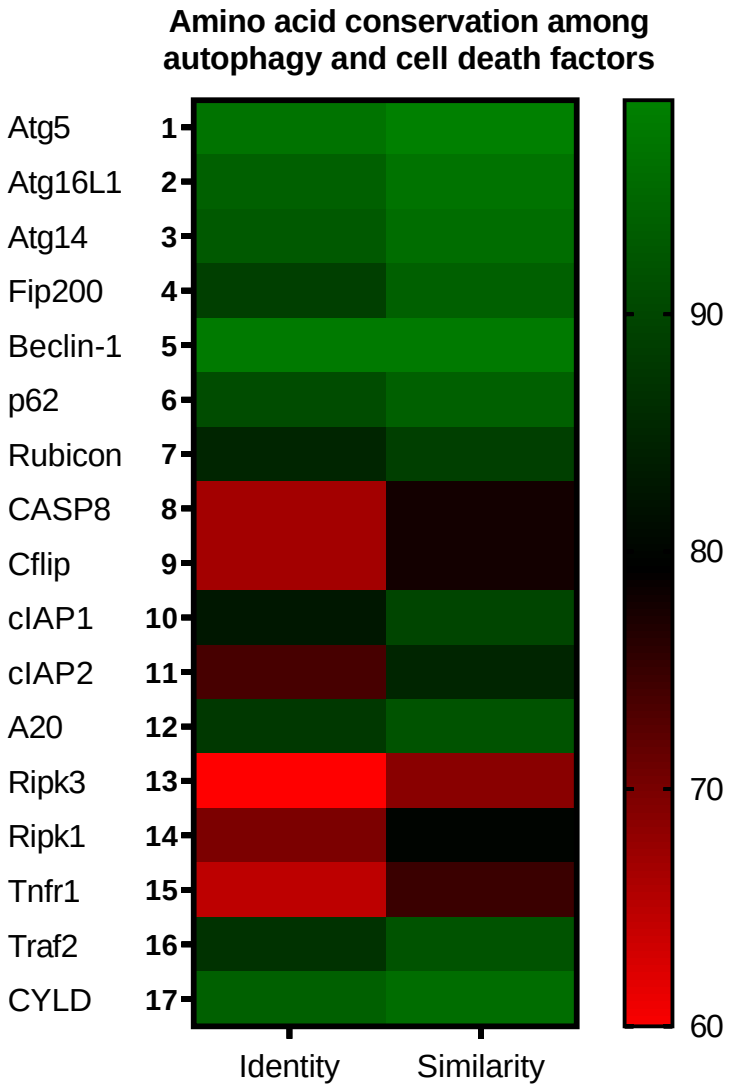

Factors involved in cell death diverge between mouse and human cells. A. Heat map of to illustrate conservation at the amino acid level between mouse and human. Values indicate percentage of shared identity at the amino acid level. Pairwise comparisons were generated using the BLASTp algorightm; Data current as of May 2020.

Figure 43 Divergence between human and mouse CFLIP isoforms

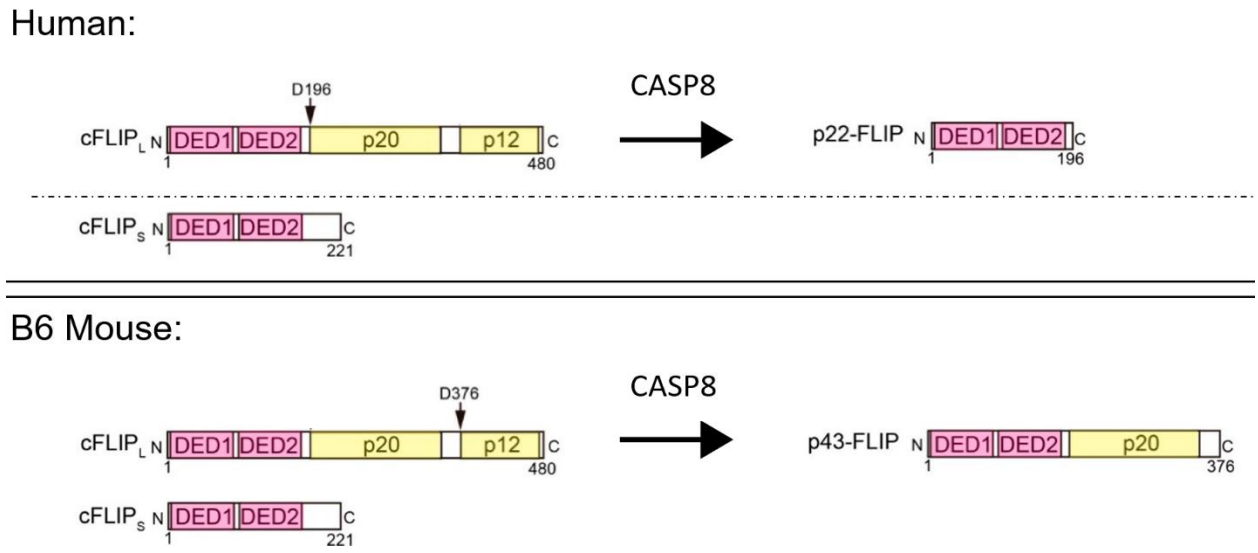

sp|O35732|CFLAR_MOUSE CASP8 and FADD-like apoptosis regulator OS=Mus musculus OX=10090 GN=Cflar PE=1 SV=3

Sequence ID: Query_30157 Length: 481 Number of Matches: 1

Range 1: 6 to 481 Graphics ▼ Next Match ▲ Previous Match

Score	Expect	Method	Identities	Positives	Gaps
630 bits(1624)	0.0	Compositional matrix adjust.	322/481(67%)	379/481(78%)	6/481(1%)

```
Query  1    MSAEVIHQVEEALDTDEKEMLLFLCRDVAIDVVPPNVRDLLDILRERGKLSVGDLAELLY  60
            +SAEVIHQVEE LD DEKEM+LFLCRDV  ++  PNVRDLLD L ERG+LS   LAELLY
Sbjct  6    VSAEVIHQVEECLDEDEKEMMLFLCRDVTENLAAPNVRDLLDSLSERGQLSFATLAELLY  65

Query  61   RVRRFDLLKRILKMDRKAVETHLLRNPHLVSDYRVLMAEIGEDLDKSDVSSLIFLMKDYM  120
            RVRRFDLLKRILK D+  VE HL RNPHLVSDYRVL+ EIGE LD++DVSSL+FL +DY
Sbjct  66   RVRRFDLLKRILKTDKATVEDHLRRNPHLVSDYRVLLMEIGESLDQNDVSSLVFLTRDYT  125

Query  121  GRGKISKEKSFLDLVVELEKLNLVAPDQLDLLEKCLKNIHRIDLKTKIQKYKQSVQGAGT  180
            GRGKI+K+KSFLDLV+ELEKLNL+A DQL+LLEKCLKNIHRIDL TKIQKY QS QGA +
Sbjct  126  GRGKIAKDKSFLDLVIELEKLNLIASDQLNLLEKCLKNIHRIDLNTKIQKYTQSSQGARS  185

Query  181  SYRNVLQAAIQK-SLKDPSNNFRLHNGRSKEQRLKEQLGAQQEPVKKSIQESEAFLPQSI  239
            +  N LQA++ K S+K    N RL NGRSKE R  E   +Q+  VK SIQES AFLP  I
Sbjct  186  NM-NTLQASLPKLSIK---YNSRLQNGRSKEPRFVEYRDSQRTLVKTSIQESGAFLPPHI  241

Query  240  PEERYKMKSKPLGICLIIDCIGNETELLRDTFTSLGYEVQKFLHLSMHGISQILGQFACM  299
             EE Y+M+SKPLGICLIIDCIGN+T+ L++TFTSLGY +Q FL    H I+QI+ ++A M
Sbjct  242  REETYRMQSKPLGICLIIDCIGNDTKYLQETFTSLGYHIQLFLFPKSHDITQIVRRYASM  301

Query  300  PEHRDYDSFVCVLVSRGGSQSVYGVDQTHSGLPLHHIRRMFMGDSCPYLAGKPKMFFIQN  359
             +H+DYDSF CVLVS GGSQS+ G DQ HSG  L H++ MF GD+CP L GKPK+FFIQN
Sbjct  302  AQHQDYDSFACVLVSLGGSQSMMGRDQVHSGFSLDHVKNMFTGDTCPSLRGKPKLFFIQN  361

Query  360  YVVSEGQLEDSSLLEVDGPAMKNVEFKAQKRGLCTVHREADFFWSLCTADMSLLEQSHSS  419
            Y     QLEDSS LEVDGP++KNV+ K  +   CT H EAD FWSLCTAD+S LE+  SS
Sbjct  362  YESLGSQLEDSS-LEVDGPSIKNVDSKPLQPRHCTTHPEADIFWSLCTADVSHLEKPSSS  420

Query  420  PSLYLQCLSQKLRQERKRPLLDLHIELNGYMYDWNSRVSAKEKYYVWLQHTLRKKLILSY  479
             S+YLQ LSQ+L+Q R+RPL+DLH+EL   +Y WNS VS+KEKY + LQHTLRKKLIL+
Sbjct  421  SSVYLQKLSQQLKQGRRRPLVDLHVELMDKVYAWNSGVSSKEKYSLSLQHTLRKKLILAP  480

Query  480  T  480
            T
Sbjct  481  T  481
```

Top: Schematic to compare B6 mouse vs human isoforms of CFLIP based upon literature reports. Humans express cFLIP-L carrying a CASP8 cleavage site at D196. This isoform can be cleaved into cFLIP-p22 upon CASP8 cleavage, which induces protection against CASP8 activation. Human cells can also express a splice isoform called cFLIP-s which is also protective against CASP8
Mice (B6) express cFLIP-L carrying a CASP8 cleavage site at D376. This isoform can be cleaved into cFLIP-p43 upon CASP8 cleavage, which induces partial to no protection CASP8 activation. cFLIP-s is not expressed in mouse. Adapted from Tsuchiya, Y et. al. *Int. J. Mol. Sci.* **2015**, *16*(12), 30321-30341 [1]

Bottom: BLASTp alignment of human cFLIP-L and mouse cFLIP-L to show the divergence at the amino acid level between these two factors. Note amino acid substitutions around D196 eliminating a CASP8 cleavage motif

Figure 44 Immunoblot assessment of the proximal TNF-triggered signaling pathway

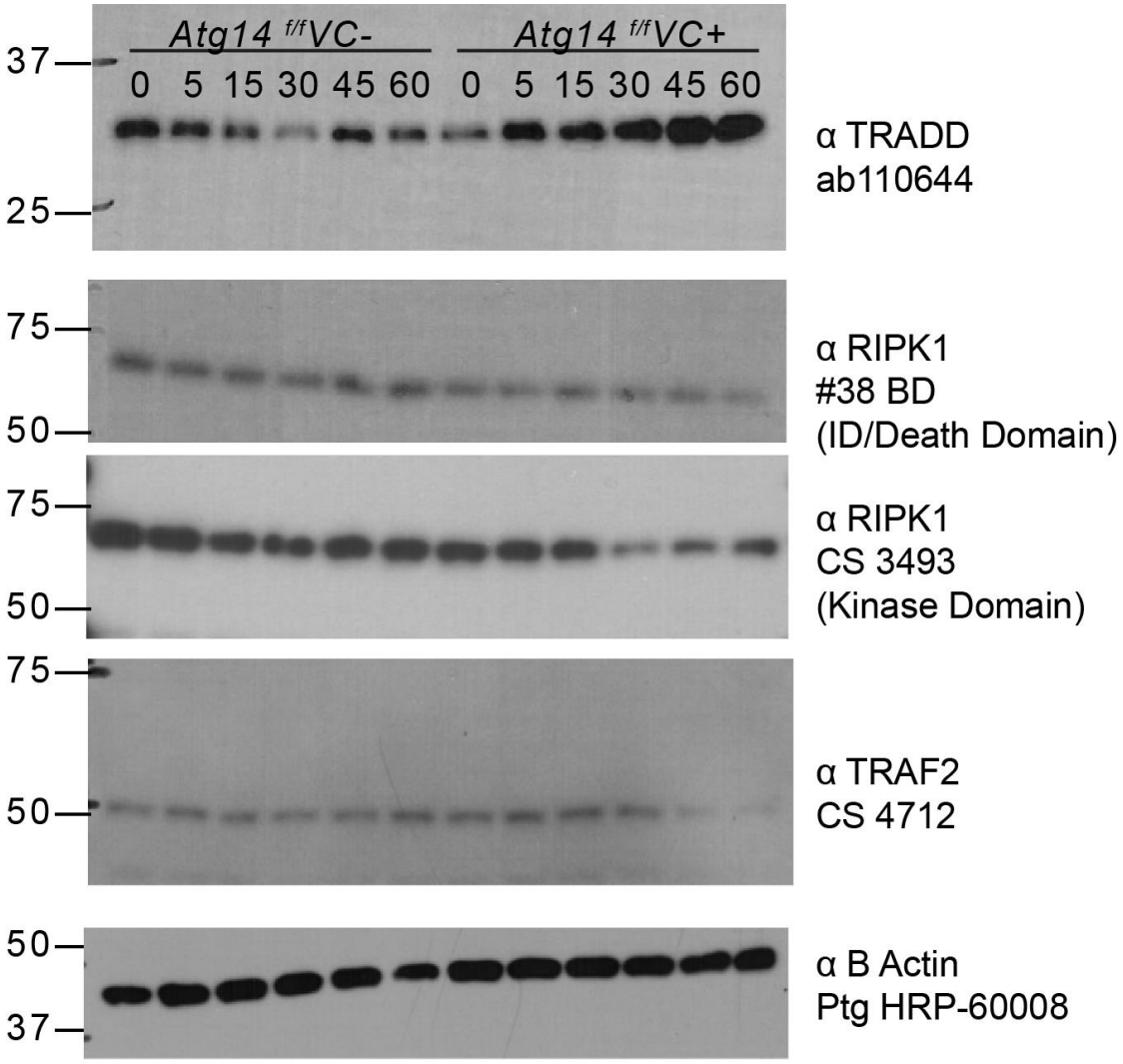

Immunoblots of mouse jejunal stem cell spheroids treated with the indicated duration (in minutes) of 25ng/ml Mouse TNF. Representative of 3 experiments. Ripk1 and Traf2 levels are decreased in *Atg14 F/F VC+* cells relative to controls. Tradd levels are increased.

Figure 45 Immunoblot assessment of the ubiquitin ligases of the TNF-triggered cell death pathway

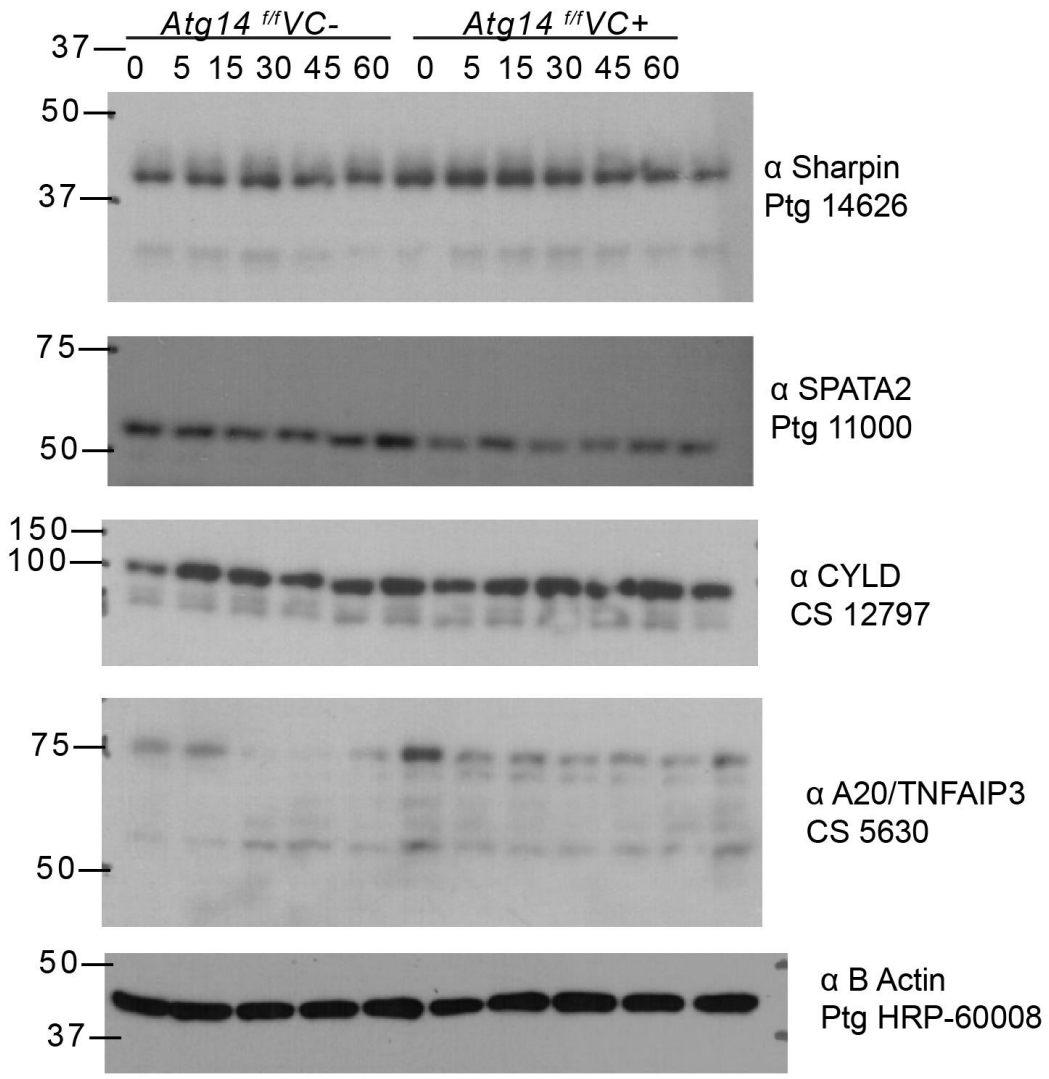

Immunoblots of mouse jejunal stem cell spheroids treated with the indicated duration (in minutes) of 25ng/ml Mouse TNF. Representative of 3 experiments.

Figure 46 Immunoblot assessment of the TNF-triggered cell death pathway

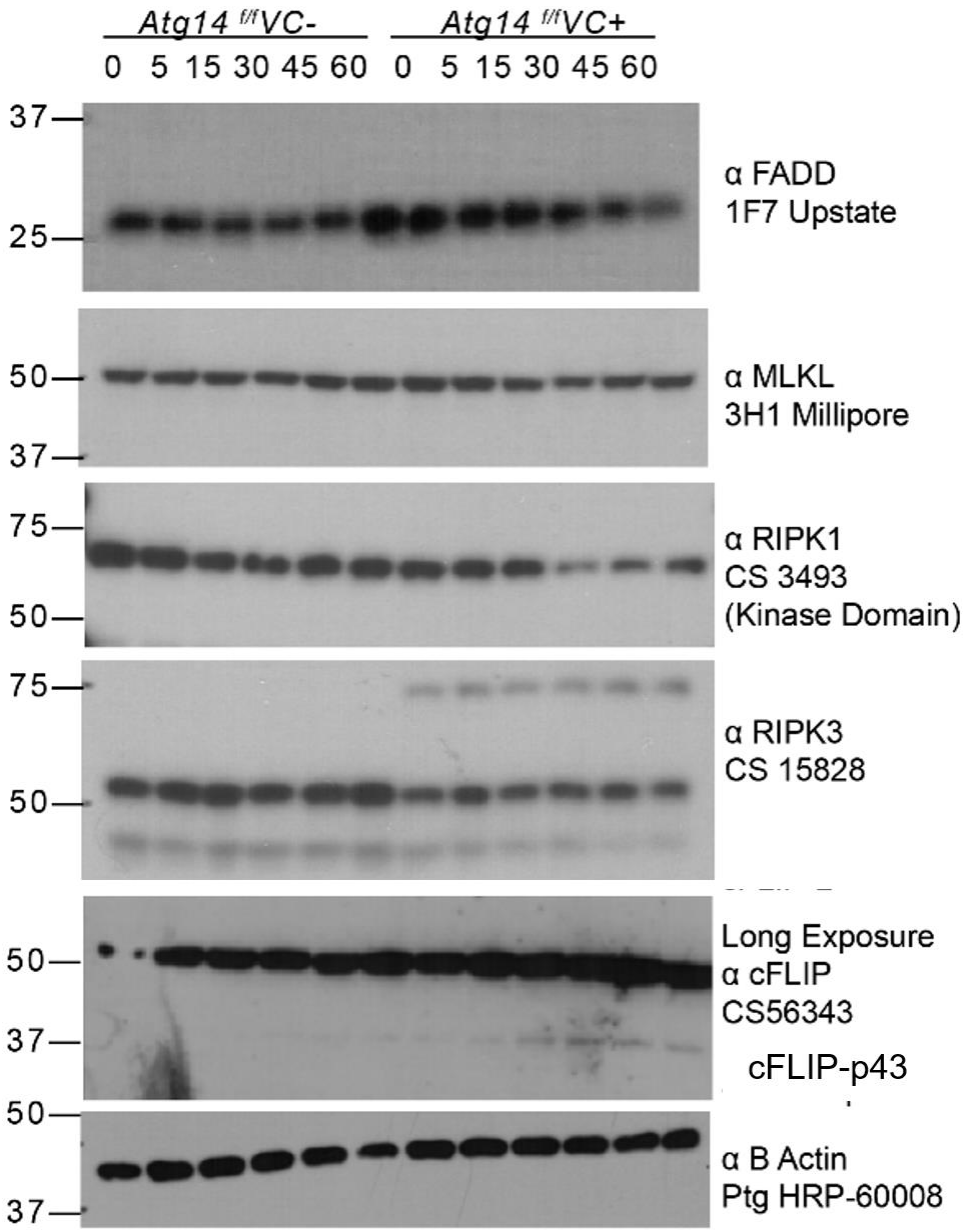

Immunoblots of mouse jejunal stem cell spheroids treated with the indicated duration (in minutes) of 25ng/ml Mouse TNF. An unknown large molecular weight band is consistently observed in *Atg14* deficient cells independent of TNF treatment. A p43 cleavage band of Cflip is observed in the *Atg14* deficient cells specifically upon TNF treatment Representative of 3 experiments.

Figure 47 Generation of cFLIP-p43 requires caspase activity

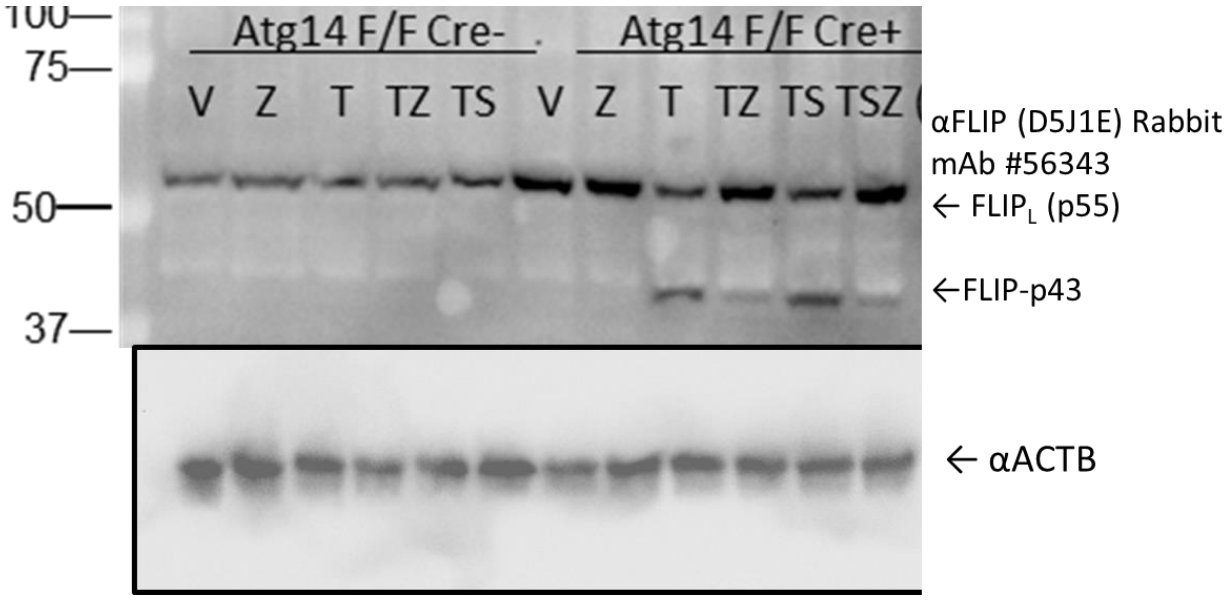

Immunoblots of mouse SV40 immortalized intestinal cells treated with media with: 0.1% DMSO (**V**), 20ug/ml Z-VAD-FMK (**Z**), 100ng/ml mouse TNF + 0.1% DMSO (**T**), 100ng/ml mouse TNF + 20ug/ml Z-VAD-FMK (**TZ**), 100ng/ml mouse TNF + 10μm BV6 SMAC + 0.1% DMSO (**TS**), 100ng/ml mouse TNF + 10μm BV6 SMAC mimetic + 20ug/ml Z-VAD-FMK (**TSZ)**. Cells were pretreated with 1 hour of Z0VAD or DMSO, and then treated with 3 hours of the indicated compounds, A p43 cleavage band of Cflip is observed in the *Atg14* deficient cells specifically upon TNF treatment. This band is rescued by caspase blockade, suggesting that the band is generated by direct Casp8 cleavage. Representative of 3 experiments.

Figure 48 Generation of cFLIP-S in HeLa cells in response to TNF stimulation

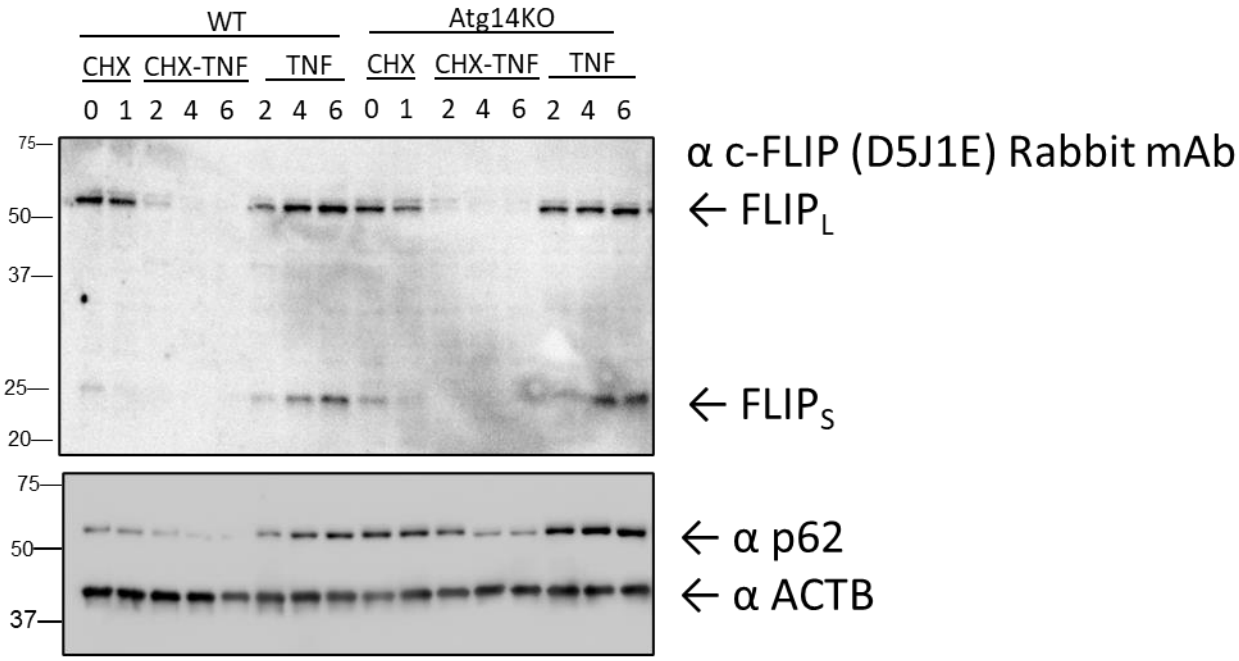

Hela cells do not generate cFLIP-p43 upon TNF stimulation, but instead produce cFLIP-S the splice isoform that protects the cell against TNF triggered death.. P62 levels re increased in the KO group relative to controls. Immunoblots of D10A CRISPR edited HeLa cells along with the parental WT line (ATCC CCL2) after challenge with TNF or TNF+ CHX. Cell were treated with 100ng.ml Human TNF or 100ng/ml CHX for the indicated period of time (0-6 hours) Lysates were probed with antibodies against p62, β-Actin, or cFLIP.

Summary and final conclusions

In this body of work, I have generated evidence that Atg14, through the canonical degradative autophagy pathway, plays a fundamental role in the regulation of cell death. Loss of autophagy leads to enhanced sensitivity through TNF triggered cell death, linking this important extracellular signaling pathways to host autophagy. Sqstm1/p62 plays a critical role in this juncture; acting not only as a biomarker of cells that are sensitive to TNF triggered apoptosis, but playing a functional role, co-localizing with caspase-8 and ubiquitin. I have demonstrated that the initiation cascade of autophagy, specifically Atg14's interaction with Beclin-1's coiled-coil domain is required for protection against cell death and for the accumulation of p62. P62 deletion in enterocytes rescue cell death in the autophagy-deficient mouse and in cultured primary cells. Lastly, I have observed that *ATG14* deficient human and mouse cells respond differently to TNF, despite the fact that autophagy is highly conserved among species. I have defined one point of divergence between mouse and human, Atg14 KO and control, with the caspase regulator cFLIP. Experiments are currently in progress to define A) the role of ATG14 in the cell death of human primary intestinal cells and B) to define the functional contribution of mouse and human cFLIP isoforms on TNF-triggered death.

This ongoing work fills a critical niche in our understanding of the application of reductionist mouse models to that of human physiology and pathophysiology. Autophagy is a fundamental cellular progress that is required in eukaryotic cells from yeast to mice to human. The degree of protein conservation among autophagy factors (>90%) across species suggest a strong conserved role for this pathway among model organisms and humans, while the variance among cell death

factors suggest that natural selection may have favored an evasion strategy in humans to prevent cell death in the context of autophagy blockade.

An improved understanding of the crosstalk among these pathways can greatly inform future approaches to develop molecular-oriented therapies to modulate autophagy and cell death. Death of the epithelial barrier can be diminished among patients with IBD to reduce tissue damage, while death of cancer intestinal epithelial cells can be augmented to prevent growth and metastasis. A lack of understanding of these pathways - in both mouse model systems and in human cells - constrain our current efforts to design therapeutics.

References/Bibliography/Works Cited

1. Tsuchiya, Y., O. Nakabayashi, and H. Nakano, *FLIP the Switch: Regulation of Apoptosis and Necroptosis by cFLIP.* Int J Mol Sci, 2015. **16**(12): p. 30321-41.
2. Parzych, K.R. and D.J. Klionsky, *An overview of autophagy: morphology, mechanism, and regulation.* Antioxid Redox Signal, 2014. **20**(3): p. 460-73.
3. Wellcome Trust Case Control, C., *Genome-wide association study of 14,000 cases of seven common diseases and 3,000 shared controls.* Nature, 2007. **447**(7145): p. 661-78.
4. Stappenbeck, T.S., et al., *Notes from some crypt watchers: regulation of renewal in the mouse intestinal epithelium.* Curr Opin Cell Biol, 1998. **10**(6): p. 702-9.
5. Nenci, A., et al., *Epithelial NEMO links innate immunity to chronic intestinal inflammation.* Nature, 2007. **446**(7135): p. 557-61.
6. Kaser, A., et al., *XBP1 links ER stress to intestinal inflammation and confers genetic risk for human inflammatory bowel disease.* Cell, 2008. **134**(5): p. 743-56.
7. Garside, P., et al., *Analysis of enteropathy induced by tumour necrosis factor alpha.* Cytokine, 1993. **5**(1): p. 24-30.
8. Miyoshi, H. and T.S. Stappenbeck, *In vitro expansion and genetic modification of gastrointestinal stem cells in spheroid culture.* Nat Protoc, 2013. **8**(12): p. 2471-82.
9. Cadwell, K., et al., *A common role for Atg16L1, Atg5 and Atg7 in small intestinal Paneth cells and Crohn disease.* Autophagy, 2009. **5**(2): p. 250-2.
10. Patel, K.K. and T.S. Stappenbeck, *Autophagy and intestinal homeostasis.* Annu Rev Physiol, 2013. **75**: p. 241-62.
11. Matsunaga, K., et al., *Autophagy requires endoplasmic reticulum targeting of the PI3-kinase complex via Atg14L.* J Cell Biol, 2010. **190**(4): p. 511-21.
12. Williamson, R.C., *Intestinal adaptation (first of two parts). Structural, functional and cytokinetic changes.* N Engl J Med, 1978. **298**(25): p. 1393-402.
13. Creamer, B., *The turnover of the epithelium of the small intestine.* Br Med Bull, 1967. **23**(3): p. 226-30.
14. Potten, C.S. and T.D. Allen, *Ultrastructure of cell loss in intestinal mucosa.* J Ultrastruct Res, 1977. **60**(2): p. 272-7.
15. Gavrieli, Y., Y. Sherman, and S.A. Ben-Sasson, *Identification of programmed cell death in situ via specific labeling of nuclear DNA fragmentation.* J Cell Biol, 1992. **119**(3): p. 493-501.
16. Kerr, J.F., A.H. Wyllie, and A.R. Currie, *Apoptosis: a basic biological phenomenon with wide-ranging implications in tissue kinetics.* Br J Cancer, 1972. **26**(4): p. 239-57.
17. Duan, H., et al., *ICE-LAP6, a novel member of the ICE/Ced-3 gene family, is activated by the cytotoxic T cell protease granzyme B.* J Biol Chem, 1996. **271**(28): p. 16720-4.
18. Tummers, B. and D.R. Green, *Caspase-8: regulating life and death.* Immunol Rev, 2017. **277**(1): p. 76-89.
19. Kischkel, F.C., et al., *Cytotoxicity-dependent APO-1 (Fas/CD95)-associated proteins form a death-inducing signaling complex (DISC) with the receptor.* EMBO J, 1995. **14**(22): p. 5579-88.
20. Muzio, M., et al., *FLICE, a novel FADD-homologous ICE/CED-3-like protease, is recruited to the CD95 (Fas/APO-1) death--inducing signaling complex.* Cell, 1996. **85**(6): p. 817-27.
21. Reggiori, F. and D.J. Klionsky, *Autophagy in the eukaryotic cell.* Eukaryot Cell, 2002. **1**(1): p. 11-21.
22. Cadwell, K. and J. Debnath, *Beyond self-eating: The control of nonautophagic functions and signaling pathways by autophagy-related proteins.* J Cell Biol, 2018. **217**(3): p. 813-822.
23. Kim, J., et al., *AMPK and mTOR regulate autophagy through direct phosphorylation of Ulk1.* Nat Cell Biol, 2011. **13**(2): p. 132-41.
24. Itakura, E., et al., *Beclin 1 forms two distinct phosphatidylinositol 3-kinase complexes with*

mammalian Atg14 and UVRAG. Mol Biol Cell, 2008. **19**(12): p. 5360-72.
25. Noda, T., K. Matsunaga, and T. Yoshimori, *Atg14L recruits PtdIns 3-kinase to the ER for autophagosome formation.* Autophagy, 2011. **7**(4): p. 438-9.
26. Jaber, N., et al., *Class III PI3K Vps34 plays an essential role in autophagy and in heart and liver function.* Proc Natl Acad Sci U S A, 2012. **109**(6): p. 2003-8.
27. Tsuboyama, K., et al., *The ATG conjugation systems are important for degradation of the inner autophagosomal membrane.* Science, 2016. **354**(6315): p. 1036-1041.
28. Wold, M.S., et al., *ULK1-mediated phosphorylation of ATG14 promotes autophagy and is impaired in Huntington's disease models.* Mol Neurodegener, 2016. **11**(1): p. 76.
29. Nguyen, T.N., et al., *Atg8 family LC3/GABARAP proteins are crucial for autophagosome-lysosome fusion but not autophagosome formation during PINK1/Parkin mitophagy and starvation.* J Cell Biol, 2016. **215**(6): p. 857-874.
30. Kimmey, J.M., et al., *Unique role for ATG5 in neutrophil-mediated immunopathology during M. tuberculosis infection.* Nature, 2015. **528**(7583): p. 565-9.
31. Boyle, K.B. and F. Randow, *The role of 'eat-me' signals and autophagy cargo receptors in innate immunity.* Curr Opin Microbiol, 2013. **16**(3): p. 339-48.
32. Stolz, A., A. Ernst, and I. Dikic, *Cargo recognition and trafficking in selective autophagy.* Nat Cell Biol, 2014. **16**(6): p. 495-501.
33. Bjorkoy, G., et al., *p62/SQSTM1 forms protein aggregates degraded by autophagy and has a protective effect on huntingtin-induced cell death.* J Cell Biol, 2005. **171**(4): p. 603-14.
34. Pankiv, S., et al., *p62/SQSTM1 binds directly to Atg8/LC3 to facilitate degradation of ubiquitinated protein aggregates by autophagy.* J Biol Chem, 2007. **282**(33): p. 24131-45.
35. Sanz, L., et al., *The interaction of p62 with RIP links the atypical PKCs to NF-kappaB activation.* EMBO J, 1999. **18**(11): p. 3044-53.
36. Goodall, M.L., et al., *The Autophagy Machinery Controls Cell Death Switching between Apoptosis and Necroptosis.* Dev Cell, 2016. **37**(4): p. 337-349.
37. Jin, Z., et al., *Cullin3-based polyubiquitination and p62-dependent aggregation of caspase-8 mediate extrinsic apoptosis signaling.* Cell, 2009. **137**(4): p. 721-35.
38. Zatloukal, K., et al., *p62 Is a common component of cytoplasmic inclusions in protein aggregation diseases.* Am J Pathol, 2002. **160**(1): p. 255-63.
39. Piras, A., et al., *Autophagic and lysosomal defects in human tauopathies: analysis of post-mortem brain from patients with familial Alzheimer disease, corticobasal degeneration and progressive supranuclear palsy.* Acta Neuropathol Commun, 2016. **4**: p. 22.
40. Kaizuka, T. and N. Mizushima, *Atg13 Is Essential for Autophagy and Cardiac Development in Mice.* Mol Cell Biol, 2016. **36**(4): p. 585-95.
41. Wang, C., et al., *Elevated p62/SQSTM1 determines the fate of autophagy-deficient neural stem cells by increasing superoxide.* J Cell Biol, 2016. **212**(5): p. 545-60.
42. Nemazanyy, I., et al., *Defects of Vps15 in skeletal muscles lead to autophagic vacuolar myopathy and lysosomal disease.* EMBO Mol Med, 2013. **5**(6): p. 870-90.
43. Park, J.S., et al., *p62/SQSTM1 is required for the protection against endoplasmic reticulum stress-induced apoptotic cell death.* Free Radic Res, 2016. **50**(12): p. 1408-1421.
44. Mathew, R., et al., *Autophagy suppresses tumorigenesis through elimination of p62.* Cell, 2009. **137**(6): p. 1062-75.
45. Chen, K., et al., *Regulation of glucose metabolism by p62/SQSTM1 through HIF1alpha.* J Cell Sci, 2016. **129**(4): p. 817-30.
46. Carswell, E.A., et al., *An endotoxin-induced serum factor that causes necrosis of tumors.* Proc Natl Acad Sci U S A, 1975. **72**(9): p. 3666-70.
47. Decker, K., *Biologically active products of stimulated liver macrophages (Kupffer cells).* Eur J Biochem, 1990. **192**(2): p. 245-61.
48. Loffreda, S., et al., *Bile ducts and portal and central veins are major producers of tumor necrosis factor alpha in regenerating rat liver.* Gastroenterology, 1997. **112**(6): p. 2089-98.

49. Bischoff, S.C., et al., *Mast cells are an important cellular source of tumour necrosis factor alpha in human intestinal tissue.* Gut, 1999. **44**(5): p. 643-52.
50. Roulis, M., et al., *Intestinal epithelial cells as producers but not targets of chronic TNF suffice to cause murine Crohn-like pathology.* Proc Natl Acad Sci U S A, 2011. **108**(13): p. 5396-401.
51. MacDonald, T.T., et al., *Tumour necrosis factor-alpha and interferon-gamma production measured at the single cell level in normal and inflamed human intestine.* Clin Exp Immunol, 1990. **81**(2): p. 301-5.
52. Targan, S.R., et al., *A short-term study of chimeric monoclonal antibody cA2 to tumor necrosis factor alpha for Crohn's disease. Crohn's Disease cA2 Study Group.* N Engl J Med, 1997. **337**(15): p. 1029-35.
53. Vandenabeele, P., et al., *Two tumour necrosis factor receptors: structure and function.* Trends Cell Biol, 1995. **5**(10): p. 392-9.
54. Tartaglia, L.A., et al., *The two different receptors for tumor necrosis factor mediate distinct cellular responses.* Proc Natl Acad Sci U S A, 1991. **88**(20): p. 9292-6.
55. Kovalenko, A., et al., *The tumour suppressor CYLD negatively regulates NF-kappaB signalling by deubiquitination.* Nature, 2003. **424**(6950): p. 801-5.
56. Wagner, S.A., et al., *SPATA2 links CYLD to the TNF-alpha receptor signaling complex and modulates the receptor signaling outcomes.* EMBO J, 2016. **35**(17): p. 1868-84.
57. Trompouki, E., et al., *CYLD is a deubiquitinating enzyme that negatively regulates NF-kappaB activation by TNFR family members.* Nature, 2003. **424**(6950): p. 793-6.
58. Ashkenazi, A. and G. Salvesen, *Regulated cell death: signaling and mechanisms.* Annu Rev Cell Dev Biol, 2014. **30**: p. 337-56.
59. Schneider-Brachert, W., et al., *Compartmentalization of TNF receptor 1 signaling: internalized TNF receptosomes as death signaling vesicles.* Immunity, 2004. **21**(3): p. 415-28.
60. Bertsch, U., et al., *Compartmentalization of TNF-receptor 1 signaling: TNF-R1-associated caspase-8 mediates activation of acid sphingomyelinase in late endosomes.* Adv Exp Med Biol, 2011. **691**: p. 605-16.
61. Foger, N., et al., *Subcellular compartmentalization of FADD as a new level of regulation in death receptor signaling.* FEBS J, 2009. **276**(15): p. 4256-65.
62. Schleich, K., et al., *Stoichiometry of the CD95 death-inducing signaling complex: experimental and modeling evidence for a death effector domain chain model.* Mol Cell, 2012. **47**(2): p. 306-19.
63. Tenev, T., et al., *The Ripoptosome, a signaling platform that assembles in response to genotoxic stress and loss of IAPs.* Mol Cell, 2011. **43**(3): p. 432-48.
64. Guicciardi, M.E. and G.J. Gores, *Life and death by death receptors.* FASEB J, 2009. **23**(6): p. 1625-37.
65. Tschopp, J., M. Irmler, and M. Thome, *Inhibition of fas death signals by FLIPs.* Curr Opin Immunol, 1998. **10**(5): p. 552-8.
66. Micheau, O. and J. Tschopp, *Induction of TNF receptor I-mediated apoptosis via two sequential signaling complexes.* Cell, 2003. **114**(2): p. 181-90.
67. Matsuzawa-Ishimoto, Y., et al., *Autophagy protein ATG16L1 prevents necroptosis in the intestinal epithelium.* J Exp Med, 2017. **214**(12): p. 3687-3705.
68. Burger, E., et al., *Loss of Paneth Cell Autophagy Causes Acute Susceptibility to Toxoplasma gondii-Mediated Inflammation.* Cell Host Microbe, 2018. **23**(2): p. 177-190 e4.
69. Pott, J., A.M. Kabat, and K.J. Maloy, *Intestinal Epithelial Cell Autophagy Is Required to Protect against TNF-Induced Apoptosis during Chronic Colitis in Mice.* Cell Host Microbe, 2018. **23**(2): p. 191-202 e4.
70. Jung, H., et al., *Atg14 protects the intestinal epithelium from TNF-triggered villus atrophy.* Autophagy, 2019. **15**(11): p. 1990-2001.
71. Hsu, H., et al., *TNF-dependent recruitment of the protein kinase RIP to the TNF receptor-1 signaling complex.* Immunity, 1996. **4**(4): p. 387-96.
72. Stanger, B.Z., et al., *RIP: a novel protein containing a death domain that interacts with Fas/APO-1*

(CD95) in yeast and causes cell death. Cell, 1995. **81**(4): p. 513-23.
73. Grimm, S., B.Z. Stanger, and P. Leder, *RIP and FADD: two "death domain"-containing proteins can induce apoptosis by convergent, but dissociable, pathways.* Proc Natl Acad Sci U S A, 1996. **93**(20): p. 10923-7.
74. Ting, A.T., F.X. Pimentel-Muinos, and B. Seed, *RIP mediates tumor necrosis factor receptor 1 activation of NF-kappaB but not Fas/APO-1-initiated apoptosis.* EMBO J, 1996. **15**(22): p. 6189-96.
75. Kelliher, M.A., et al., *The death domain kinase RIP mediates the TNF-induced NF-kappaB signal.* Immunity, 1998. **8**(3): p. 297-303.
76. Takahashi, N., et al., *RIPK1 ensures intestinal homeostasis by protecting the epithelium against apoptosis.* Nature, 2014. **513**(7516): p. 95-9.
77. Dannappel, M., et al., *RIPK1 maintains epithelial homeostasis by inhibiting apoptosis and necroptosis.* Nature, 2014. **513**(7516): p. 90-4.
78. Cuchet-Lourenco, D., et al., *Biallelic RIPK1 mutations in humans cause severe immunodeficiency, arthritis, and intestinal inflammation.* Science, 2018. **361**(6404): p. 810-813.
79. Li, Y., et al., *Human RIPK1 deficiency causes combined immunodeficiency and inflammatory bowel diseases.* Proc Natl Acad Sci U S A, 2019. **116**(3): p. 970-975.
80. Ofengeim, D. and J. Yuan, *Regulation of RIP1 kinase signalling at the crossroads of inflammation and cell death.* Nat Rev Mol Cell Biol, 2013. **14**(11): p. 727-36.
81. Peltzer, N., M. Darding, and H. Walczak, *Holding RIPK1 on the Ubiquitin Leash in TNFR1 Signaling.* Trends Cell Biol, 2016. **26**(6): p. 445-461.
82. Kondylis, V., et al., *The interplay of IKK, NF-kappaB and RIPK1 signaling in the regulation of cell death, tissue homeostasis and inflammation.* Immunol Rev, 2017. **277**(1): p. 113-127.
83. Feltham, R. and J. Silke, *The small molecule that packs a punch: ubiquitin-mediated regulation of RIPK1/FADD/caspase-8 complexes.* Cell Death Differ, 2017. **24**(7): p. 1196-1204.
84. Zhang, D.W., et al., *RIP3, an energy metabolism regulator that switches TNF-induced cell death from apoptosis to necrosis.* Science, 2009. **325**(5938): p. 332-6.
85. Matsuzawa, Y., et al., *RIPK3 regulates p62-LC3 complex formation via the caspase-8-dependent cleavage of p62.* Biochem Biophys Res Commun, 2015. **456**(1): p. 298-304.
86. Moquin, D.M., T. McQuade, and F.K. Chan, *CYLD deubiquitinates RIP1 in the TNFalpha-induced necrosome to facilitate kinase activation and programmed necrosis.* PLoS One, 2013. **8**(10): p. e76841.
87. Geng, J., et al., *Regulation of RIPK1 activation by TAK1-mediated phosphorylation dictates apoptosis and necroptosis.* Nat Commun, 2017. **8**(1): p. 359.
88. Seo, J., et al., *CHIP controls necroptosis through ubiquitylation- and lysosome-dependent degradation of RIPK3.* Nat Cell Biol, 2016. **18**(3): p. 291-302.
89. Park, H.H., et al., *Regulation of RIP3 protein stability by PELI1-mediated proteasome-dependent degradation.* BMB Rep, 2018. **51**(10): p. 484-485.
90. Choi, S.W., et al., *PELI1 Selectively Targets Kinase-Active RIP3 for Ubiquitylation-Dependent Proteasomal Degradation.* Mol Cell, 2018. **70**(5): p. 920-935 e7.
91. Wang, H., et al., *PELI1 functions as a dual modulator of necroptosis and apoptosis by regulating ubiquitination of RIPK1 and mRNA levels of c-FLIP.* Proc Natl Acad Sci U S A, 2017. **114**(45): p. 11944-11949.
92. Feng, S., et al., *Cleavage of RIP3 inactivates its caspase-independent apoptosis pathway by removal of kinase domain.* Cell Signal, 2007. **19**(10): p. 2056-67.
93. Lin, Y., et al., *Cleavage of the death domain kinase RIP by caspase-8 prompts TNF-induced apoptosis.* Genes Dev, 1999. **13**(19): p. 2514-26.
94. Micheau, O., et al., *NF-kappaB signals induce the expression of c-FLIP.* Mol Cell Biol, 2001. **21**(16): p. 5299-305.
95. Ram, D.R., et al., *Balance between short and long isoforms of cFLIP regulates Fas-mediated apoptosis in vivo.* Proc Natl Acad Sci U S A, 2016. **113**(6): p. 1606-11.
96. Kreuz, S., et al., *NF-kappaB inducers upregulate cFLIP, a cycloheximide-sensitive inhibitor of death*

receptor signaling. Mol Cell Biol, 2001. **21**(12): p. 3964-73.
97. Blanpain, C., V. Horsley, and E. Fuchs, *Epithelial stem cells: turning over new leaves.* Cell, 2007. **128**(3): p. 445-58.
98. Hall, P.A., et al., *Regulation of cell number in the mammalian gastrointestinal tract: the importance of apoptosis.* J Cell Sci, 1994. **107 (Pt 12)**: p. 3569-77.
99. Potten, C.S., J.W. Wilson, and C. Booth, *Regulation and significance of apoptosis in the stem cells of the gastrointestinal epithelium.* Stem Cells, 1997. **15**(2): p. 82-93.
100. Edelblum, K.L., et al., *Regulation of apoptosis during homeostasis and disease in the intestinal epithelium.* Inflamm Bowel Dis, 2006. **12**(5): p. 413-24.
101. Cliffe, L.J., et al., *Accelerated intestinal epithelial cell turnover: a new mechanism of parasite expulsion.* Science, 2005. **308**(5727): p. 1463-5.
102. Sun, L., et al., *Type I interferons link viral infection to enhanced epithelial turnover and repair.* Cell Host Microbe, 2015. **17**(1): p. 85-97.
103. Wang, Y., et al., *Chemotherapy drugs induce pyroptosis through caspase-3 cleavage of a gasdermin.* Nature, 2017. **547**(7661): p. 99-103.
104. Heazlewood, C.K., et al., *Aberrant mucin assembly in mice causes endoplasmic reticulum stress and spontaneous inflammation resembling ulcerative colitis.* PLoS Med, 2008. **5**(3): p. e54.
105. Strater, J., et al., *Rapid onset of apoptosis in vitro follows disruption of beta 1-integrin/matrix interactions in human colonic crypt cells.* Gastroenterology, 1996. **110**(6): p. 1776-84.
106. Lee, E.G., et al., *Failure to regulate TNF-induced NF-kappaB and cell death responses in A20-deficient mice.* Science, 2000. **289**(5488): p. 2350-4.
107. Cadwell, K., T.S. Stappenbeck, and H.W. Virgin, *Role of autophagy and autophagy genes in inflammatory bowel disease.* Curr Top Microbiol Immunol, 2009. **335**: p. 141-67.
108. Liu, T.C., et al., *Interaction between smoking and ATG16L1T300A triggers Paneth cell defects in Crohn's disease.* J Clin Invest, 2018.
109. Sun, Q., et al., *Identification of Barkor as a mammalian autophagy-specific factor for Beclin 1 and class III phosphatidylinositol 3-kinase.* Proc Natl Acad Sci U S A, 2008. **105**(49): p. 19211-6.
110. Hara, T., et al., *FIP200, a ULK-interacting protein, is required for autophagosome formation in mammalian cells.* J Cell Biol, 2008. **181**(3): p. 497-510.
111. Patel, K.K., et al., *Autophagy proteins control goblet cell function by potentiating reactive oxygen species production.* EMBO J, 2013. **32**(24): p. 3130-44.
112. Madison, B.B., et al., *Cis elements of the villin gene control expression in restricted domains of the vertical (crypt) and horizontal (duodenum, cecum) axes of the intestine.* J Biol Chem, 2002. **277**(36): p. 33275-83.
113. Peschon, J.J., et al., *TNF receptor-deficient mice reveal divergent roles for p55 and p75 in several models of inflammation.* J Immunol, 1998. **160**(2): p. 943-52.
114. Miyoshi, H., et al., *Wnt5a potentiates TGF-beta signaling to promote colonic crypt regeneration after tissue injury.* Science, 2012. **338**(6103): p. 108-13.
115. Kaiko, G.E., et al., *The Colonic Crypt Protects Stem Cells from Microbiota-Derived Metabolites.* Cell, 2016. **165**(7): p. 1708-20.
116. Miyoshi, H., et al., *Prostaglandin E2 promotes intestinal repair through an adaptive cellular response of the epithelium.* EMBO J, 2017. **36**(1): p. 5-24.
117. Brown, S.L., et al., *Myd88-dependent positioning of Ptgs2-expressing stromal cells maintains colonic epithelial proliferation during injury.* J Clin Invest, 2007. **117**(1): p. 258-69.
118. Cadwell, K., et al., *A key role for autophagy and the autophagy gene Atg16l1 in mouse and human intestinal Paneth cells.* Nature, 2008. **456**(7219): p. 259-63.
119. Cadwell, K., et al., *Virus-plus-susceptibility gene interaction determines Crohn's disease gene Atg16L1 phenotypes in intestine.* Cell, 2010. **141**(7): p. 1135-45.
120. Lee, G., et al., *Response of small intestinal epithelial cells to acute disruption of cell division through CDC25 deletion.* Proc Natl Acad Sci U S A, 2009. **106**(12): p. 4701-6.
121. Kang, S.S., et al., *An antibiotic-responsive mouse model of fulminant ulcerative colitis.* PLoS Med,

2008. **5**(3): p. e41.
122. Filler, S.G., et al., *Pharmacokinetics of murine p75-Fc fusion protein and MP6-XT22 anti-murine TNF-alpha mAb in mice.* J Investig Dermatol Symp Proc, 2007. **12**(1): p. 52-6.
123. Baud, V. and M. Karin, *Signal transduction by tumor necrosis factor and its relatives.* Trends Cell Biol, 2001. **11**(9): p. 372-7.
124. Piguet, P.F., et al., *TNF-induced enterocyte apoptosis in mice is mediated by the TNF receptor 1 and does not require p53.* Eur J Immunol, 1998. **28**(11): p. 3499-505.
125. Wang, L., F. Du, and X. Wang, *TNF-alpha induces two distinct caspase-8 activation pathways.* Cell, 2008. **133**(4): p. 693-703.
126. Mizushima, N., et al., *A protein conjugation system essential for autophagy.* Nature, 1998. **395**(6700): p. 395-8.
127. Itakura, E. and N. Mizushima, *Characterization of autophagosome formation site by a hierarchical analysis of mammalian Atg proteins.* Autophagy, 2010. **6**(6): p. 764-76.
128. Adolph, T.E., et al., *Paneth cells as a site of origin for intestinal inflammation.* Nature, 2013. **503**(7475): p. 272-6.
129. Gan, B., et al., *Role of FIP200 in cardiac and liver development and its regulation of TNFalpha and TSC-mTOR signaling pathways.* J Cell Biol, 2006. **175**(1): p. 121-33.
130. Meichle, A., et al., *Protein kinase C-independent activation of nuclear factor kappa B by tumor necrosis factor.* J Biol Chem, 1990. **265**(14): p. 8339-43.
131. Hsu, H., et al., *TRADD-TRAF2 and TRADD-FADD interactions define two distinct TNF receptor 1 signal transduction pathways.* Cell, 1996. **84**(2): p. 299-308.
132. McKnight, N.C., et al., *Beclin 1 is required for neuron viability and regulates endosome pathways via the UVRAG-VPS34 complex.* PLoS Genet, 2014. **10**(10): p. e1004626.
133. Choi, J., et al., *The parasitophorous vacuole membrane of Toxoplasma gondii is targeted for disruption by ubiquitin-like conjugation systems of autophagy.* Immunity, 2014. **40**(6): p. 924-35.
134. Lu, Q., et al., *Homeostatic Control of Innate Lung Inflammation by Vici Syndrome Gene Epg5 and Additional Autophagy Genes Promotes Influenza Pathogenesis.* Cell Host Microbe, 2016. **19**(1): p. 102-13.
135. Zhao, Z., et al., *Autophagosome-independent essential function for the autophagy protein Atg5 in cellular immunity to intracellular pathogens.* Cell Host Microbe, 2008. **4**(5): p. 458-69.
136. Codogno, P., M. Mehrpour, and T. Proikas-Cezanne, *Canonical and non-canonical autophagy: variations on a common theme of self-eating?* Nat Rev Mol Cell Biol, 2011. **13**(1): p. 7-12.
137. Takeshige, K., et al., *Autophagy in yeast demonstrated with proteinase-deficient mutants and conditions for its induction.* J Cell Biol, 1992. **119**(2): p. 301-11.
138. Johansen, T. and T. Lamark, *Selective Autophagy: ATG8 Family Proteins, LIR Motifs and Cargo Receptors.* J Mol Biol, 2020. **432**(1): p. 80-103.
139. Matsumoto, G., et al., *Serine 403 phosphorylation of p62/SQSTM1 regulates selective autophagic clearance of ubiquitinated proteins.* Mol Cell, 2011. **44**(2): p. 279-89.
140. Pilli, M., et al., *TBK-1 promotes autophagy-mediated antimicrobial defense by controlling autophagosome maturation.* Immunity, 2012. **37**(2): p. 223-34.
141. Lamark, T., S. Svenning, and T. Johansen, *Regulation of selective autophagy: the p62/SQSTM1 paradigm.* Essays Biochem, 2017. **61**(6): p. 609-624.
142. Boldin, M.P., et al., *Involvement of MACH, a novel MORT1/FADD-interacting protease, in Fas/APO-1- and TNF receptor-induced cell death.* Cell, 1996. **85**(6): p. 803-15.
143. Fernandes-Alnemri, T., et al., *In vitro activation of CPP32 and Mch3 by Mch4, a novel human apoptotic cysteine protease containing two FADD-like domains.* Proc Natl Acad Sci U S A, 1996. **93**(15): p. 7464-9.
144. Cohen, G.M., *Caspases: the executioners of apoptosis.* Biochem J, 1997. **326 (Pt 1)**: p. 1-16.
145. Mosselmans, R., et al., *Endocytic pathway of recombinant murine tumor necrosis factor in L-929 cells.* J Immunol, 1988. **141**(9): p. 3096-100.
146. Diao, J., et al., *ATG14 promotes membrane tethering and fusion of autophagosomes to*

endolysosomes. Nature, 2015. **520**(7548): p. 563-6.
147. Doi, H., et al., *p62/SQSTM1 differentially removes the toxic mutant androgen receptor via autophagy and inclusion formation in a spinal and bulbar muscular atrophy mouse model.* J Neurosci, 2013. **33**(18): p. 7710-27.
148. Kurosawa, M., et al., *Depletion of p62 reduces nuclear inclusions and paradoxically ameliorates disease phenotypes in Huntington's model mice.* Hum Mol Genet, 2015. **24**(4): p. 1092-105.
149. Rodriguez-Muela, N., et al., *Blocking p62-dependent SMN degradation ameliorates spinal muscular atrophy disease phenotypes.* J Clin Invest, 2018. **128**(7): p. 3008-3023.
150. Zach, F., et al., *p62/sequestosome 1 deficiency accelerates osteoclastogenesis in vitro and leads to Paget's disease-like bone phenotypes in mice.* J Biol Chem, 2018. **293**(24): p. 9530-9541.
151. Harada, H., et al., *Deficiency of p62/Sequestosome 1 causes hyperphagia due to leptin resistance in the brain.* J Neurosci, 2013. **33**(37): p. 14767-77.
152. Rodriguez, A., et al., *Mature-onset obesity and insulin resistance in mice deficient in the signaling adapter p62.* Cell Metab, 2006. **3**(3): p. 211-22.
153. Zeissig, S., et al., *Downregulation of epithelial apoptosis and barrier repair in active Crohn's disease by tumour necrosis factor alpha antibody treatment.* Gut, 2004. **53**(9): p. 1295-302.
154. Wirtz, S., et al., *Chemically induced mouse models of acute and chronic intestinal inflammation.* Nat Protoc, 2017. **12**(7): p. 1295-1309.
155. Lassen, K.G., et al., *Atg16L1 T300A variant decreases selective autophagy resulting in altered cytokine signaling and decreased antibacterial defense.* Proc Natl Acad Sci U S A, 2014. **111**(21): p. 7741-6.
156. Marmenout, A., et al., *Molecular cloning and expression of human tumor necrosis factor and comparison with mouse tumor necrosis factor.* Eur J Biochem, 1985. **152**(3): p. 515-22.
157. Slee, E.A., et al., *Benzyloxycarbonyl-Val-Ala-Asp (OMe) fluoromethylketone (Z-VAD.FMK) inhibits apoptosis by blocking the processing of CPP32.* Biochem J, 1996. **315 (Pt 1)**: p. 21-4.
158. Staelens, J., et al., *Hyporesponsiveness of SPRET/Ei mice to lethal shock induced by tumor necrosis factor and implications for a TNF-based antitumor therapy.* Proc Natl Acad Sci U S A, 2002. **99**(14): p. 9340-5.
159. Mahieu, T., et al., *The wild-derived inbred mouse strain SPRET/Ei is resistant to LPS and defective in IFN-beta production.* Proc Natl Acad Sci U S A, 2006. **103**(7): p. 2292-7.
160. Ueffing, N., et al., *Mutational analyses of c-FLIPR, the only murine short FLIP isoform, reveal requirements for DISC recruitment.* Cell Death Differ, 2008. **15**(4): p. 773-82.
161. VanDussen, K.L., et al., *Development of an enhanced human gastrointestinal epithelial culture system to facilitate patient-based assays.* Gut, 2015. **64**(6): p. 911-20.